Deformation twinning in nanocrystalline materials

Y.T. Zhu [a,*], X.Z. Liao [b], X.L. Wu [c]

[a] Department of Materials Science & Engineering, North Carolina State University, Raleigh, NC 27695, USA
[b] School of Aerospace, Mechanical and Mechatronic Engineering, The University of Sydney, NSW 2006, Australia
[c] State Key Laboratory of Nonlinear Mechanics, Institute of Mechanics, Chinese Academy of Sciences, Beijing 100080, China

ARTICLE INFO

ABSTRACT

Nanocrystalline (nc) materials can be defined as solids with grain sizes in the range of 1–100 nm. Contrary to coarse-grained metals, which become more difficult to twin with decreasing grain size, nanocrystalline face-centered-cubic (fcc) metals become easier to twin with decreasing grain size, reaching a maximum twinning probability, and then become more difficult to twin when the grain size decreases further, i.e. exhibiting an inverse grain-size effect on twinning. Molecular dynamics simulations and experimental observations have revealed that the mechanisms of deformation twinning in nanocrystalline metals are different from those in their coarse-grained counterparts. Consequently, there are several types of deformation twins that are observed in nanocrystalline materials, but not in coarse-grained metals. It has also been reported that deformation twinning can be utilized to enhance the strength and ductility of nanocrystalline materials. This paper reviews all aspects of deformation twinning in nanocrystalline metals, including deformation twins observed by molecular dynamics simulations and experiments, twinning mechanisms, factors affecting the twinning, analytical models on the nucleation and growth of deformation twins, interactions between twins and dislocations, and the effects of twins on mechanical and other properties. It is the authors' intention for this review paper to serve not only as a valuable reference for researchers in the field of nanocrystalline metals and alloys, but also as a textbook for the education of graduate students.

© 2011 Elsevier Ltd. All rights reserved.

* Corresponding author. Tel.: +1 919 513 0559; fax: +1 919 515 3419.
E-mail address: ytzhu@ncsu.edu (Y.T. Zhu).

Contents

1. Introduction

When a metal or alloy is plastically deformed, its shear strain is usually produced by dislocation slip and/or deformation twinning, especially at low temperatures and low strain rates [1,2]. Other deformation mechanisms include grain rotation, grain boundary sliding, and diffusion, but these mechanisms only become significant at relatively high temperatures, especially when the grain sizes are large [3]. Deformation twinning is a common and important phenomenon in metals and alloys. The twinning tendency of a face-centered-cubic (fcc) metal is largely determined by its stacking fault energy. For example, coarse-grained fcc metals with high stacking fault energies such as Al and Ni normally deform by dislocation slip, while fcc metals with low stacking fault energy such as Ag primarily deform by twinning [4,5]. The following deformation conditions also promote deformation twinning [1,2,6–11]: (1) high strain rate and (2) low deformation temperature. Deformation twinning in coarse-grained materials has been reviewed by Christian and Mahajan [1], and therefore will not be reviewed in detail in the present paper. The focus of this paper is on nanocrystalline fcc metals. Nanocrystalline bcc and hcp metals have not been extensively studied, and will only be briefly discussed.

Nanocrystalline (nc) materials can be defined as solids with grain sizes in the range of 1–100 nm [12]. They have been reported to be considerably stronger than their coarse-grained counterparts, but their ductility is usually disappointingly low [13]. Bulk nc materials are usually synthesized by either two-step approaches such as nano-powder synthesis and consolidation [14,15], or one-step approaches such as severe plastic deformation (SPD) [16–18]. The low ductility of nc materials synthesized by the two-step approach is usually attributed to flaws such as cracks, air bubbles, etc. [19]. SPD is capable of synthesizing flaw-free nc materials with higher ductility than those synthesized by nano-powder consolidation. However, even these flaw-free nc materials usually exhibit very low uniform tensile elongation (the strain before necking), which is the measure for useful ductility. It should be also noted that very small samples are often used to measure the mechanical properties of nc materials, due to the difficulty in synthesizing large nc samples. This presents a serious problem because small sample size (e.g. gauge length smaller than 5 mm) may lead to an artificially high ductility, although the yield strength is not affected [20,21].

The mechanical properties, including ductility, of nc materials are controlled by their unique deformation mechanisms [6,9,10,18,22,23]. Deformation mechanisms identified in nc materials include partial dislocation emission from grain boundaries [8,24–31], deformation twinning [8,24–30,32], perfect dislocation slip [24,26,28], grain boundary sliding [24,33–37], and grain rotation [25,28,38,39]. In addition, since deformation twinning usually occurs simultaneously with the slip of perfect and partial dislocations, interactions between twins and gliding dislocations at twin boundaries inevitably occur and have been observed both experimentally [40–44] and by molecular dynamics (MD) simulations [45–50]. These interactions make twins effective in simultaneously increasing the strength and ductility of nc materials [40,51]. In addition, it is also reported that nc Cu with high density of twins have good electrical conductivity and excellent resistance to current-induced diffusion [40,52]. Therefore, deformation twinning in nc materials is of both fundamental and practical importance, and can be utilized to design nc materials for superior mechanical and physical properties.

Significant progress has been made in understanding the deformation twins in the last decade. In this paper we review all aspects of deformation twinning in nc metals and alloys, including deformation twins observed by MD simulations and experiments, twinning mechanisms, factors affecting the twinning, analytical models on the nucleation and growth of deformation twins, and the effects of deformation twinning on mechanical and other properties.

This paper is organized in the following way. We will first briefly introduce some basics on the deformation twinning to help with the reading of the paper, especially for those young scientists such as graduate students. The deformation twinning in coarse-grained fcc materials will be briefly reviewed to provide a comparison for the twinning in nc materials. Then the deformation mechanisms in nc materials will be discussed to put the deformation twinning in an appropriate perspective relative to all other active mechanisms in nc materials. This is followed by all aspects of deformation twin-

ning in nc materials. The interaction between dislocations and twin boundaries will be reviewed because it significantly affects the mechanical properties of nc materials. Finally, the effect of twinning on the mechanical behaviors and electrical conductivity of nc materials will be discussed.

2. Basics of deformation twinning in fcc metals

Deformation twinning as a common deformation mechanism has been described in textbooks [53] as well as specialized books dealing with dislocations and deformation of metals [54]. Here we will only briefly describe some selected aspect of it to help with the discussions in the following sections of the paper. Conventionally, deformation twins in fcc metals are believed to be formed by the glide of partial dislocations with the same Burgers vector on successive [55] planes. This collectively produces a macroscopic strain to accommodate the imposed strain. The twinning partial in fcc metals has a Burgers vector of $\mathbf{b}_1 = a/6\langle 1\,1\,2\rangle$ with a magnitude of $a/\sqrt{6}$. As shown in Fig. 1 [56], if deformation twinning occurs above the twin boundary a spherical grain via partials with a Burgers vector $\mathbf{b}_1$, a grain will be sheared into a new shape. Note that a grain boundary kink will be produced at the twin boundary with a kink angle of 141°, which is twice of the angle between two close-packed {1 1 1} planes.

The twinning partial dislocations are all Shockley partials that can glide on the slip plane. There are three equivalent Shockley partials on each slip plane. For example, as shown in Fig. 2, on the (1 1 1) slip plane the three partials are $\mathbf{b}_1 = \mathbf{B}\delta = a/6[2\,\bar{1}\,\bar{1}]$, $\mathbf{b}_2 = \mathbf{A}\delta = a/6[\bar{1}\,2\,\bar{1}]$, and $\mathbf{b}_3 = \mathbf{C}\delta = a/6[\bar{1}\,\bar{1}\,2]$. Note that there are also three partials with opposite Burgers vectors, $-\mathbf{b}_1$, $-\mathbf{b}_2$, and $-\mathbf{b}_3$. The implications of these partials with opposite Burgers vectors will be discussed later.

Fig. 2b shows the magnitude and orientation of the three Burgers vectors of partial dislocations, $\mathbf{b}_1$, $\mathbf{b}_2$, and $\mathbf{b}_3$, as overlaid on the close-packed atoms in the (1 1 1) slip plane. It also shows the atomic stacking positions A, B, and C. For fcc metals, the stacking sequence of atoms in successive close-packed planes is ABCABCABCABC. When a partial dislocation glides across a slip plane, a stacking fault is produced and all atoms above the stacking fault change their positions. From magnitude and orientation of the Burgers vectors shown in Fig. 2b, the atom stacking position shift caused by the gliding of a partial dislocation can be described below:

Partial $\mathbf{b}_1$: $A \rightarrow B$, $B \rightarrow C$, $C \rightarrow A$
Partial $\mathbf{b}_2$: $A \rightarrow B$, $B \rightarrow C$, $C \rightarrow A$
Partial $\mathbf{b}_3$: $A \rightarrow B$, $B \rightarrow C$, $C \rightarrow A$

In other words, although the three Burgers vectors have different orientations, they cause the same stacking position shift. As will be shown later, this has important implications for deformation twinning in nc fcc metals. Note that partials with opposite orientations, i.e. $-\mathbf{b}_1$, $-\mathbf{b}_2$, and $-\mathbf{b}_3$, will shift the stacking sequence to the opposite direction, i.e. $B \rightarrow A$, $C \rightarrow B$, $A \rightarrow C$.
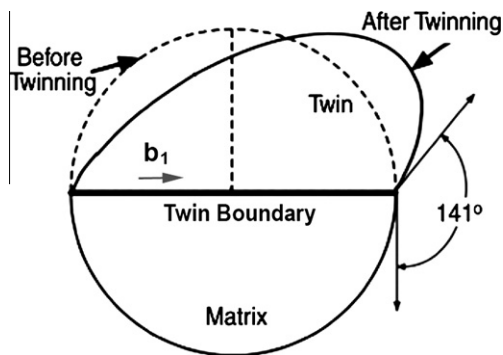
Fig. 1. Conventional deformation twinning by the gliding of partials on successive slip planes above the twin boundary changes the shape of the spherical grain above the twin boundary [56].
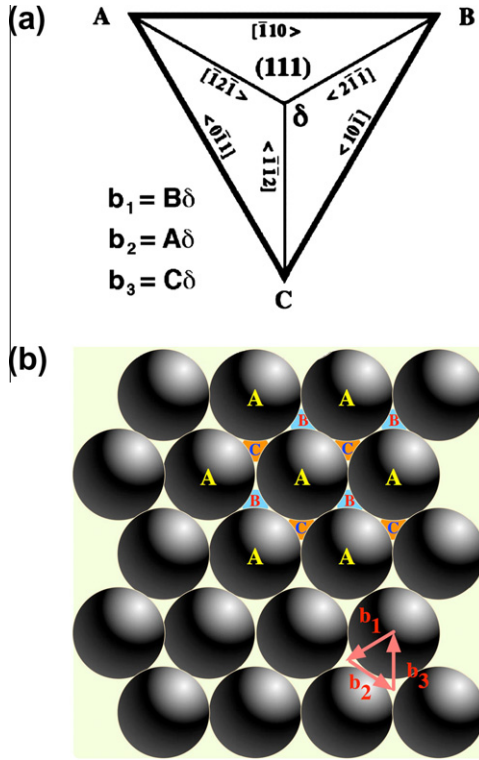
Fig. 2. (a) Three equivalent Burgers vectors $\mathbf{b}_1$, $\mathbf{b}_2$, and $\mathbf{b}_3$ on the (1 1 1) slip plane for Shockley partials. (b) The magnitude and orientation of the three partial Burgers vectors, $\mathbf{b}_1$, $\mathbf{b}_2$, and $\mathbf{b}_3$, on the (1 1 1) plane of closely-packed atoms, and the atomic stacking positions A, B, C (note that they are not related to the letter A, B and C in (a)).
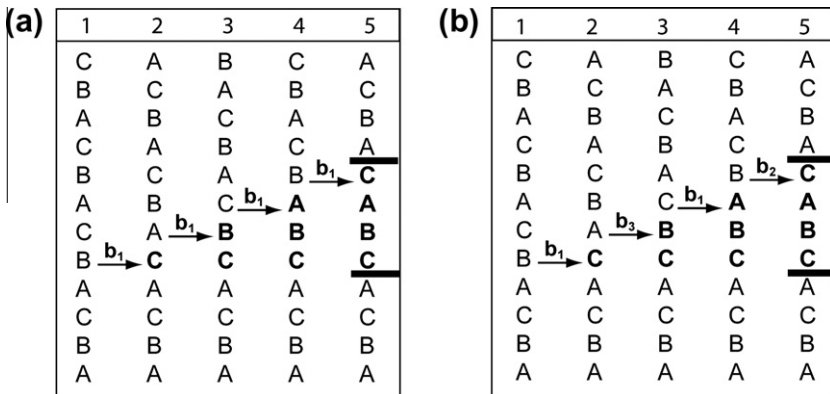
Fig. 3. (a) The process of forming a four-layer deformation twin by the slip of four partials with the *same* Burgers vector ($\mathbf{b}_1$) on successive slip planes. (b) The process of forming a four-layer deformation twin by the slip of four partials with a mixture of Burgers vectors $\mathbf{b}_1$, $\mathbf{b}_2$, and $\mathbf{b}_3$ on successive slip planes.

As stated earlier, a deformation twin can be formed by the slip of Shockley partials on successive slip planes. Fig. 3a shows the formation of a four-layer twin via the slip of partials with the same Burgers vector, marked by the bold letter **CBAC**. As shown, the column 1 has a normal fcc stacking

sequence ABCABCABCABC. The slip of first partial $\mathbf{b}_1$ produces an intrinsic stacking fault (see the bold letter **C** in column 2), which is identical to removing a layer of B atoms. The slip of the second $\mathbf{b}_1$ partial on an adjacent slip plane converts the stacking fault into a two-layer twin nucleus (**CB**, see column 3) [34,42,56–59]. Note that the two-layer twin nucleus is also identical to an extrinsic staking fault, e.g. a stacking fault formed by inserting an extra C layer between the A and B layers. [54]. Further slip of $\mathbf{b}_1$ partials grows the twin nucleus into a four-layer twin **CBAC**, with the twin boundaries represented by two horizontal lines (see column 5). Since the twinning process described in Fig. 3a involves only partials with the same Burgers vector, we name such a process as monotonic twinning process.

Fig. 3b shows that a four-layer twin with identical stacking sequence as in Fig. 3a can also be produced by the slip of four partials with mixture of three Burgers vector ($\mathbf{b}_1$, $\mathbf{b}_2$, and $\mathbf{b}_3$) on successive slip planes. In other words, a twin can be formed by the slip of identical partials or different partials. This is because the three partials, $\mathbf{b}_1$, $\mathbf{b}_2$, and $\mathbf{b}_3$, produce the same stacking sequence shifts despite of their orientation difference.

It should be noted that the macroscopic strain produced by the two twinning processes described in Fig. 3 are very different. In Fig. 3a, all partials have the same Burgers vector, and therefore produce a shear strain in the same direction. This can collectively produce a relatively large macroscopic strain and change the grain shape as shown in Fig. 1. In contrast, the twinning process described in Fig. 3b will produce a much smaller macroscopic strain because partials with different Burgers vectors shear the lattice to different directions.

The two twinning processes described in Fig. 3 will have implications in the twin morphologies. As discussed later, most twinning mechanisms proposed for the fcc metals with coarse grains are consistent with the twinning process described in Fig. 3a, while the twinning process described in Fig. 3b could be very common in nanocrystalline fcc metals. Materials with grain sizes in the range of 1 μm to 1000 μm are hereafter defined as coarse-grained materials [3,16,18,28,60–64].

A crystallographic feature of the twin is the mirror symmetry of atomic arrangement across the coherent twin boundary plane. For an fcc metal, this symmetry can be best viewed along the [1 1 0] orientation that is on the coherent twin boundary plane (see Fig. 4a). As shown, the coherent twin boundary plane is the $(1\bar{1}1)$ close-packed plane, and it has a 70.53° angle with other close packed planes. Each lattice point in the two-dimensional illustration (Fig. 4a) represents an atom column, with the dark circles below the light circle by a distance of atomic radius, i.e. 1/4[1 1 0]. However, under the high-resolution electron microscope, these two types of columns give identical images, as shown in Fig. 4b. The mirror symmetry in the high-resolution electron microscopy (HREM) image shown in Fig. 4b is often used to identify twins in fcc metals.

Regular low-resolution transmission electron microcopy (TEM) is also often used to identify deformation twins in metals, although it cannot obtain atomic-resolution images. TEM can detect the microstructural feature of twins, which is often in a plate shape with straight twin boundaries. Examples of low-resolution twin images are shown in Fig. 5a. However, in nc fcc metals, multiple twins often form, which show no obvious plate-like morphology (see Fig. 5b) [34,42,56,65–70]. Under such circumstances, HREM is needed to identify and study the deformation twins.

3. Deformation twinning in coarse-grained fcc metals

3.1. Twinning mechanisms in coarse-grained fcc metals

Deformation twinning in coarse-grained fcc metals and alloys has been comprehensively reviewed by Christian and Mahajan [1]. Therefore, we will only give a brief summary here. Coarse-grained fcc metals are believed to twin via several conventional mechanisms including the pole mechanism [71], prismatic glide mechanism [72], faulted dipole mechanism [73], or other mechanisms [74–76]. These mechanisms often require a dislocation source in the grain interior to operate. As will be discussed later, this poses a problem for nc metals and alloys since their grain interior are often free of dislocations [25,61], although dislocations can exist in nc grains under certain deformation conditions [77,78]. In addition, the deformation mechanisms in nc materials are dramatically different from those in their coarse-grained counterparts due to a strong grain size effect below 100 nm.
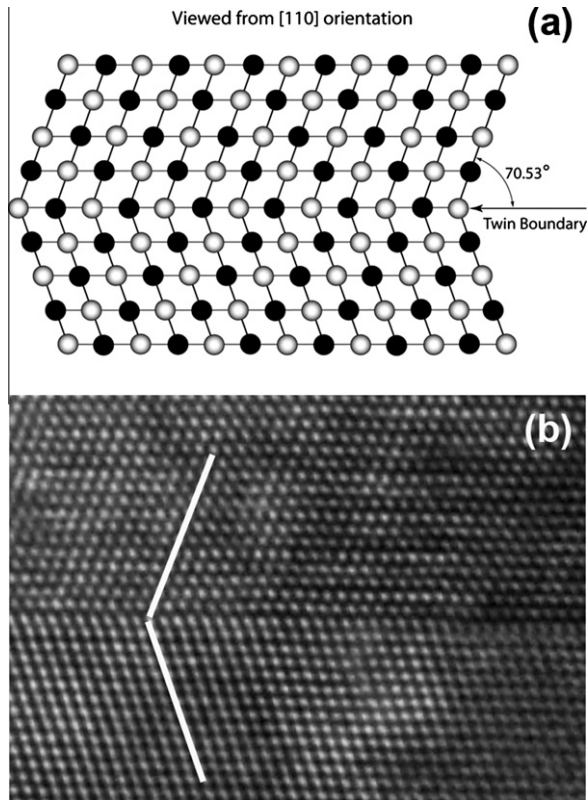
Fig. 4. (a) The mirror symmetry of atoms in a twin in fcc metals, when viewed from a [1 1 0] direction that is on the coherent twin boundary plane. A dark filled circle represents an atom column that is shifted for half an atomic distance below an atom column represented by a light circle. (b) A typical HREM image of a twin in an fcc metal. Columns represented by lighter and dark circles in (a) are not differentiated by HREM in (b).

One exception is a 3-layer twin nucleation model proposed by Mahajan and Chin for fcc metals [74]. In theory, this model can be easily applied to nc metals. Furthermore, Kibey et al. recently calculated the critical stress for the nucleation of such a three-layer twin, incorporating the general planar fault energies (GPFE) obtained from the *ab initio* density functional theory (DFT) [79]. The predicted stress is very close to experimentally measured values for many fcc metals. However, the "three-layer" twin nucleation is yet to be observed in nc fcc metals.

3.2. Grain size effect

According to the experimental results reported in the literature, smaller grain size impedes deformation twinning [11,80–83] in coarse-grained metals and alloys, irrespective of their crystal structure. Meyers et al. [11] summarized the Hall–Petch slopes for both perfect dislocation slip and twinning in a number of *coarse-grained* metals with fcc, body-centered cubic (bcc) and hexagonal-close-pack (hcp) crystal structures. In each case, the experimentally observed Hall–Petch slope for twinning is much higher than that for the slip of perfect dislocations. In other words, for coarse-grained metals, the stress required for activating twinning increases much faster with decreasing grain size than the stress for perfect dislocation slip, as illustrated in Fig. 6. Therefore, smaller grain size make the deformation twinning more difficult. The grain size effect was demonstrated in many examples. El-Danaf et al. [81] reported that 70/30 brass showed much greater twin density in samples with the grain size of 250 μm than in samples with grain sizes of 9 and 30 μm. Meyers et al. [84] observed that shock compression at
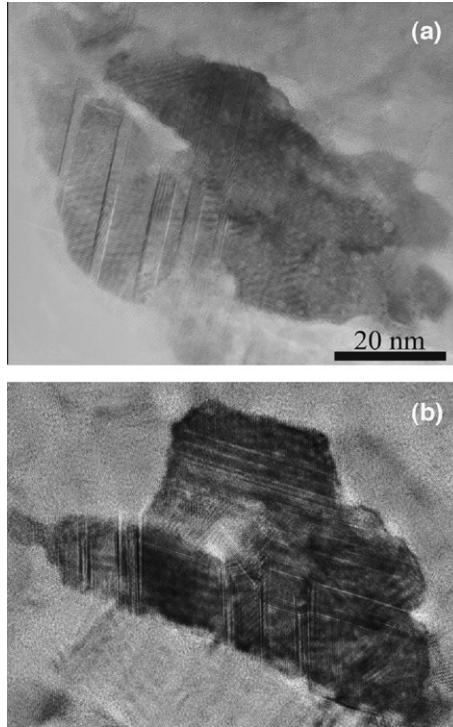
Fig. 5. Morphology of deformation twins in nc fcc Cu under low resolution. (a) Twins with plate-like morphology. (b) Multiple twins without obvious plate-like morphology. Both (a) and (b) are from the original HREM images with reduced resolutions.
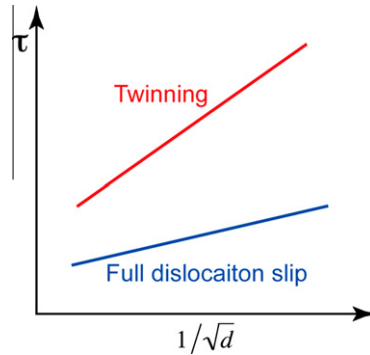
Fig. 6. The schematic of Hall–Petch relationship for twinning and full dislocation slip in coarse-grained metals and alloys. τ is the shear stress and d is the grain size. The higher slope for twinning indicates that twinning is more difficult than the slip of full dislocations in smaller grains.

35 GPa produced profuse deformation twins in Cu samples with average grain sizes of 117 and 315 µm, but virtually no twin in Cu samples with an average grain size of 9 µm.

3.3. Temperature and strain rate effect

The strain rate and temperature effect on deformation twinning in coarse-grained fcc metals and alloys have been summarized by Meyers et al. [11] and by Christian and Mahajan [1]. There is a
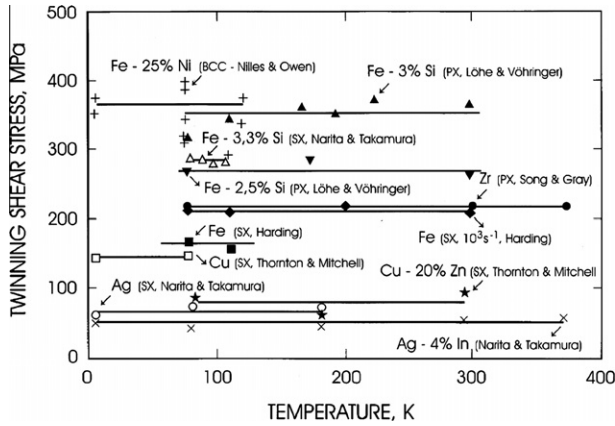
Fig. 7. Effect of temperature on twinning stress for several single crystalline and polycrystalline metals and alloys [11].

general equivalency of low temperature and high strain rate [1]. Specifically, lower temperature and higher strain rate usually promote deformation twinning. For example, fcc Cu was found to deform by twinning at 4 K at a low strain rate [85], although it only deforms by dislocation slip at room temperature and low strain rate. Therefore, there is a transition to twinning with decreasing temperature. This transition temperature increases with decreasing stacking fault energy [1]. Generally, the tendency for twinning increases rather slowly with decreasing temperature but much faster with increasing strain rate. For example, shock deformation has been found to produce twins in metals and alloys with medium-to-high stacking fault energy [84,86–88], which usually does not deform by twinning at quasi-static strain rate and room temperature.

The observed temperature and strain rate effect can be understood from two aspects. The first is how the critical twinning stress varies with the temperature and strain rate, and the second is how the material flow stress changes with the temperature and strain rate. Meyers et al. [11] summarized the twinning stress as a function of temperature for a number of single-crystal and polycrystalline metals and alloys (see Fig. 7), and found that the twinning stress is insensitive to temperature. However, there are debates on this issue [89–92]. Mahajan suggested that the bcc metals have a negative twinning stress dependence on temperature, while fcc metals have a sight positive twinning stress dependence on temperature [1]. The strain rate effect on twinning stress is not well studied. Harding [93,94] found that the twinning shear stress increased from 170 MPa to 220 MPa when the strain rate was increased from 10^{-3} s^{-1} to 10^3 s^{-1}.

The flow stress of metals and alloys usually increases with decreasing temperature and/or increasing strain rate. The increase in flow stress at low temperature is believed caused, at least in part, by the strong dependence of the work-hardening on temperature, which may increase the flow stress to the critical twinning stress. During the deformation process, dynamic hardening and recovery occurs simultaneously. The dynamic recovery process needs the climbing of dislocations, which is a thermally activated process [95]. It becomes slower at lower temperatures [28,95–104], and this causes higher work-hardening rate, and consequently higher flow stress. At higher strain rate the overall work hardening rate increases because the dislocation generation rate is faster than the dislocation annihilation, which leads to the increase in flow stress. Therefore, the increase in twinning tendency at low temperatures and higher strain rates can be largely attributed to the increase in flow stress.

4. Deformation mechanisms in nanocrystalline materials

Due to their small grain size, nc materials deform via mechanisms that are different from those in their coarse-grained counterparts [6,8,9,22–24,27,42,66]. As discussed in the introduction, several deformation mechanisms have been identified in nc materials. The significance of each deformation

mechanism changes with decreasing grain size. For example, for fcc metals and alloys with medium-to-high stacking fault energy, perfect dislocation slip dominates in large grains (e.g. larger than 50 nm) [3]. However, more than one deformation mechanisms may be active at any grain size, although the significance of each mechanism changes with grain size. In other words, for each deformation mechanism, there is a grain size range in which it plays a significant role. In the following subsections, we will briefly summarize several deformation mechanisms to set the stage for the detailed review of deformation twinning in Section 5.

It should be noted that the HREM observations have been extensively used to support proposed twinning mechanisms. These observations were mostly postmortem because of the difficulty of in situ HREM. Early HREM observations were mostly used to validate twinning mechanisms observed by molecular dynamics (MD) simulations. New twinning mechanisms were later proposed based on analysis of postmortem HREM observations. Some of these HREM findings were verified by MD simulations. HREM and MD simulations are complementary means for studying deformation twinning, and then are especially powerful when combined to study deformation mechanisms in nc materials.

4.1. Grain boundary sliding

Grain boundary sliding in nc materials was first observed by MD simulations [24,36,37,105], later reported experimentally [27,106–108], and modeled analytically [109–112]. Importantly, such grain boundary sliding may occur in a coordinated way [27,105–107,113–115]. For example, shown in Fig. 8 is the alignment of grain boundaries of many grains to facilitate the grain boundary sliding [107]. The small grain sizes of nc materials [37] make it easier for the grain alignment [80,116]. Such a coordinated grain boundary sliding may play a significant role in the deformation of nc materials, as shown in Fig. 9, which reveals prevalent grain boundary aligning in nc Ti. More study is needed on this issue.

4.2. Grain rotation

Grain rotation in nc metals was first observed under in situ HREM by Ke et al. [38], and later confirmed by Shan et al. [25,117], Jin et al. [118] and Wang et al. [119]. Grain rotation as a deformation mechanism was also revealed by MD simulations [105,120,121] and has been analytically modeled [111,122,123]. The unambiguous means to observe grain rotation is in situ TEM. However, experimental evidence of grain rotation from such observation is also controversial because the TEM samples are very thin and may not represent bulk nc materials. More recently, texture measurement confirmed that grain rotation indeed plays a significant role in the deformation of bulk nc materials [28,124–127]. However, the grain rotation was also found to accompany grain growth during the deformation
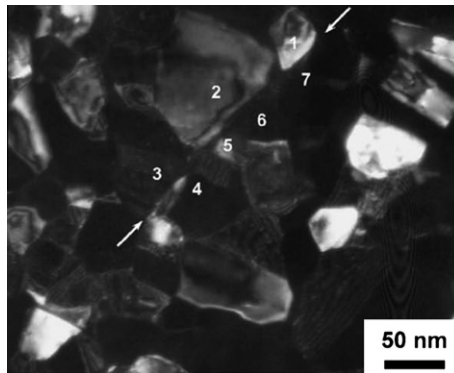
Fig. 8. The alignment of grains in nc Pd after deformation by high-pressure torsion, suggesting coordinated grain boundary sliding [107].
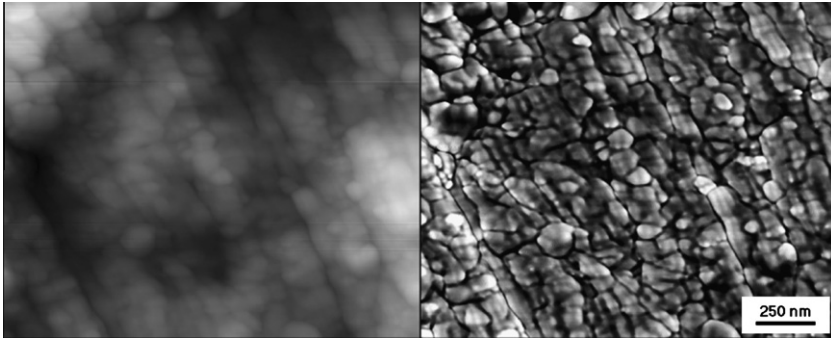
Fig. 9. Atomic Force Microscope (AFM) topography (left) and phase contrast (right) images taken from the surface of a nc Ti sample processed by HPT after being tested in tension at 250 °C for a strain of ∼30%.

[28,39,124,125,128]. Such stress (strain) assisted grain growth has been reported by several groups [28,39,118–121,124–126,128–139] and can occur at even liquid nitrogen temperature [129,130]. These observations suggest that grain rotation play a significant role in the deformation of nc metals and alloys and it often leads to grain growth. Wang et al. concluded that grain rotation first converts high-angle grain boundaries to low-angle grain boundaries. The low-angle grain boundaries will then disappear, leaving behind higher density of dislocations, which is consistent with MD simulations by Haslam et al. [128].

4.3. Dislocation emission from grain boundaries

Grain boundaries become the primary dislocation source and sink when the grain is smaller than a critical size [140–143]. This is because dislocation sources often no longer exist in the grain interior of nc materials. For example, in ultrafine-grained hexagonal close-packed (hcp) Ti processed by severe plastic deformation [142], grains and subgrains smaller than 100 nm are often dislocation free (see Fig. 10). This critical grain size is determined by material properties such as stacking fault energy and deformation parameters such as temperature and strain rate. High stacking fault energy and low melting temperature make dislocation recovery easier, which consequently leads to larger critical grain size. For example, for pure Al, which has high stacking fault energy (122 mJ/m^2 [54,144]) and
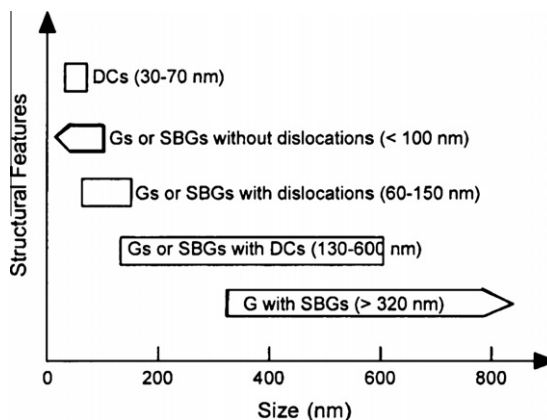
Fig. 10. Hierarchy of microstructure in Ti processed by severe plastic deformation [142]. The acronyms are G – grains, SBG – subgrains, DC – dislocation cells.

low melting temperature (660.32 °C), the critical grain size is relatively large. Grains of a few hundred nanometers may be dislocation free [145–147]. The lack of dislocation in the grain interior has been attributed to the lacking of strain hardening in nc materials [51,140,148–154].

When dislocation source is unavailable inside the grain interior, grain boundary becomes the primary source for dislocation generation. Indeed, in situ TEM revealed extensive emission of dislocations from grain boundaries of nc materials [25,143,155,118,156]. However, in situ TEM is often done under low-resolution mode and cannot differentiate partial dislocations from perfect dislocations. Partial dislocation emissions from grain boundaries were extensively observed by MD simulations [9,10,26,22,144,157,158], and was verified experimentally by ex situ HREM observations [8]. As will be discussed in later sections, the emission of dislocations from the grain boundaries play a critical role in the nucleation and growth of deformation twins in nc fcc metals, and is responsible for several unique twinning mechanisms.

It should be noted that under certain deformation conditions, high-dislocation density is still possible in nc metals and alloys. For example, high-density of dislocation defect structure was found in the grain interior of nc Ni deformed under constrained rolling at liquid nitrogen temperature [77].

4.4. Stacking fault and deformation twinning

In coarse-grained fcc and bcc materials, stacking faults and deformation twins usually occur in metals and alloys with low stacking fault energy, although high strain rate and low deformation temperature can significantly promote twinning. In coarse-grained hcp metals and alloys, twinning is a common deformation mechanism because their small number of slip systems [56,159–170]. In comparison, nc materials have a very different behavior in the formation of stacking faults and deformation twins. First, nc hcp metals are rarely observed to deform by twinning. Second, nc fcc metals are found to generally deform by twinning more easily, especially in those fcc metals with medium to high stacking fault energy, although twinning may become difficult again at very small grain sizes [171]. Deformation twinning in nc fcc metals and alloys is the focus of this review, and is discussed in detail in the next section.

5. Deformation twinning in nanocrystalline fcc materials

5.1. Molecular dynamics simulations

The MD simulation of deformation twinning in nc fcc materials has been comprehensively reviewed by Wolf et al. [22]. Here we will only give a brief summary on the features of MD simulations as well as the major results on deformation twinning obtained by MD simulations. Early insights on the deformation mechanisms of nc materials are almost exclusively obtained by MD simulations [9,24,26,36,105,144,157,172–176], largely because of the difficulty in synthesizing nc materials for experimental studies. For example, extensive early studies were performed on nc samples synthesized by inert gas condensation [15,177–184], which did not have clean grain boundaries and had flaws such as cracks and pores after consolidation due to the adsorption of O, H, and N atoms during the synthesis of nano-powders. It is still a challenge even today to synthesize nc materials with certain structural characteristics to systematically investigate a specific deformation mechanism.

MD simulation has several advantages over experimental investigation, which makes it a powerful tool for studying nc materials [22]. First, MD simulation can elucidate the atomic level deformation mechanisms in nc materials in a degree of detail that cannot be obtained experimentally. Second, it is capable of investigating the real-time deformation behavior, including twinning and detailed defect evolution and interaction, which are not possible by any experimental technique. Third, it can simulate a well-characterized and idealized model nc system to study specific deformation mechanisms. Fourth, it is capable of deforming samples to very large plastic strains, which make it possible to investigate the deformation behavior under high dislocation densities.

MD simulation also has its own limitations [22]. First it is typically limited to relatively small model systems. As a result, many researchers often use model systems with very small grain sizes. This could

sometimes lead to serious problems because it is known that grain sizes affect the deformation mechanisms [24,37,57,59,171,185]. For example, it was observed by MD simulations that nc Al, Cu and Ni rarely deform by twinning [10], which contradicts the experimental observations [2,6,23, 33–35,66,68,77,186–189]. This controversy was later found caused by the grain size effect, i.e. the small grain size used in the MD simulation is so small that the deformation twins are hard to form, due to an inverse grain size effect on twinning [171]. This limitation will be gradually relaxed as faster computers become more available to researchers. The second limitations of MD simulations is its short time duration [22], which results in extremely high strain rate (typically larger than $10^7 \, \text{s}^{-1}$). Although such high strain rate is physically plausible [190–192], they are much higher than what we can normally obtain experimentally. This makes it more complex to compare with experimental results, because it is well known that the strain rate has significant effect on deformation mechanisms. For example, it is generally agreed that higher strain rate promotes deformation twinning [2,11,80,84,171,188,193–195].

MD simulation has revealed many important deformation mechanisms of nc materials despite of its limitations. Below we will list only a few that are relevant to deformation twinning: First, emission of Shockley partials from grain boundaries are extensively observed by several groups [9,10,24,26,37,45,46,144,157,158,185,196–210]. Second, three mechanisms for twin nucleation and growth were clearly revealed by Yamakov et al. (see Fig. 11) [9]. As shown in Fig. 11, a twin nucleus (marked by A) is formed by the overlapping of two extended dislocations on adjacent slip planes. There are also three other similar twin nuclei in the same grain. A twin marked by B is formed by successive emission of five Shockley partials from the grain boundary. C represents a twin formed by grain boundary splitting and migration, which leaves behind a coherent twin boundary (marked by α) and produces another coherent twin boundary (marked by β), while the migrating twin boundary (marked by δ) consists of a Shockley partial dislocations.
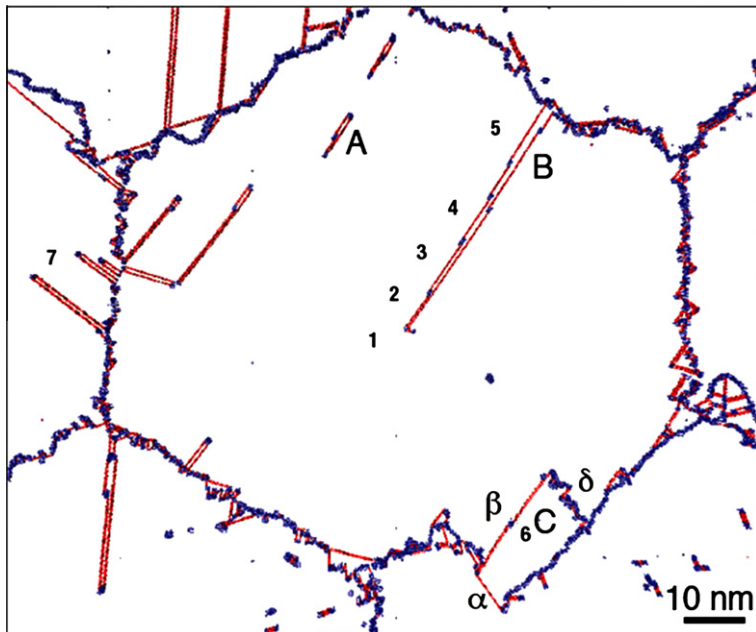
Fig. 11. Three twinning mechanisms are revealed in this MD simulation snapshot of nc Al with columnar grains [9]. As marked in the figure, A represents a twin nucleus formed by the overlapping of two extended dislocations on adjacent slip planes, B represents a twin formed by successive emission of Shockley partials from the grain boundary, and C represents a twin formed by grain boundary splitting and migration. Seven marks a few partial dislocations emitted from the grain boundary.

5.2. Experimental observations

The experimental observations of deformation twins were summarized in a previous paper [56]. Experimental results can validate and provide input to the MD simulations. Nanocrystalline samples for experimental studies are usually much larger and more complex than the model systems used by MD simulations, and therefore may reveal some deformation phenomena that are missed by the MD simulations. Early experimental observations of deformation twins were limited to the validation of MD simulation results. Examples include the experimental observation of partial dislocations emitted from grain boundaries (see Fig. 12) [6–8,23,186,211,212], and deformation twinning [3,6–8,18,23,31,65,66,186,213,214]. In recent years, several new phenomena have been first revealed by experimental investigations, including fivefold twins [8,65,70], twins with reduced macroscopic strain [2], inverse grain size effect on twinning [171], V-shaped twins by a self-thickening mechanism [67,69], and reversible twinning process [215]. Interestingly, a proposed formation mechanism [70] based on the experimentally observations for fivefold twins was later verified by MD simulation [216].

Experimental techniques for investigating deformation twinning include HREM, in situ HREM, and diffraction analysis (X-ray, synchrotron or neutron analysis). HREM is used most because it is easily accessible and provides direct atomic-resolution observation of twins. However, it is a postmortem technique, which makes the analysis of the twinning process non-trivial. In recent years, in situ HREM has been used to observe the twinning process, twin-dislocation interactions and other deformation mechanisms in nc materials [119,156,215,217,218]. Such experiments are still relatively difficult, and the quality of the atomic images is expected to improve in the near future. X-ray analysis has been used to analyze the twin boundary density in nc materials [51,149,153,219–222]. However, such analysis is usually qualitative and the absolute value of density of twin boundaries may depend on the method/model used in the analysis. Nevertheless, relative comparison of twin densities can be made if the X-ray diffraction data are taken and analyzed in a consistent manner.

The samples used for experimental studies have been prepared by mechanical attrition [65], physical vapor deposition [6], high-pressure torsion [8], surface mechanical attrition [223], electro-deposition [35,40,41,68], inert gas condensation [15], etc. Each of these methods may have its own intrinsic issue such as impurities, unclean grain boundaries, and non-equilibrium grain boundaries. One common feature of experimental samples is the relatively wide grain size distribution, especially in samples produced by deformation methods. In comparison, MD simulations often use relatively
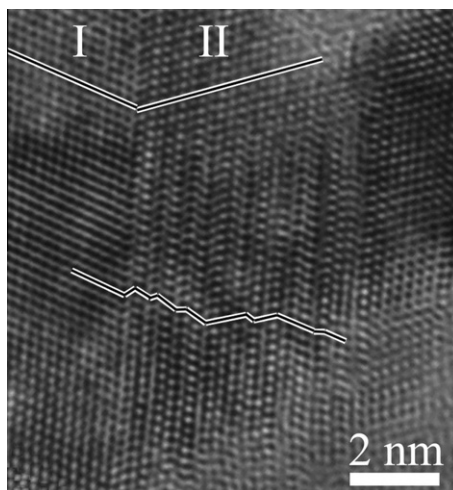

Fig. 12. An HREM image of nc Cu processed by high-pressure torsion (HPT), showing Shockley partial dislocations that were emitted from the lower grain boundary and stopped in the grain interior before reaching the upper grain boundary, leaving behind stacking faults [8].

uniform grain sizes. The wide grain size distribution may be an advantage in some cases. For example, the inverse grain size effect on deformation twinning was found by statistical HREM investigation of electro-deposited Ni with grain sizes ranging from 10 nm to 76 nm [171].

Experimental techniques available so far have much lower spatial and temporal resolutions than the MD simulations. It is also a challenge to observe the deformation process and defect evolutions in real time. Therefore, it would be desirable to combine experiments and MD simulations to probe the deformation process of nc materials.

5.3. Twinning mechanisms

In this section, we will describe the twinning mechanisms that are proposed basing on the experimental observations and MD simulation results.

5.3.1. Overlapping of stacking fault ribbons

The nucleation of deformation twins via overlapping of two stacking fault ribbons are first observed by MD simulations (see Fig. 11) [9]. Fig. 13 shows an HREM image of such a twin nucleus with a thickness of two atomic planes in the interior of a nc Al grain. It was formed by the dynamic overlapping of two extended partial dislocations with stacking faults on adjacent slip planes. As shown, the two stacking faults are only partially overlapped. The twin can grow thicker by adding more SFs on either side of the twin. However, no deformation twins of this type that are thicker than two layers have been reported. Therefore, this twinning mechanism does not play a significant role in the deformation of nc materials. This is because of the lacking of a continuous mechanism for it to grow. It depends on the incidental overlapping of other slipping dissociated dislocations with stacking fault ribbons to grow.

A variant of this twinning mechanism is the overlapping of a dissociated dislocation with a stacking fault connected with the grain boundary [187]. As shown in Fig. 14, close to the grain boundary, the two-layer twin nucleus turned into a stacking fault. This suggests that a stacking fault was first formed from the grain boundary and extended toward grain interior. A dissociated dislocation with a wide stacking fault slipped toward the grain boundary on an adjacent slip plane and then incidentally overlapped with the stacking fault, forming a two-layer twin nucleus. Such a twin nucleus was also predicted by MD simulation (see Fig. 11).

If the leading partial of the dissociated dislocation shown in Fig. 14 reaches the grain boundary, the twin nucleus will become identical to a normal twin nucleus formed by emission of two Shockley partials from the grain boundary. This twin nucleation mechanism could be significant in nc materials with non-equilibrium grain boundaries. High density of dissociated partials with one end pinned on the grain boundary has been observed in nc Ni with non-equilibrium grain boundaries (see Fig. 15) [187], which provides a high probability for such a mechanism to operate.

The two scenarios of twin nucleation via overlapping of stacking faults are schematically illustrated in Fig. 16, in which the thin hairlines across the grain represent the slip planes and the thick shorter lines represent the stacking faults. A twin is nucleated when two stacking faults on two adjacent slip
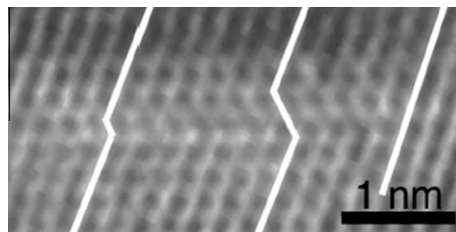
Fig. 13. A deformation twin formed by the overlapping of two extended dislocations on adjacent slip planes in the interior of a grain of nc Al deformed by ball-milling [23].
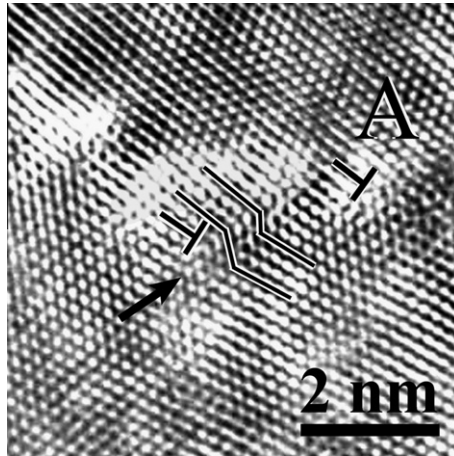
Fig. 14. A twin nucleus formed by overlapping of a dissociated dislocation with a stacking fault from grain boundary in nc Ni [187].
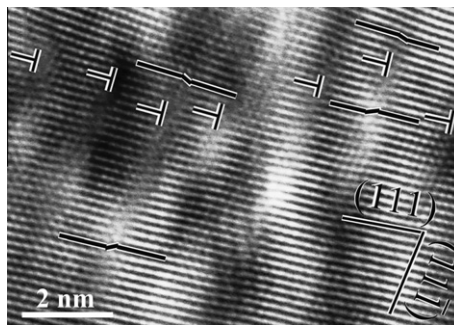
Fig. 15. HREM images showing 60° dislocations that are dissociated into Shockley partials bounding stacking faults.

planes overlap with each other. The twin nucleus marked as A corresponds to that in Fig. 13, while the twin nucleus marked as B corresponds to that in Fig. 14.

5.3.2. Partial emission from grain boundaries

Formation of deformation twins via emission of Shockley partials from grain boundaries was first predicted by MD simulations (see Fig. 11) [9]. Such deformation twins were later verified by HREM. For example, Fig. 17a shows a deformation twin, T_1, which has a curved twin boundary with the matrix, T_2, in nc Ni deformed by surface mechanical attrition treatment (SMAT) [56,224]. This twin was formed by successive emission of Shockley partials from the grain boundary on the left. However, the partials did not reach the other side of the grain, and the stopped front of these partials formed a curved twin boundary (see the broken white line). Another example is seen in Fig. 17b, which shows a single twin growing from a grain boundary but terminated inside a grain [214]. The twin was formed by plastically deforming an electrodeposited nc Ni. Such a twin can only be formed by the partial emissions from the grain boundary on the left.

To form the twins shown in Fig. 17, Shockley partials need to be emitted from the grain boundaries on successive slip planes. This type of twinning is the most commonly observed in nc fcc metals and alloys [6,8,9,23,37,66,157,187,203,214]. Therefore, it is scientifically important to understand how the partials are emitted from the grain boundary. It has been reported that partial dislocations can readily
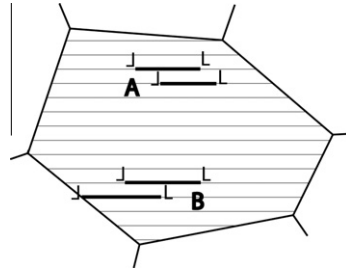
Fig. 16. Two scenarios of twin nucleation via overlapping of stacking faults. The thin hairlines across the grain represent the slip planes and the thick shorter lines represent the stacking faults. Each "L" at the end of a stacking fault indicates a partial dislocation. The twin nucleus marked as A corresponds to that in Fig. 13, while the twin nucleus marked as B corresponds to that in Fig. 14.
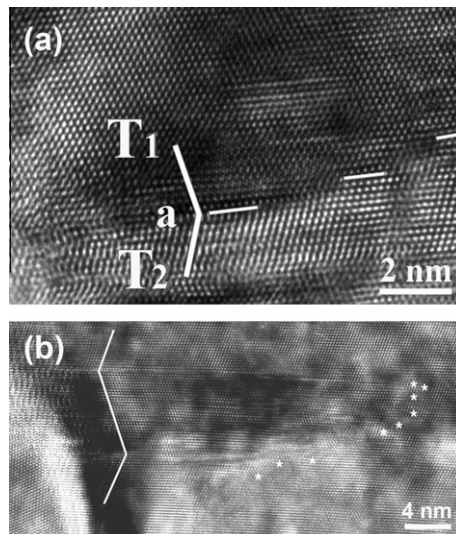
Fig. 17. (a) A deformation twin (T_1) formed by successive emission of partials on adjacent slip planes from the grain boundary on the left in nc Ni deformed by surface mechanical attrition treatment [56]. (b) An HREM image of a twin formed by plastically deforming electrodeposited nc Ni. The twin was formed by the emission of partials from the grain boundary on the left, and it ended in the grain interior as marked by the white asterisks [214].

emit from non-equilibrium grain boundary to nucleate a deformation twin [7,187,225]. However, it is statistically and practically impossible for a partial dislocation to exist on every slip plane to grow a single twin. Nucleation of a new partial on every slip plane is difficult because of the required high energy. Therefore, there must be a partial multiplication mechanism at the grain boundary that will supply a twinning partial on every successive slip plane for twin nucleation and growth. This has been proposed recently by Zhu et al. [214], and is delineated below.

Two dislocation reaction and cross-slip mechanisms have been proposed to supply twinning partials on successive slip planes from the grain boundary to grow a twin continuously. The first mechanism involves the emission of partials with the same Burgers vector, while the second mechanism involves the emission of partials with two different Burgers vectors, which produce a single twin with reduced shear strain. The details of these two mechanisms are described below.

For simplicity, a square grain is used in the description of the two mechanisms. As shown in Fig. 18, the line parallel to the left grain boundary represents a full dislocation with a Burgers vector of
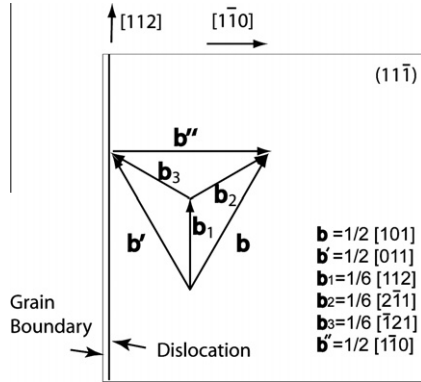
Fig. 18. Schematics of a square grain with a dislocation line parallel to the grain boundary [207]. The slip plane is $(1\,1\,\bar{1})$, which is parallel to the page. The dislocation line near at the left grain boundary has a Burgers vector of $\mathbf{b} = 1/2[1\,0\,1]$. Other Burgers vectors in the figure are $\mathbf{b}' = 1/2[0\,1\,1]$, $\mathbf{b}_1 = 1/6[1\,1\,2]$, $\mathbf{b}_2 = 1/6[2\,\bar{1}\,1]$, $\mathbf{b}_2 = 1/6[\bar{1}\,2\,1]$, $\mathbf{b}'' = 1/2[1\,\bar{1}\,0]$.

$\mathbf{b} = 1/2[1\,0\,1]$. The orientation of the dislocation line is $[1\,1\,2]$. The plane represented by the square is the $(1\,1\,\bar{1})$ close-packed slip plane. Below we will delineate the first mechanism for Shockley partial multiplication.

5.3.2.1. Mechanism A: multiplication of partials with the same Burgers vector. Let's start with Fig. 18, the perfect dislocation, $\mathbf{b}$, dissociates into two partials under an appropriate applied stress,

$$\mathbf{b} \rightarrow \mathbf{b}_1 + \mathbf{b}_2 \tag{1}$$

where $\mathbf{b}_1 = 1/6[1\,1\,2]$ is parallel to the dislocation line, while $\mathbf{b}_2 = 1/6[2\,\bar{1}\,1]$ has a 60° angle with the dislocation line. This dissociation is energetically favorable and therefore can proceed easily. Under an applied shear stress with appropriate orientation, the partial with the Burgers vector $\mathbf{b}_2$ glides on the $(1\,1\,\bar{1})$ slip plane across the grain to form a stacking fault. Partial $\mathbf{b}_1$ is a pure screw partial and cross-slips to the next $(1\,1\,\bar{1})$ plane, where it undergoes the following dislocation reaction

$$\mathbf{b} \rightarrow \mathbf{b} + (-\mathbf{b}_2) \tag{2}$$

where $-\mathbf{b}_2$ stays at the grain boundary and the perfect dislocation $\mathbf{b}$ is driven toward the grain interior by the applied stress. The reaction in Eq. (2) has a very high energy barrier and therefore needs a large applied stress to activate. The $\mathbf{b}$ can subsequently dissociate into $\mathbf{b}_1$ and $\mathbf{b}_2$ according to Eq. (1), forming a wide stacking fault ribbon [212]. $\mathbf{b}_2$ would be the leading partial because the applied stress favors its slip. The slip of $\mathbf{b}_2$ nucleates a single twin, and $\mathbf{b}_1$ returns to the grain boundary due to insufficient resolved shear stress to drive it across the grain. Note that in the above process $\mathbf{b}_1$ separates $-\mathbf{b}_2$ and $\mathbf{b}_2$ and keeps them at a large distance to reduce their mutual attraction so that $\mathbf{b}_2$ can easily glide away.

Repetition of the above dislocation reactions (Eqs. (1) and (2)) and cross-slip of $\mathbf{b}_1$ enables the single twin to grow continuously. Such a twin growth process leaves a partial $-\mathbf{b}_2$ on the left grain boundary and another partial $\mathbf{b}_2$ on the right grain boundary on every slip plane in the twin. This changes the grain shape from the original square to what is shown in Fig. 19, as viewed in the $\mathbf{b}' = [0\,1\,1]$ direction, which is perpendicular to $\mathbf{b}_2$.

In an HREM micrograph taken from any $\langle 1\,1\,0 \rangle$ direction that is on the twin boundary plane, the atomic-scale image has mirror symmetry across the coherent twin boundary. This is the way to identify a twin using HREM. As shown in Fig. 18, there are three orientations from which a twin with $(1\,1\,\bar{1})$ twinning plane can be viewed by HREM: $\mathbf{b} = 1/2[1\,0\,1]$, $\mathbf{b}' = 1/2[0\,1\,1]$, and also $\mathbf{b}'' = 1/2[1\,\bar{1}\,0]$. The view from $\mathbf{b}'$ is illustrated in Fig. 19, which shows a 141° grain boundary kink. However, if the twin is viewed from the $\mathbf{b}$ and $\mathbf{b}''$ direction, the projection of the twinning partial $\mathbf{b}_2$ on the direction perpendicular to the $\mathbf{b}$ and $\mathbf{b}''$ in the $(1\,1\,\bar{1})$ plane will be reduced by half because the $\mathbf{b}$ and $\mathbf{b}''$ has a 30°
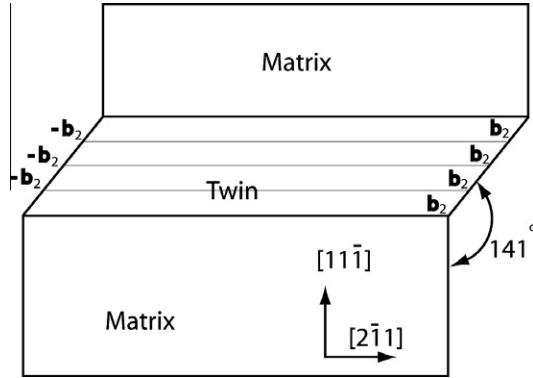
Fig. 19. The grain shape change caused by the first twinning mechanism in which all twinning partials have the same Burgers vector [207]. The 141° grain boundary kink can be seen from an orientation perpendicular to the Burgers vector of the twinning partial and parallel to the slip plane.

angle with the $\mathbf{b}_2$. In other words, the grain boundary kink angle will now be increased to 158°, as shown in Fig. 20. This makes twinning strain appear less than what is viewed from $\mathbf{b}'$ orientation (Fig. 19).

5.3.2.2. Mechanism B: multiplication of partials with the two different Burgers vectors. Next we will describe the second twinning mechanism, which involves the emission of partials with two different Burgers vectors, $\mathbf{b}_2$ and $\mathbf{b}_3$. It produces less macroscopic strain than the twinning mechanism A. One can see from Fig. 19 that, after cross-slip, the partial $\mathbf{b}_1$ under appropriate applied stress can have another dislocation reaction:

$$\mathbf{b}_1 \rightarrow \mathbf{b}' + (-\mathbf{b}_3) \tag{3}$$

where $\mathbf{b}_3 = 1/6[\bar{1}\,2\,1]$ and $\mathbf{b}' = 1/2[0\,1\,1]$. The partial $-\mathbf{b}_3$ stays at the grain boundary and the perfect dislocation $\mathbf{b}'$ dissociates into $\mathbf{b}_1$ and a new partial $\mathbf{b}_3$. The applied shear stress drives the new partial $\mathbf{b}_3$ away from the grain boundary to glide on the $(1\,1\,\bar{1})$ plane across the grain, which grows the twin.

If the dislocation reactions described in Eqs. (2) and (3) occur on alternative slip planes or occur for approximately the same number of times, the grain will change its shape along the $\mathbf{b}_1$ direction (see
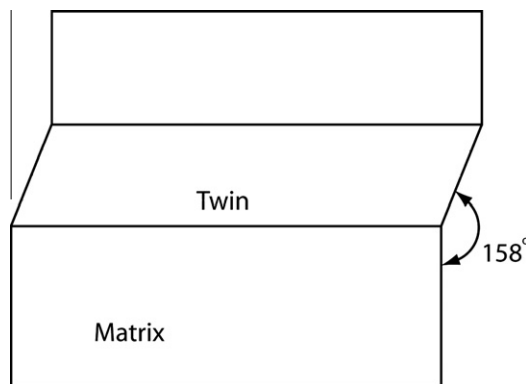
Fig. 20. The grain shape change caused by the first twinning mechanism in which all twinning partials have the same Burgers vector, but viewed from the orientation of $\mathbf{b}$ and $\mathbf{b}''$ [207]. The grain boundary kink is 158°. As will be described later, this can also be caused by the second twinning mechanism in which approximately equal numbers of $\mathbf{b}_2$ partials and $\mathbf{b}_3$ partials are involved. In the second twinning mechanism, the 158° grain boundary kink can be seen from an orientation perpendicular to $\mathbf{b}_1$.

Fig. 18), but the macroscopic strain will be only half of that shown in Fig. 19. This is because the slip of the partial $\mathbf{b}_2$ produces a strain of $a/\sqrt{6}$ along the $\mathbf{b}_2$ direction, while the slip of the partial $\mathbf{b}_3$ produces a strain of $a/\sqrt{6}$ along the $\mathbf{b}_3$ direction. From Fig. 18 we have the following relationship $\mathbf{b}_2 + \mathbf{b}_3 = \mathbf{b}_1$. Therefore, the total strain in every two slip planes is $a/\sqrt{6}$ along the $\mathbf{b}_1$ direction, producing a change in grain shape as shown in Fig. 20 when viewed from the $[1\bar{1}0]$ orientation (along $\mathbf{b}''$). However, if the twin is viewed from the $\mathbf{b}$ or $\mathbf{b}'$ orientation, the grain boundary kink angle will be ~169° (see Fig. 21). Note that it is also possible to form a twin by the mixture of the first and the second mechanisms. This could happen when the twined grain rotates during the twinning process, which changes the stress orientation.

As described in Figs. 19–21, three possible grain boundary kinks could be observed under HREM if a twin is formed by the mechanism A or B. If the HREM image shows a twinned grain with a 141° grain boundary kink as shown in Fig. 19, then the twin was formed by the mechanism A described by Eq. (2), in which only one type of twinning partial is involved to produce the twin. On the other hand, if the HREM image shows a twinned grain with a 158° grain-boundary kink as shown in Fig. 20, it is not possible to determine if the twin is produced by the first mechanism or the second mechanism. However, if the HREM image shows a twinned grain with a 169° grain-boundary kink as shown in Fig. 21, the twin is formed by the Mechanism B, in which about equal number of $\mathbf{b}_2$ partials and $\mathbf{b}_3$ partials are involved.

In practice, the grain boundary kink in an HREM micrograph is sharp enough for angle measurement only when the grain boundary is close to the edge-on orientation, which does not happen very often statistically. This makes the kink-angle measurement a tedious task. For example, the grain boundary kinks in Fig. 17 are not obvious because grain boundary is far from the edge-on condition.

In the above discussion, we specified the dislocation type and Burgers vector so that $\mathbf{b}_1$ is a pure screw partial dislocation, making it easy for $\mathbf{b}_1$ to cross-slip into the next $(1\,1\bar{1})$ plane. This is the easiest path for twin growth. However, we shall point out that even if $\mathbf{b}_1$ is a pure edge or a mixed type, it can still move to the next $(1\,1\bar{1})$ slip plane by climbing alone or by climbing plus cross-slip, although higher applied stress is needed for such a process. Note also that the dislocation climbing on the grain boundary should be much easier than in the grain interior because of higher diffusion rate at the grain boundary and the probability of higher local residual stress.

5.3.3. Twinning with low macroscopic strain

In the last section, we demonstrated that deformation twins in nc fcc metals may have a grain boundary kink of 141° if formed by partials with the same burger vector and viewed from an appropriate $\langle 1\,1\,0 \rangle$ orientation under HREM (see Fig. 22) [2]. This represents the highest macroscopic strain that can be formed by a deformation twin in fcc materials. It is also demonstrated that if the partials
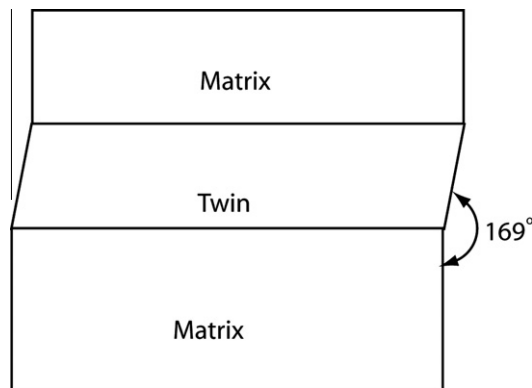

Fig. 21. The grain shape change caused by the second twinning mechanism (Mechanism B) in which approximately equal numbers of $\mathbf{b}_2$ partials and $\mathbf{b}_3$ partials are involved. The 158° grain boundary kink can be seen from the orientation of $\mathbf{b}''$.
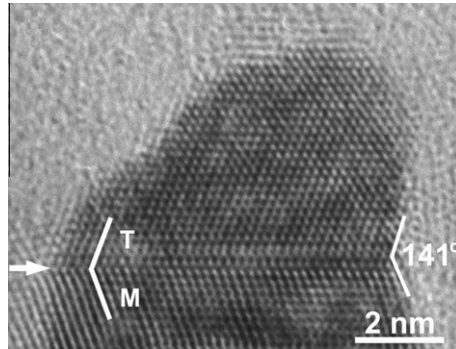
Fig. 22. HREM micrograph of a twin in nc Cu synthesized by high-pressure torsion. The arrow indicates the twin boundary. The grain boundary has a 141° kink at its intersection with the twin boundary. This twin was formed by partials with the same Burgers vector [2]. Note that this twin morphology is the same as that of a deformation twins in coarse-grained fcc metals.

have different Burgers vectors, the macroscopic strain will be lower. In this section, we further deliberate on the observation and mechanisms of deformation twins with low or even zero macroscopic strain.

Fig. 23 shows typical HREM images of deformation twins in nc Al, Ni and Cu that were produced by cryogenic milling, cryo-tension, and high-pressure torsion, respectively [2]. As shown, the grain boundary segments are smooth even at locations where they intersect the twin boundaries, suggesting that the deformation twins shown in Fig. 23 did not change the morphology of the grains.

It is proposed that the twins shown in Fig. 23 were formed via a twinning mechanism named *random activation of partials* (*RAP*) [2]. Fig. 2 illustrates a set of Shockley partials involved in the RAP process. As shown, on the (1 1 1) slip plane, there are three Shockley partials, $\mathbf{b}_1 = \mathbf{B\delta}$, $\mathbf{b}_2 = \mathbf{A\delta}$ and $\mathbf{b}_3 = \mathbf{C\delta}$. Note that $\mathbf{A\delta}$ means a Burgers vector that starts at $\mathbf{A}$ and ends at $\mathbf{\delta}$. It is obvious that

$$\mathbf{b}_1 + \mathbf{b}_2 + \mathbf{b}_3 = 0 \qquad (4)$$

As discussed in Section 2 and Fig. 3, a twin can be formed by the slip of identical partials or different partials, because the three partials, $\mathbf{b}_1$, $\mathbf{b}_2$, and $\mathbf{b}_3$, produce the same stacking sequence shifts despite of their orientation difference. Therefore, if all of the three partials propagate in equal number of times, one after another, there will be no net accumulation of macroscopic strain.

The RAP mechanism involves three Shockley partials with different Burgers vectors. Below we discuss how the emission of three Shockley partials can be realized in a nano grain with the help of

Fig. 23. HREM images of typical deformation twins in three nc fcc metals. (a) Al processed by cryo-milling, (b) electro-deposited Ni deformed by cryo-tension, and (c) Cu processed by high-pressure torsion. It is evident that the deformation twins did not change the shape of the grains. The arrows indicate the twin boundaries. The broken curves indicate grain boundaries. Twins and matrix are labeled T and M, respectively [2].

Fig. 24. Consider a Shockley partial dislocation loop on a (1 1 1) plane with the Burgers vector $\mathbf{b}_1$ = 1/6[2 $\bar{1}$ $\bar{1}$]. Fig. 24 illust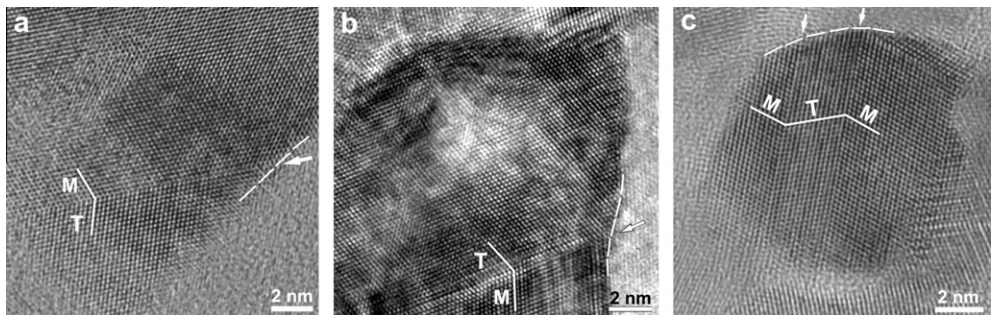rates such a dislocation loop emitted from a grain boundary triple junction and deposited on other segments of the grain boundary of a hexagonal grain. Part of the dislocation line segments parallel to grain edges AB and DE has pure screw character and can easily cross-slip in the GB to the next slip plane. On the next slip plane, $\mathbf{b}_1$ can slip by itself under appropriate stress or produce other dislocations via the following two reactions:

$$\frac{a}{6}[2\,\bar{1}\,\bar{1}] = \frac{a}{6}[\bar{1}\,2\,\bar{1}] + \frac{a}{2}[1\,\bar{1}\,0] \tag{5}$$

$$\frac{a}{6}[2\,\bar{1}\,\bar{1}] = \frac{a}{6}[\bar{1}\,\bar{1}\,2] + \frac{a}{2}[1\,0\,\bar{1}] \tag{6}$$

From Fig. 2a, we can also rewrite Eq. (5) as $\mathbf{b}_1$ = BA + $\mathbf{b}_2$, and Eq. (6) as $\mathbf{b}_1$ = BC + $\mathbf{b}_3$. Thus it is possible to randomly emit the three Shockley partials, $\mathbf{b}_1$, $\mathbf{b}_2$, and $\mathbf{b}_3$, on the next (1 1 1) slip plane.

A global shear stress cannot drive the three partials simultaneously. So what drives the $\mathbf{b}_1$, $\mathbf{b}_2$, and $\mathbf{b}_3$ partial slip? It is argued that it is possible for these partials to randomly nucleate and slip one at a time, driven by changing local shear stresses [2]. These stresses could significantly differ from the global shear stress. That such a scenario is possible is revealed by atomistic simulations of stress concentration of 3–3.5 GPa, which is many times higher than the applied shear stress, near the edge of a stacking fault [203]. Furthermore, grain boundary sliding and grain rotation, significant in nc materials [25,38,39,108], alter local stress state [80] and/or change the orientation of the twinning grain. These local stress variations can promote the random emission of partials. Other locations for high local stress concentration include triple junctions, and grain boundary steps. Also, once a twin is nucleated, it is relatively easy to grow the twin [57,59,226], thus explaining why the RAP twins could form instead of producing many stacking faults. It has been recently reported that the three partials $\mathbf{b}_1$, $\mathbf{b}_2$, and $\mathbf{b}_3$ can indeed move in the same direction by a stop-and-start mechanism. This mechanism has been predicted by MD simulation and verified by in situ TEM observation at the incoherent twin boundaries in Cu film produced by magnetron sputtering [227]. This mechanism can also produce deformation twins without macroscopic strain.

A global strain is necessary to relieve the global stress. Although the grains with RAP twins do not change their shape, they indeed contribute to the global strain by grain boundary sliding and grain rotation. Also, during the RAP twinning, the applied stress, and the attendant accumulated energy, is effectively dissipated locally by the random nucleation and slip of three Shockley partials from grain boundaries. However, their Burgers vectors add up to zero macroscopic strain, without violating laws of thermodynamics. It should be noted that although the RAP twins have negligible direct contribution to the macroscopic deformation at the grain level, they indirectly contribute to the bulk deformation by favorably reorienting the crystal lattice to change the applied resolved shear stresses on slip systems.
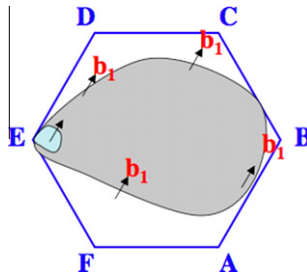

Fig. 24. A Shockley partial dislocation loop with Burgers vector $\mathbf{b}_1$ emitted from a grain boundary triple junction at E, grows, and deposits on other grain boundaries of a hexagonal grain [2]. Part of the dislocation line segments parallel to grain edges AB and DE has pure screw character and can move along the grain boundary to the next slip plane.

Note that the RAP twins form only if the numbers of $\mathbf{b}_1$, $\mathbf{b}_2$, and $\mathbf{b}_3$ partials are about the same. If this condition is not met, there will be macroscopic strain in the twinned grain. The magnitude of the strain is determined by the relative numbers of the three partials.

5.3.4. Grain boundary splitting and migration

This type of twins was first proposed by Ashby and Harper in 1967 [228]. The twinning mechanism was first verified by the MD simulation [157], and then experimentally observed recently [66]. This twinning mechanism was already shown in Fig. 11 and described in Section 5.1. Fig. 25 is an HREM image of a twin formed by grain boundary splitting and migration in nc Al processed by cryogenic ball milling. As shown, some segments of the boundary are straight, coherent $(1\bar{1}1)$ twin boundaries as indicated by white arrows. Mirror images typical of twins are shown on the two sides of these coherent twin boundaries. These segments, which are connected by non-crystallographic segments, form a zigzag boundary between the twinned area and the matrix. A twin lamella was formed via the migration of the new twin boundary. The boundaries of twin lamellae formed at different time frames joined together to form the zigzag boundary.

The non-crystallographic segments observed here were actually the new twin boundaries in this mechanism. As discussed earlier in Section 5.1, the non-crystallographic segments are formed by Shockley partial dislocations, which exist on every slip plane. It is likely that these partials are $\mathbf{b}_1$, $\mathbf{b}_2$, and $\mathbf{b}_3$ mixed in about the equal numbers, because if all partials have the same Burgers vector, there should be a large strain field in front of the non-crystallographic twin boundary. Such a strain field should be reflected by lattice distortion and/or high density of dislocations in the matrix in front of the non-crystallographic twin boundary, which is not observed in Fig. 25.

5.3.5. Sequential twinning mechanism

The mechanism of sequential twinning via emissions of Shockley partials from grain boundaries and twin boundaries was proposed based on the experimental observation of multifold twins, including fivefold twins (see Fig. 26) [70]. Fivefold twins were often observed to form by the nucleation and growth mechanism in nanosized particles, annealed nc fcc metals, or nano-wires [229–233]. However, these fivefold *growth* twins are very different from the fivefold *deformation* twins discussed here, which are formed by the partial-dislocation mediated sequential twinning mechanism. Fivefold deformation twins have been observed in an nc Al alloy [65], pure Cu [8,70,234], and an ulrafine-grained Cu alloy [235]. In this twinning mechanism, a regular twofold twin will be formed first, and then a three-fold twin is formed by the successive interaction of Shockley partials with the twin boundary. Repetition of this process leads to the formation of fourfold and fivefold twins. This twinning mechanism was later verified by MD simulation [216]. More details are described below.

The first step of this mechanism is the formation of a simple twin with domains I and II (Fig. 27a) via partial dislocation emissions from grain boundaries. Such a type of twins occur frequently in nc fcc metals [7,70,214], and can be formed via several twinning mechanisms [42,214]. The second step (Fig. 27b) starts with the emission of a 90° Shockley partial, $\mathbf{b}_1 = 1/6[\bar{1}\bar{1}\bar{2}]$, from the upper grain boundary in domain II. The partial glides on a $(1\,1\,\bar{1})$ slip plane toward the twin boundary TB1. A 90° Shockley partial has a Burgers vector perpendicular to the dislocation line.
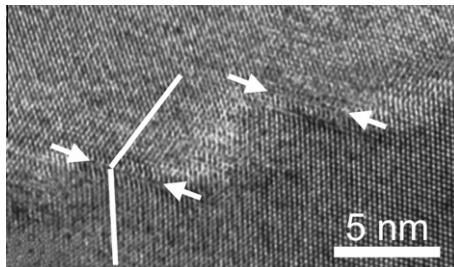
Fig. 25. A deformation twin formed by GB splitting and migration in nc Al deformed by ball milling [66].
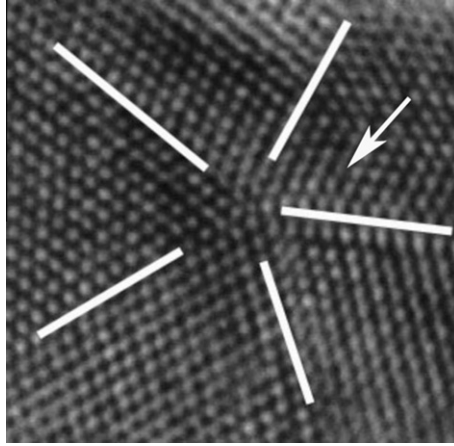
Fig. 26. A fivefold twin formed by the sequential twinning in nc Cu deformed by high-pressure torsion [70].
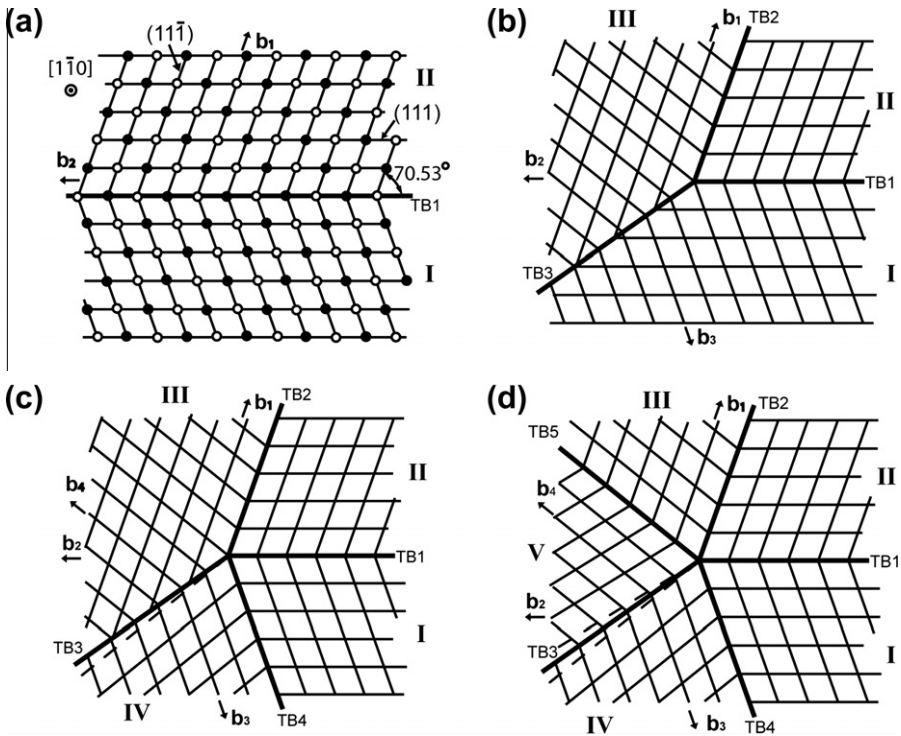
Fig. 27. (a) Illustration of a regular twin (step 1). (b) A threefold deformation twin (step 2) formed by the emission of a series of 90° partials, b_1. These partials form new 90° partials with a Burgers vector b_2 on the twin boundary TB1, which glides away from TB1, forming a new twin boundary TB3. (c) A fourfold deformation twin (step 3) formed from a threefold deformation twin by emitting a series of 90° partials, b_3. (d) A fivefold deformation twin (step 4) formed from a fourfold deformation twin by emitting a series of 90° partials, b_4. The dotted lines form an angle of 7.33°, which has to be accommodated by elastic strain [70].

A deformation twin can be defined by the twin plane K_1, shear direction $\boldsymbol{\eta}_1$, undistorted plane K_2, and direction $\boldsymbol{\eta}_2$. $\boldsymbol{\eta}_2$ lies on K_2 (see Fig. 28) [54]. Deformation twins in an fcc metal are of compound type, in which a twin formed by Shockley partials with the Burgers vector parallel to $\boldsymbol{\eta}_1$ gliding on K_1 is the same as a twin formed by partials with the Burgers vector parallel to $\boldsymbol{\eta}_2$ gliding on K_2. In Fig. 27a, we can regard K_1 and K_2 as $(1\,1\,\bar{1})$ and $(1\,1\,1)$ slip planes, respectively. $\boldsymbol{\eta}_1$ is parallel to $\mathbf{b}_1$, and $\boldsymbol{\eta}_2$ is parallel to another 90° Shockley partial $\mathbf{b}_2 = 1/6[1\,1\,\bar{2}]$. In other words, when a 90° Shockley partial $\mathbf{b}_1$ reaches the twin boundary TB1, it becomes equivalent to another 90° partial $\mathbf{b}_2$ on the $(1\,1\,1)$ plane. Under an appropriate external shear stress, the $\mathbf{b}_2$ partial could glide to the left, which consequently moves the twin boundary downward by one atomic plane. When a series of Shockley partials with a Burgers vector $\mathbf{b}_1$ emit from the grain boundary successively on adjacent $(1\,1\,\bar{1})$ planes, with each $\mathbf{b}_1$ partial converting to a $\mathbf{b}_2$ partial that glides to the left, a twin domain III will form, which effectively converts the regular twin in Fig. 27a into a threefold twin as shown in Fig. 27b. An incoherent twin boundary, TB3, is also formed.

A threefold deformation twin can be transformed into a fourfold deformation twin via the emissions of a series of 90° Shockley partials from a grain boundary in domain I or III (step 3). Assuming that a 90° Shockley partial $\mathbf{b}_3$ first emits from a point on a grain boundary in domain I (see Fig. 2) and moves toward the twin boundary TB3, a stacking fault will form, and a twin will nucleate and grow on both side of the stacking fault via the stress-controlled twin growth mechanism, resulting in a new twin domain IV (Fig. 27c). The fourfold deformation twin can be transformed into a fivefold deformation twin (step 4) by emitting another series of Shockley partials ($\mathbf{b}_4$) from grain boundaries in

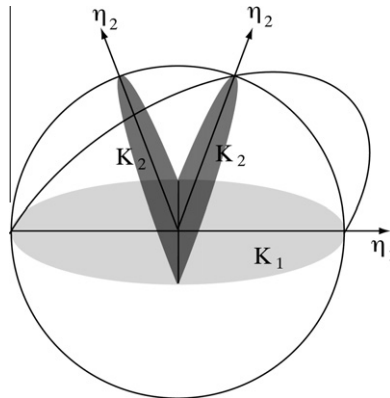Fig. 28. Illustration of twinning elements $\boldsymbol{\eta}_1$, $\boldsymbol{\eta}_2$, K_1 and K_2.
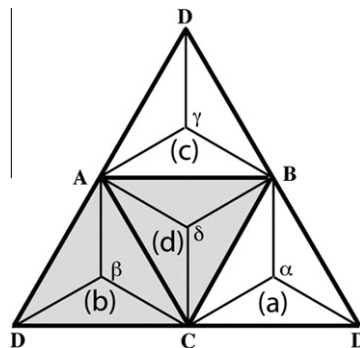

Fig. 29. The Thompson tetrahedron illustrating the possible slip systems and dislocations thereof in an fcc crystal.

twin domain III (Fig. 27c), following the same process as the formation of twin domain IV. When a Shockley partial with a Burgers vector $\mathbf{b}_4$ reaches the twin boundary TB3, it forms an edge dislocation in the displacement shift complete (DSC) lattice, with a Burgers vector opposite to the Burgers vector of the edge dislocation previously formed by a $\mathbf{b}_3$ partial in the DSC lattice. Therefore, these two types of edge dislocations will cancel each other, which converts TB3 into a coherent twin boundary. In addition, another coherent twin boundary, TB5, is also formed, which transforms the fourfold twin into a fivefold twin. It is also possible that the $\mathbf{b}_3$ and $\mathbf{b}_4$ partials are activated simultaneously, directly transforming a threefold deformation twin into a fivefold deformation twin.

Note that the above ideal twinning process would leave a 7.33° gap (see the angle between the two dashed lines in Fig. 27d). This is because the angle between two $\langle 1\,1\,1 \rangle$ planes in an fcc metal is ~70.53°, which is 1.47° smaller than the 72° that is required to cover 360° by five twins. This angle difference is accommodated by elastic strain [229,236]. The lattice distortion from elastic strain can be seen near twin boundaries of the fivefold twin in Fig. 26 (see the white arrow).

5.3.6. Partial multiplication at twin boundaries

One of the major issues in the formation of deformation twins in nc fcc metals is the source of partial dislocations that are needed on consecutive {1 1 1} slip planes. As discussed earlier, in coarse-grained fcc metals, several continuous partial-supply mechanisms have been proposed, including the pole mechanism [71], prismatic glide mechanism [72], faulted dipole mechanism [73], and others [1,74–76]. However, these mechanisms cannot operate in nc metals due to the lack of dislocation sources in the grain interior. The partial multiplication mechanisms discussed in Section 5.3.2 and the RAP mechanism discussed in Section 5.3.3 are two examples of partial dislocation self-generation mechanisms via dislocation reaction at grain boundaries. Below we will describe several mechanisms for partial multiplication at twin boundaries, which can form single and multiple twins in a self sustained way [42].

To assist with the description of the twinning mechanisms, we show the unfolded Thompson tetrahedron in Fig. 29. As shown, the four {1 1 1} slip planes (represented by four triangles) can be denoted as (a)–(d). The (b) and (d) planes are shaded here because they will be used to help describe the formation of deformation twins in the following sections. Note also that points α, β, γ and δ are at the center of the triangles BCD, ACD, ABD, and ABC, respectively. The lines that link the center of a triangle with its corners, e.g. $\mathbf{A\beta}$, and $\mathbf{\delta C}$, represent the Burgers vectors of partial dislocations on that slip plane. $\mathbf{A\beta}$ represents a Burgers vector from A to β. Other Burgers vectors herein are defined in the same way. A dislocation whose Burgers vector links the centers of two slip planes is defined here as a stair-rod dislocation (e.g. $\mathbf{\beta\delta}$), which follows the definition by Thompson [54,76].

5.3.6.1. Single twin via partial reactions at twin boundary.

As shown in Fig. 30a, a partial dislocation, $\mathbf{C\beta}$, glides on the (b) plane toward a stacking fault, SF, on the (d) plane, and is stopped on the slip plane next to the SF. Driven by applied stress, the partial $\mathbf{C\beta}$ dissociates into a partial dislocation $\mathbf{C\delta}$ on the (d) plane and a stair rod dislocation $\mathbf{\delta\beta}$ according to Fig. 29:

$$\mathbf{C\beta} \rightarrow \mathbf{C\delta} + \mathbf{\delta\beta} \qquad (7)$$

According to Fig. 30b, $\mathbf{C\delta}$ glides to the right to nucleate the twin, leaving behind the stair-rod dislocation $\mathbf{\delta\beta}$. The stair-rod dislocation $\mathbf{\delta\beta}$ can further dissociate into a partial $\mathbf{\delta C}$ on the (d) plane and a partial $\mathbf{C\beta}$ on the (b) plane according to Fig. 29:
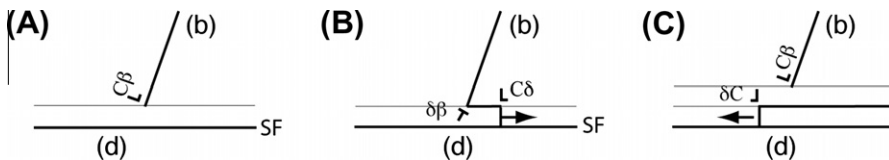

Fig. 30. Schematics of dislocation reactions between partial $\mathbf{C\beta}$ on the (b) plane and a stacking fault, SF, on the (d) plane to nucleate a single twin. Repetition of these reactions leads to the growth (thickening) of this twin [42].

$$\delta\beta \rightarrow \delta C + C\beta \qquad\qquad(8)$$

This reaction, and others to follow, needs applied stress to overcome the energy barrier. As shown in Fig. 30c, δC glides to the left to extend the twin nucleus and the partial $C\beta$ glides up by one atomic plane.

The above dislocation reactions at the stacking fault SF nucleate a two-layer twin, and leave behind the original partial dislocation $C\beta$ at the twin boundary. The partial $C\beta$ can continue the above dislocation reaction and slip with each reaction cycle growing the twin by one slip plane.

In this twinning mechanism, the self partial-multiplication mechanism involves a Shockley partial at the twin boundary (see Fig. 30c). This Shockley partial should be associated with, and located at the end of, a stacking fault. Therefore, we should see a twin in the (d) plane and a stacking fault in the (b) plane. Such a configuration is indeed observed in nc Cu processed by high-pressure torsion, as shown in Fig. 31.

5.3.6.2. V-shaped twin via dislocation reaction and cross-slip [42,67,69]. This mechanism is different from the cross-slip mechanism proposed by Fujita and Mori [237]. The latter does not provide for a mechanism for the twin to grow (thicken) by itself. To describe this mechanism, we start with the situation described in Fig. 30a, in which the partial $C\beta$ is stopped at the stacking fault SF. The partial $C\beta$ now dissociates into the following dislocations (see Fig. 29) under an applied stress with appropriate stress magnitude and orientation:

$$C\beta \rightarrow CA + A\delta + \delta\beta \qquad\qquad(9)$$

$A\delta$ glides to the right to nucleate a twin on the (d) plane, while CA cross-slips to the next intersection of the (d) and (b) planes (see Fig. 32a). The stair-rod dislocation $\delta\beta$ is sessile. CA now dissociates into two partials on the (b) plane:

$$CA \rightarrow C\beta + \beta A \qquad\qquad(10)$$

βA glides upward to nucleate a twin on the (b) plane, forming the nucleus of a V-shaped twofold twin (see Fig. 32b).

The partial $C\beta$ can repeat the above dislocation reactions and processes, causing growth (thickening) of the twofold twin, as illustrated in Fig. 32c. As shown, there is a stair-rod dislocation $\delta\beta$ at every intersection of the (d) and (b) planes. This results in a high stress at the ends of the stair-rod pileup at the intersecting boundary of the two twins. When the stress is very high, partial or perfect dislocations could be emitted or absorbed to relieve these stress concentrations.
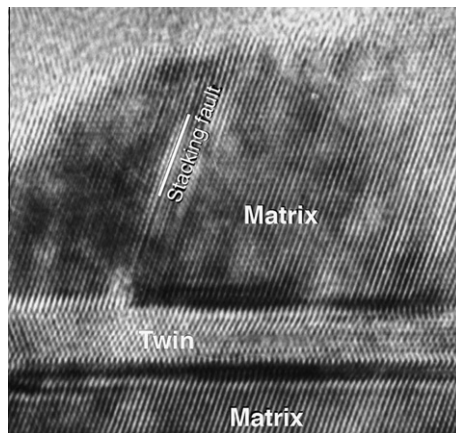
Fig. 31. A single twin that is consistent with the self-multiplication mechanism [42].

Such a V-shaped twin has been observed in electrodeposited nc Ni after cryo-rolling at liquid nitrogen temperature [69]. Shown in Fig. 33a is the HREM image of a nc Ni grain marked as A. The image inside the white frame is shown in Fig. 33b. As shown, two intersecting twins are visible, labeled as T_1 and T_2, respectively. The T_1 is observed to extend all the way from the grain boundary on the right side. One end of the T_2 intersects with T_1 in the area marked by *B*, while the other end terminates inside the grain (marked as *D*). This V-shaped twin was formed by the *dislocation reaction and cross-slip* mechanism illustrated in Fig. 32.

5.3.6.3. T-shaped twin via dislocation reaction and cross-slip. A T-shaped twin can be formed in a process similar to the V-shaped twin. Assuming that a V-shaped twin is already formed (see Fig. 34A). A partial dislocation **Cδ**, emitted from the grain boundary or another source, glides to the right on a (d) plane adjacent to the original stacking fault (see Fig. 34A). The partial **Cδ** is stopped by the twin boundary and dissociates into the following dislocations (see Fig. 29) under the applied stress:

$$\mathbf{C\delta \rightarrow CA + A\beta + \beta\delta} \tag{11}$$

Aβ glides upward to nucleate a twin on the (b) plane, while **CA** cross-slips to the intersection of the next (d) plane and (b) plane (similar to that shown in Fig. 32a). The stair-rod dislocation **βδ** is sessile and cannot move. **CA** now dissociates into two partials on the (d) plane:

$$\mathbf{CA \rightarrow C\delta + \delta A} \tag{12}$$

δA lides to the left to grow the twin on the (d) plane (see Fig. 34B). The partial **Cδ** can repeat the above dislocation reactions and processes, causing growth (thickening) of the T-shaped twin, as illustrated in Fig. 34c.
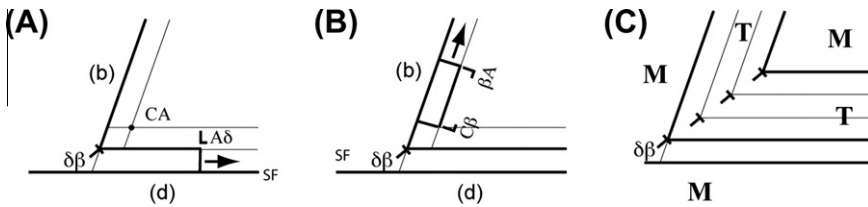
Fig. 32. Schematics of the nucleation and growth of a V-shaped twofold deformation twin by dislocation reaction and cross-slip at the twin boundary. (A) Nucleation of a twin on the (D) plane. (B) Nucleation of the second twin on the (B) plane. (C). A V-shaped twofold twin after some growth. A stair-rod dislocation **δβ** is at every intersection of the (D) and (B) planes [42].
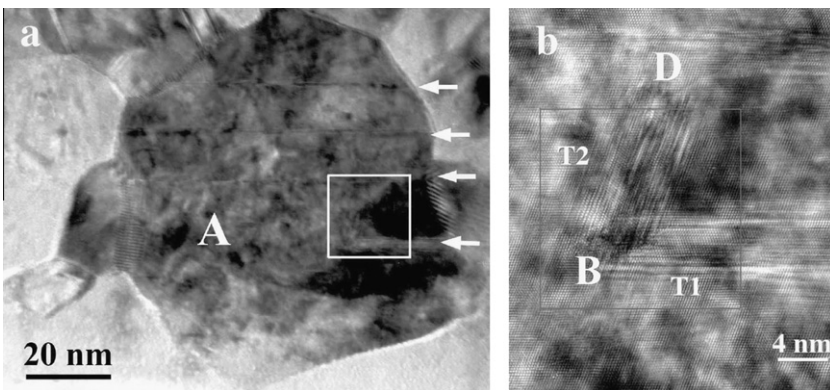
Fig. 33. HREM images showing (a) a grain that contains a cross-slip twin in the white frame and (b) an enlarged image of the area in the white frame in (a) [66].
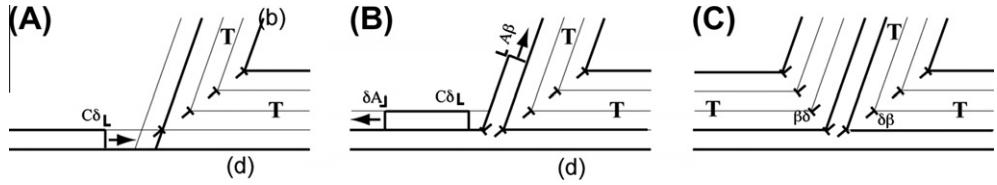
Fig. 34. Formation of a T-shaped twin. (A) A partial, **Cδ**, slip toward the twin boundary. (B) After the dislocation reactions (Eqs. (5) and (6)), a T-shaped twin is nucleated, leaving behind the partial **Cδ** to repeat another dislocation reaction cycle. (C) The final T-shaped twin with two arrays of stair-rod dislocations [42].

As shown in Fig. 34C, the above process produces a stair-rod dislocation **βδ** at every intersection of (d) and (b) planes, which is of the opposite sign to the **δβ** stair-rod dislocations formed earlier in the twofold twin. The arrays of **βδ** and **δβ** stair-rod dislocations partially cancel each other's long-range stress fields [238]. However, the pileup tips would still have local stress concentration. Note that following the processes similar to what are described in the Figs. 32 and 34, an X-shaped twin can also form [42].

5.3.7. Dislocation rebound mechanism

The single and multiple twins could also be formed by the dislocation rebound mechanism [239]. The elastic field of a partial dislocation is reflected (or partially reflected) at grain boundaries or twin boundaries (analogous to shock wave reflection) [239]. The reverse shear field can aid in nucleation of an opposite-sign dislocation where the first one impinged, especially if the velocity of the dislocation approaches the Rayleigh velocity (sound velocity) [42,48,239]. This dislocation rebound mechanism can produce the single twin, V-shaped twin, T-shaped twin, and X-shaped twins described above [42]. The rebound mechanism is deliberated in the following sections.

As shown in Fig. 35a, a partial, **Cδ** nucleates from the grain boundary on the left, glides to the right to form a stacking fault. Such events have been observed both in MD simulations [9,10] and by HREM [8]. The elastic field of the partial dislocation is reflected by the grain boundary on the right, which helps with the nucleation of a partial dislocation with an opposite sign, **δC** on the next slip plane. This partial glides to the left, nucleating a single twin, as shown in Fig. 35b. Note that the nucleation and glide of **δC** leaves behind a partial of opposite sign, **Cδ**, on the right grain boundary (see Fig. 35b).

5.4. Grain size effect

Grain size is an essential factor that affects the formation of deformation twins in metals and alloys. It has been extensively reported in the literature that larger grain sizes are more favorable to twin nucleation for conventional coarse-grained (CG) materials [11,240]. This is rationalized as follows. Both the critical stresses σ for dislocation slip and twinning follow a Hall–Petch type (H–P) behavior, $\sigma = \sigma_0 + kd^{-\alpha}$, where d is grain size, σ_0 and k are constants and α is an exponent typically equal to 0.5. For many CG metals and alloys, the H–P slope for deformation-twinning-mediated plasticity (k_{DT}) is
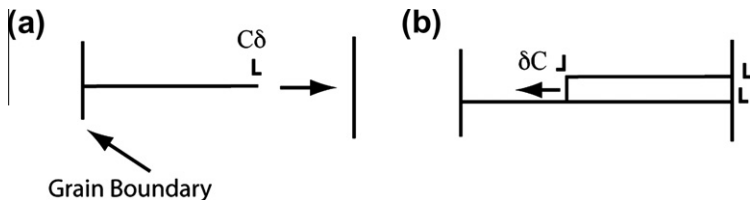
Fig. 35. The formation of a single twin by the rebound mechanism. (a) A partial **Cδ** glides to the right to form a stacking fault. (b) **Cδ** rebounds as **δC** from a grain boundary or twin boundary to nucleate a single twin. Two partials **Cδ** are left superposed on the grain boundary at the right [40].

much larger (up to 10 times) than that for dislocation slip (k_{DS}) [11,81]. Therefore, for coarse-grained metals and alloys, decreasing grain size favors dislocation slip and makes twinning more difficult. The physical reason for such a grain size effect in coarse-grained metals is not understood. Yu et al. [241] recently attempted to explain such a phenomenon by a "stimulated slip" mechanism. More studies are needed to probe its fundamental physics.

However, when the grain size is further refined down to nanometer regions (below 100 nm), deformation twinning has been frequently observed even in materials with medium to high stacking fault energies such as copper and nickel. Therefore, twinning was considered as one of the major plastic deformation mechanisms of nanostrutured materials [8,24–30]. The grain size effect on deformation twinning in the nc fcc Ni was systematically investigated in a recent study [171]. An electrodeposited nc-Ni foil with grains in the range of 10–75 nm and an average grain size of ~25 nm were deformed at liquid nitrogen temperature at a strain rate of $3 \times 10^{-3} \, s^{-1}$ to a strain of 5.5% and at a flow stress of 1.5 GPa. About 130 grains were examined under HREM to check if they contain deformation twins and stacking faults. Fig. 36 shows the histograms of (a) grain size distribution, (b) the number of grains containing stacking faults and twins, and (c) fractions of grains containing stacking faults and twins in samples deformed under tension. Fig. 36b shows that with decreasing grain size the number of grains containing twins (hereafter referred to as twinned grains) first increases and then decreases, while the number of grains containing stacking faults increases monotonically. The fraction of twinned grains is a good statistical indicator of twinning propensity. Therefore, Fig. 36 indicates that the twinning
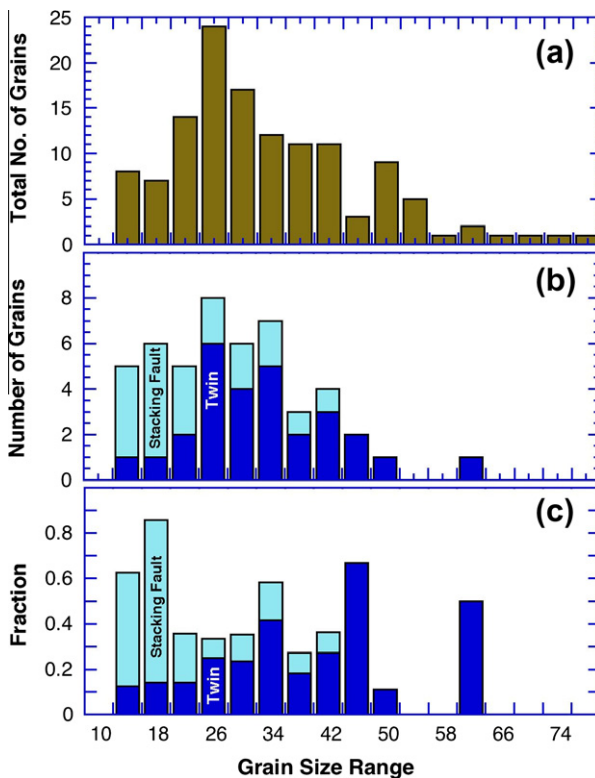
Fig. 36. Statistical grain size effect on the formations of stacking faults and deformation twins in nc Ni deformed under tension at liquid nitrogen temperature. The twin is defined as consisting of two or more layers of stacking faults on consecutive slip planes. (a) The size distribution of all grains examined under TEM. (b) The number distributions of grains containing stacking faults and twins. (c) The *fraction* distribution of grains containing stacking faults and twins. Each fraction was calculated as the ratio of the number of grains containing stacking faults and twins to the total number of grains in the corresponding size range [164].

propensity first increases and then drops with decreasing grain size. The decrease of twinning propensity with decreasing grain size is called the *inverse grain-size effect* [171]. This inverse grain size effect was also verified by synchrotron and neutron diffraction [242], and later observed in nc Cu [243], which has a lower stacking fault energy and very different general planar fault energies from the Ni. This suggests that it is a common phenomenon in nc fcc metals.

The experimental observation of grain size effect shown in Fig. 36 is consistent with what is predicted by an analytical model of Zhu et al. [57,59]. Fig. 36 shows an optimum grain size at which the twinning is easiest, which is also predicted by the model. The details of this model will be discussed later in Section 5.8.3.

One of the salient features of the data in Fig. 36 is that no inverse grain-size effect exists for stacking faults. This is due to the effect of generalized planar fault energies on the nucleation of twins, which make it more difficult to activate twinning partial than to activate the first partial to form stacking fault. In other words, the grain size effect on the deformation twins and stacking faults can be explained by the combined effect of grain size effect described in Section 5.8.3 and the general planar fault energy effect described in Section 5.5 [171]. A recently proposed "stimulated slip" model [241] was also used to explain the inverse-grain size effect on twinning [243], which is not appropriate because the deformation physics assumed in the model is consistent with coarse-grained metals, but not with nanocrystalline metals. In addition, the "stimulated slip" model cannot explain the grain size effect on the formation of stacking faults.

5.5. General planar fault energy effect

Traditionally, stacking fault energy is considered as the primary intrinsic material property that affects the twinning propensity [54]. It is well known that lower stacking fault energy promotes deformation twinning in coarse-grained fcc metals and alloys. The same trend has also been observed in nc fcc metals and alloy. For example, higher density of deformation twins was observed with decreasing stacking fault energy in nanostructured Cu–Al alloys subjected to dynamic plastic deformation [244], and in the Cu–Zn alloy system subjected to HPT processing [51,101,219,221,222,245].

Recent molecular dynamics (MD) simulations, phase field simulation, analytical modeling and experimental observations reveal that the stacking fault energy alone is not sufficient to explain the observed twinning behavior, and the generalized planar fault energies (GPFEs) also significantly affect the partial-dislocation-mediated deformation processes in nc materials [10,29,188,246]. In fcc metals, the GPFE curves describe the energy change caused by rigidly shifting two semi-infinite crystals on a {1 1 1} plane along a ⟨1 1 2⟩ direction [10]. The GPFE curves can be most accurately calculated using the *ab initio* approach [201], although some errors and variation could result from boundary conditions and simulation code.

The three most important energies on the GPFE curves are the stacking fault energy (γ_{sf}), unstable stacking fault energy (γ_{usf}), and unstable twin fault energy (γ_{utf}). As shown in Fig. 37, Ni has very high stacking fault energy, and therefore, by conventional wisdom, should not deform by the slip of partial dislocations, which generate stacking faults. However, MD simulations revealed stacking faults, and experiments revealed both stacking faults and deformation twins in nc Ni. These results were explained by the GPFEs [10] and other factors [188,247]. Specifically, after a leading partial generates a stacking fault, the nucleation and gliding barrier for the trailing partial is a function of $\gamma_{usf}-\gamma_{sf}$, which is large for Ni and Cu, as compared to Al. This makes it possible for some first partials to slip without trailing partial following them, creating stacking faults. Also, since the unstable twin fault energy is not much higher than the unstable stacking fault energy, twins should be possible once a leading partial is emitted, thus making it possible to produce twins in nc Ni despite its high stacking fault energy. The GPFEs have been used to explain the differences in deformation mechanisms of nc Al, Ni and Cu with a small grain size of 12 nm, which were investigated by MD simulations [10].

The GPFE curves can also help explain the grain size effect on twinning and stacking fault shown Fig. 36. The precondition for the nucleation of a deformation twin is to first form a stacking fault. In other words, a stacking fault was first formed by a leading partial, and then a twinning partial converted the stacking fault to a twin nucleus. This suggests that leading partials were first activated in grains with a wide range of grain sizes to create stacking faults, but twinning partials become more
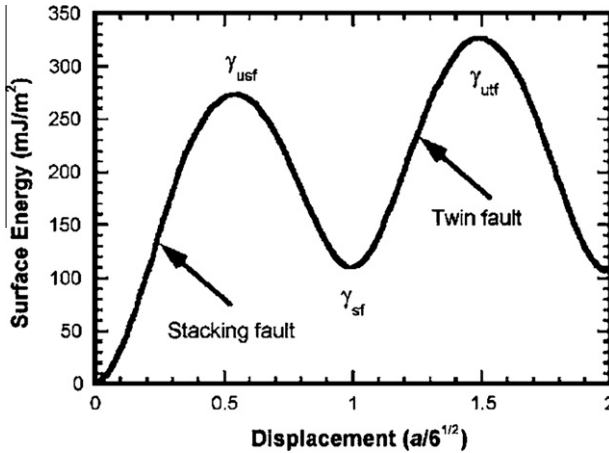
Fig. 37. Schematic of the generalized planar fault energy curves for Ni [201]. γ_{sf} is the stable stacking fault energy; γ_{usf} is the unstable stacking fault energy; γ_{utf} is the unstable twin fault energy; a is the lattice constant.

difficult to nucleate and slip with decreasing grain size if the inverse grain-size effect is operating. Therefore, it takes higher applied stress to emit a twinning partial than a leading partial that creates a stacking fault. This is consistent with the effect of GPFE energies on partial slip. As shown in Fig. 37, the unstable twin fault energy is higher than unstable stacking fault energy, which makes it more difficult to emit twinning partials. It has also been reported that higher stresses are required to emit partials in smaller grains [23,27]. One can envision that below a certain critical grain size the stress required to emit a twinning partial becomes higher than the applied stress, which stops twinning but still allows the emission of the leading partials to create extended stacking faults. Due to the variation in grain orientations and local stress states, this leads to a statistical decrease in twin density with decreasing grain size, i.e. the inverse grain-size effect on twinning. Since the stress is still high enough to emit leading partials, there is no inverse grain size effect on stacking fault.

Recently, an analytical model was proposed to quantitatively describe the twinning tendency of fcc metals basing on the GPFE curves [188]. It should be noted that the GPFE effect alone cannot explain the observed grain size effect on deformation twinning. Specifically, the grain size effect was not addressed in the reported GPFE models [10,188]. Also note that GPFE curves should be calculated using the *ab initio* method, which is much more accurate than the MD simulations in this case. The latter could lead to significantly different GPFE curves depending on the atom potentials used in the simulation [10,248]. It should be also noted that GPFE curves are not affected by grain size. MD simulations using a specific grain size can only represent that particular grain size and cannot be extrapolated to other grain sizes [171]. More discussions on the GPFE energy based models will be presented later in Section 5.8.4.

5.6. Non-equilibrium grain boundary

Nanocrystalline materials often have non-equilibrium grain boundaries with high densities of extrinsic (extra) dislocations [35,65,225,234,249,250]. This is especially true for those nc metals and alloys produced by severe plastic deformation [65]. A typical non-equilibrium grain boundary is shown in Fig. 38a, which is an HREM image of a low-angle grain boundary in a nc Cu [225]. The two grains are misoriented for about 9°. Fig. 38b is a structural model corresponding to the low-angle grain boundary. From this model, it is seen that two types of dislocations with Burgers vectors $\mathbf{b}_1$ and $\mathbf{b}_2$ are needed to accommodate the geometrical misorientation. In other words, these dislocations are geometrically necessary. Valiev et al. referred to these geometrically-necessary dislocations as intrinsic dislocations [251]. According to Fig. 38b, the spacing of type 1 dislocations is about 18 Å, which is
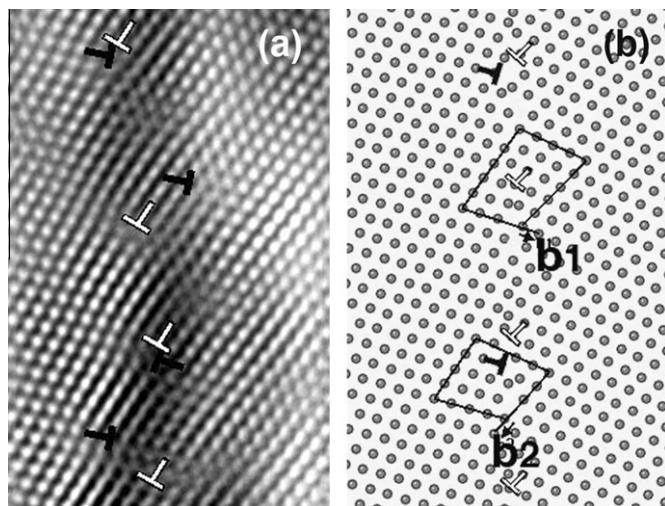
Fig. 38. (a) An HREM image of a non-equilibrium low-angle grain boundary and (b) its equilibrium structural model. Burgers vectors are **b**$_1$ and **b**$_2$ [225].

consistent with that measured from Fig. 38a. However, there are three more type 2 dislocations in Fig. 38a than in Fig. 38b, which indicates that three extrinsic (or non-geometrically-necessary) dislocations exist at the grain boundary shown in Fig. 38a. Therefore, this segment of low-angle grain boundary is in a high-energy configuration and should be called non-equilibrium grain boundary.

Dislocations on non-equilibrium grain boundaries may have unique structures. Fig. 15 shows an HREM image of a non-equilibrium low angle (∼3°) grain boundary in nanocrystalline Ni formed by surface mechanical attrition treatment [187]. 60° dislocations with (1 1 1) half planes are marked on the grain boundary. Importantly, Fig. 15 shows dissociated 60° dislocations with wide stacking faults. The boundaries of two such wide stacking faults are marked by two pair of lines, respectively. The stacking fault widths are in the range of 1.22–3.66 nm.

The existence of dissociated dislocations on non-equilibrium grain boundaries has important consequences on the deformation twinning in nc Ni. First, the leading partial can simply slip into the grain interior under an external stress, becoming an extended partial and creating a stacking fault. In other words, the emission of the leading partial is affected by the stable stacking fault energy, but not by the much higher unstable stacking fault energy. Second, since the trailing partials already exist on the grain boundary, it could also slip into the grain interior, a process that does not have to overcome the high unstable SFE predicted by the GPFE curve. The easy emissions of the trailing partials effectively erase the stacking faults created by the leading partial, which lowers the density of stacking faults. In addition, if two dissociated dislocations on a grain boundary happen to be on adjacent planes, a twin nucleus forms. Such a twin nucleation process will not need to overcome the high unstable twin fault energy on the GPFE curves. Therefore, the non-equilibrium grain boundaries would make twinning easier.

5.7. Strain rate and temperature effect

The strain rate and temperature effect on deformation twinning in nc fcc metals and alloys is similar to their effect on coarse-grained fcc metals and alloys. Specifically, lower temperature and higher strain rate usually promote deformation twinning in nc fcc metals and alloys [103,104,252]. Zhao et al. [153] reported that nanostructured Cu did not deform by twinning at room temperature but produced large quantity of deformation twins at liquid nitrogen temperature, verifying that the low temperature indeed promote deformation twinning in nanostructured materials.

Wu and Zhu [171] statistically studied the strain rate and strain effect on deformation twinning in nc Ni. An electrodeposited nc-Ni foil with grains in the range of 10–75 nm and an average grain size of ~25 nm were deformed at liquid nitrogen temperature under three deformation modes with increasing strain rate and strain: (1) quasi-static tension at a strain rate of 3×10^{-3} s^{-1} to a strain of 5.5% and at a flow stress of 1.5 GPa, (2) rolling at a strain rate of 2×10^{-2} s^{-1} to a strain of 9.8%, and (3) split Hopkinson pressure bar (SHPB) test at a strain rate of ~2.6×10^3 s^{-1} to a strain of 13.5% and a flow stress of ~2 GPa. About 130 grains for each sample were examined using HREM to obtain good statistics. Shown in Fig. 39 is the fractions of grains that contain at least one twin. The fraction of twinned grains increased from 28% under tension to 38% under rolling to 44% under SHPB. The strain rate effect is believed caused by the higher flow stress with higher strain rate [171]. The flow stress under tension was 1.5 GPa and this was increased to 2.0 GPa under SHPB [188,193]. Although the flow stress under rolling could not be measured, it should be between 1.5 GPa and 2.0 GPa, because higher stain rate usually leads to higher flow stress. This observation is somewhat different from that in a recent study using laser driven compression at an extremely high strain rate of >10^7 s^{-1} [189], but consistent with a recent MD simulation on strain rate effect [193,194].

5.8. Twin nucleation and growth models

Several models based on various assumptions have been proposed to describe the formation of deformation twins in nc fcc metals. The validity of a model is determined by how much deformation physics it is based on and it predicts. A model that is not based on the deformation physics observed by experiments or MD simulations is of little scientific value, although it sometimes can be used to fit the observed experimental data by adjusting the fitting parameters. Such a model can often mislead the scientific community. Below we discuss a few well-known models and their limitations.

5.8.1. Conventional dislocation model

Two similar models were proposed to explain the formation of deformation twins in nc metals [6,65]. In the model by Chen et al. [6], the stress needed to activate a lattice dislocation is described as

$$\tau_L = \frac{2\eta Gb}{d} \tag{13}$$

where η is a parameter that reflects the characteristics of the dislocation ($\eta = 0.5$ for an edge dislocation and $\eta = 1.5$ for a screw dislocation), G is the shear modulus, b is the magnitude of the Burgers vector of the lattice dislocation, d is the grain size. The stress to activate a partial dislocation is described as
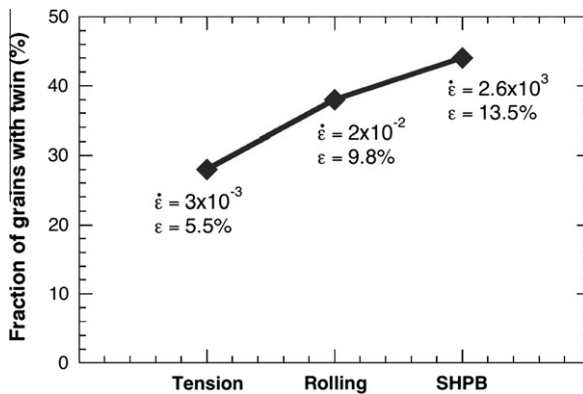

Fig. 39. The fraction of twinned grains in nc Ni deformed at liquid nitrogen temperature under tension, rolling and SHPB. Tension: strain rate = 3×10^{-3} s^{-1}, strain = 5.5%, flow stress = 1.5 GPa; rolling: strain rate = 2×10^{-2} s^{-1}, strain = 9.8%; SHPB: strain rate = ~2.6×10^3 s^{-1}, strain = 13.5%, flow stress = ~2 GPa [171].

$$\tau_P = \frac{2\eta G b_1}{d} + \frac{\gamma}{b_1} \tag{14}$$

where b_1 is the magnitude of the Burgers vector of the partial dislocation, and γ is the stacking fault energy. When $\eta = 0.5$, these two equations become identical to those in the work by Liao et al. [65].

Because $b > b_1$, τ_P will increase at a slower rate than τ_L, which means that it will be easier to activate a partial dislocation than a perfect dislocation when the grain is below a critical size. These two models seem very straightforward in explaining the activation of partial dislocations, which is a prerequisite of deformation twinning.

Unfortunately, experimental data show that smaller grain size hinders, not promotes, deformation twinning [11,81], which directly contradicts these two models [6,65]. It has been found that the critical stress for twinning follows a Hall–Petch relationship [11],

$$\sigma_t = \sigma_{t0} + \kappa_t d^{-1/2} \tag{15}$$

where σ_{t0} is a constant and κ_t is the Hall–Petch slope for twinning. Eq. (15) is similar to the well-known Hall–Petch relationship for the slip of a perfect dislocation:

$$\sigma_s = \sigma_{s0} + \kappa_s d^{-1/2} \tag{16}$$

where σ_{s0} is a constant and κ_s is the Hall–Petch slope for the slip of a perfect dislocation.

Table 1 lists the Hall–Petch slope for both twinning and for slip of lattice dislocations [11]. As shown, the Hall–Petch slope for twinning is higher than that for the slip of lattice dislocation for bcc, fcc, and hcp metals and alloys. Therefore, the models are not supported by experimental data. Moreover, these two models predict an unrealistically high critical stress for twinning [6], which reflects their problem. The models also made an inexplicit assumption that activation of partial dislocation equals formation of twinning, which, as shown later, is not correct. Another obvious evidence that this model cannot account for the deformation physics is that it cannot explain the experimentally observed inverse-grain size effect shown in Fig. 36.

The reason for the failure of this model is that Eqs. (13) and (14) are based on an early (1961) work by Venables [72], which did not account for the recently observed deformation physics of nc materials, i.e. the dislocation emission from grain boundaries, as discussed in Section 5.3.2. In other words, this model is not based on physics that prevails in nc materials, and therefore is not correct. However, unfortunately, due to its simplicity, this model has been used by many research groups to explain why deformation twinning occurs in nc materials [6,65,80].

Table 1
The Hall–Petch slopes for bcc, fcc and hcp metals and alloys [11].

Material	H–P slope for slip, κ_s (MPa mm$^{1/2}$)	H–P slope for twinning, κ_t (MPa mm$^{1/2}$)
bcc		
Fe–3 wt.% Si	12	100
Armco Fe	20	124
Fe–25 at.% Ni	33	100
Cr	10.08	67.75
Va	3.46 (20 K)	22.37
fcc		
Cu	5.4 (RT)	21.66 (77 K)
Cu–6 wt.% Sn	7.1	11.8 (77 K), 7.9 (RT)
Cu–9 wt.% Sn	8.2	15.77 (77 K)
Cu–10 wt.% Zn	7.1	11.8 (77 K)
Cu–15 wt.% Zn	8.4	16.7 (295 K)
hcp		
Zr	8.26	79.2
Ti	6 (78 K)	18 (4 K)

5.8.2. Partial emission from grain boundaries

A recent analytical dislocation model by Asaro et al. [253] considered the MD simulation and experimental results, which indicate partial dislocations emissions from boundaries of nanosized grains. The critical stress needed to move a lattice dislocation is described as

$$\tau_L = \frac{Gb}{d} \tag{17}$$

and the critical stress needed to move a partial dislocation is described as

$$\tau_P = \frac{Gb}{3d} + (1 - \delta)\frac{\gamma}{Gb} \tag{18}$$

where δ is the ratio of equilibrium stacking fault width to grain size.

This model predicts that below a certain critical grain size partial dislocations from GBs need a lower stress to move than lattice dislocations in nc metals. Most importantly, it predicts a realistic, low twinning stress that is obtainable under experimental conditions such as ball-milling. However, the model does not address one critical issue: as shown in Fig. 36, the emission of a partial dislocation does not guarantee the nucleation of a deformation twin because the trailing partial could easily follow to erase the stacking fault formed by the first partial.

5.8.3. Twinning partial from grain boundaries

To address the above issue in the above model, Zhu et al. recently developed an analytical model to describe the nucleation and growth of deformation twins in nc fcc metals [57,59]. This model is described below.

The model assumes a grain with a square (1 1 1) slip plane, as shown in Fig. 40, similar to that used in a previous study [253]. Under an external shear stress, τ, a 30° leading Shockley partial, $\mathbf{b}_1$, is emitted from grain boundary AB, depositing two segments of partial dislocation lines (Aa and Bb) on the grain boundaries. τ is oriented at an angle α with line ab. A trailing 30° partial, $\mathbf{b}_2$, is also emitted (line Aa'b'B). The two partials ab and a'b' are separated by a stacking fault (Fig. 40a). The two partials react to form two perfect dislocation segments, Aa' and Bb' at the GBs. This dislocation system is called a *Screw system* hereafter, because the two partials can form a perfect screw dislocation along the grain boundary AB.

To nucleate a deformation twin, a stacking fault needs to be first created. This can occur via: (1) emission of a 30° partial, $\mathbf{b}_1$, from grain boundary, (2) extending the stacking fault ribbon in Fig. 40a across the grain. Both scenarios may occur depending on the orientation of τ. In Fig. 40a, for the partial $\mathbf{b}_1$ to move, τ has to perform a work to overcome increases in both the stacking fault energy and dislocation energy from lengthening segments Aa and Bb [54]. The critical stress for moving partial $\mathbf{b}_1$ can be derived as [57]:

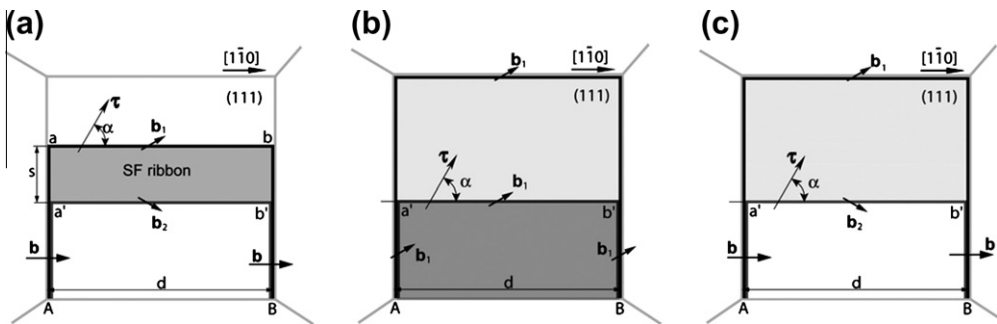**Fig. 40.** A schematic illustration of the dislocation model for the nucleation of deformation twins. (a) a perfect screw dislocation dissociated into two partials $\mathbf{b}_1$ and $\mathbf{b}_2$; (b) the nucleation of a deformation twin via the emission of a twinning partial on a (1 1 1) plane adjacent to the stacking fault plane; (c) the emission of a trailing partial that removes the stacking fault [57,59].

$$\tau_P = \frac{1}{\cos(\alpha - 30^\circ)} \left[\frac{\sqrt{6}\gamma}{a} + \frac{Ga(4-v)}{8\sqrt{6}\pi(1-v)d} \ln \frac{\sqrt{2}d}{a} \right] \tag{19}$$

where γ is the stable stacking fault energy, a is the lattice parameter, v is the Poisson's ratio, and d is the grain size defined in Fig. 40.

The τ needed to move the leading and trailing partials together is equivalent to τ for moving a screw lattice dislocation. τ has to overcome the work needed to lengthen the lattice dislocation segments Aa′ and Bb′, and can be derived as:

$$\tau_L = \frac{Ga}{2\sqrt{2}\pi(1-v)d\cos\alpha} \ln \frac{\sqrt{2}d}{a} \tag{20}$$

After the stacking fault formation, a twin may nucleate via the emission of a second 30° partial, $\mathbf{b}_1$, from the grain boundary on a plane adjacent to the stacking fault (Fig. 40b). On the other hand, a trailing partial may also emit on the stacking fault plane and erase the stacking fault in its path (Fig. 40c). The critical twin nucleation stress can be derived as:

$$\tau_{twin} = \frac{Ga(4-v)}{8\sqrt{6}\pi(1-v)d\cos(\alpha-30^\circ)} \ln \frac{\sqrt{2}d}{a} \tag{21}$$

The trailing partial requires a stress, τ_{trail}, to move, which can be derived as

$$\tau_{trail} = \frac{1}{\cos(\alpha+30^\circ)} \left[\frac{\sqrt{6}(8+v)Ga}{48\pi(1-v)d} \ln \frac{\sqrt{2}d}{a} - \frac{\sqrt{6}\gamma}{a} \right] \tag{22}$$

Once a twin is nucleated, it may grow via the emission of more $\mathbf{b}_1$ twinning partials under stress τ_{twin}. It may also shrink via the emission of a shrinking partial, $\mathbf{b}_2$, on a plane adjacent to the twin boundary but on the twin side. The stress needed to move a shrinking partial can be derived as:

$$\tau_{shrink} = \frac{1}{\cos(\alpha+30^\circ)} \frac{\sqrt{6}(8+v)Ga}{48\pi(1-v)d} \ln \frac{\sqrt{2}d}{a} \tag{23}$$

The stresses, τ_P, τ_L, τ_{twin}, τ_{trail}, and τ_{shrink}, determine the nucleation and growth of a deformation twin. For example, at $\tau_P < \tau_L$, partial dislocations will be emitted from the grain boundary, and at $\tau_{twin} < \tau_{trail}$, a twin may nucleate. In the following, Al is used as a model material to validate the model [57,59]. For Al, G = 26.5 GPa, v = 0.345, a = 0.404 nm, and γ = 122 mJ/m^2 [54,144]. In Fig. 41, the stresses, τ_P, τ_L, τ_{twin}, τ_{trail}, and τ_{shrink}, are plotted as a function of grain size d for α = 25°. The point B in Fig. 41 represents the critical grain size, d_B, below which a deformation twin nucleates because $\tau_{twin} < \tau_{trail}$.
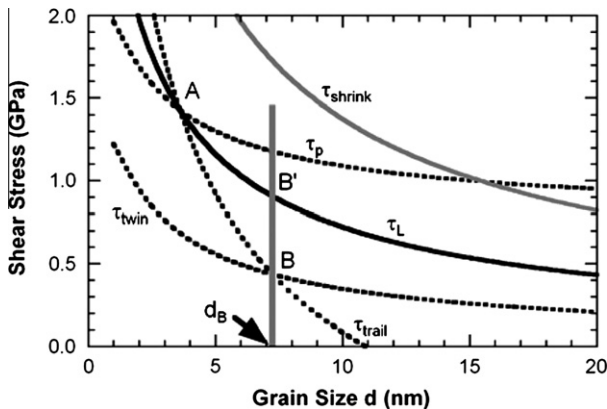

Fig. 41. The critical stresses, τ_P, τ_L, τ_{twin}, τ_{trail}, and τ_{shrink}, as a function of nc Al grain size d for a given α value of 25° [57].

However, a deformation twin can nucleate only after the formation of a stacking fault. As shown, at grain size d_B, $\tau_L < \tau_P$, i.e. the lattice dislocation is operating at point B′. It is also calculated that the stacking fault width at τ_L is far larger than d_B [57]. This means that a deformation twin nucleates after a stacking fault ribbon spreads across the grain. Interestingly, at point B′ the grain size is larger and the critical stress is lower for twin nucleation than those for the partial dislocation emission at point A, because the stacking fault of a dissociated lattice dislocation would spread across the grain before a partial is emitted. In other words, a twin will nucleate at the critical grain size d_B under the stress of d_B at B′.

The above equations and analysis are for the *Screw* system only. There are two other possible dislocation systems: a *60° I system* with a leading 90° partial and a trailing 30° partial, and a *60° II system* with a leading 30° partial and a trailing 90° partial [57]. These two systems are amenable to the same procedure, and therefore we only present the final results. It is found that the *60° II* system does not operate because it requires much higher stress to nucleate a deformation twin. In a polycrystalline nc sample, grains are likely to orient in all orientations. Therefore, a deformation map linking stresses of deformation twin nucleation and growth with grain size is very useful and desirable. Such a map can be constructed by plotting the critical (the lowest) stresses against the critical grain sizes, without the stress orientation information (see Fig. 42).

The deformation map in Fig. 42 reveals that there are optimum grain sizes for deformation twin nucleation (the lowest stress point at cup bottom), which are 4.85 nm and 7.25 nm for the *60° I* and *Screw* systems respectively. The minimum stresses for the *60° I* and screw systems in Fig. 42 were derived and simplified as [59]

$$\tau_{min}^{60°I} = \frac{1.72(4-3v)}{2.89-v}\frac{\gamma}{a} \tag{24}$$

$$\tau_{min}^{screw} = \frac{12.21}{3.73+v}\frac{\gamma}{a} \tag{25}$$

As shown in Fig. 42, these two minimum stresses are very close. For simplicity, we use their average as the critical stress for twinning, which can be derived as

$$\tau_m = \frac{\gamma}{2a}\left[\frac{1.72(4-3v)}{2.89-v}+\frac{12.21}{3.73+v}\right] \tag{26}$$

Eq. (26) can be approximated and simplified by assuming the value of v in the denominators as 0.33, which yields

$$\tau_m = \frac{(5.69-2.02v)\gamma}{2a} \tag{27}$$

Calculation shows that the error in Eq. (27) caused by the approximation is less than 2% for a wide range of v values from 0.25 to 0.45. Such a small error is negligible, considering the semi-quantitative nature of the model.
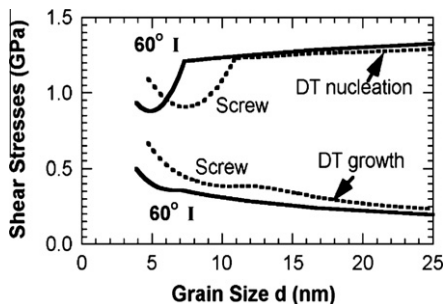

Fig. 42. A deformation map showing the critical stresses for deformation twin nucleation and growth in nc Al as a function of grain size for the 60° I and the *Screw* dislocation systems [57].

The optimum grain size for twinning, or the grain size at which the twinning stress is lowest for the 60° I and screw systems in Fig. 42 can be calculated from the following simplified equations [59]

$$\frac{d_m^{60°I}}{\ln(\sqrt{2}d_m^{60°I}/a)} = \frac{2.089 - v}{54.985(1 - v)}\frac{Ga^2}{\gamma}$$

(28)

$$\frac{d_m^{screw}}{\ln(\sqrt{2}d_m^{screw}/a)} = \frac{3.727 + v}{97.053(1 - v)}\frac{Ga^2}{\gamma}$$

(29)

For simplicity, we can use average of the Eqs. (28) and (29) as the critical grain size, d_m, for twinning:

$$\frac{d_m}{\ln(\sqrt{2}d_m/a)} = \frac{9.69 - v}{253.66(1 - v)}\frac{Ga^2}{\gamma}$$

(30)

The critical stress and optimum grain size for deformation twinning for Al, Cu and Ni calculated using Eqs. (27) and (30) are listed in Table 2. The predicted critical twinning stress is obtainable under experimental conditions and optimum grain size for twinning agrees well with experimental observations [57,59,171].

One of the most significant feature of this model is its successful prediction of normal and inverse grain size effect on deformation twinning [171]. However, it also has a major deficiency: it does not consider the effect of GPFE's, which affects the nucleation and gliding of the first and twinning partials. Consequently, this model cannot explain why no inverse grain size effect is observed for stacking faults (Fig. 36). In addition, this model treated dislocation lines as straight lines for simplicity, while they should be curved inside the grain in the real situation. Gu et al. recently developed a curved dislocation-line model to describe the partial emission from the grain boundary to form stacking faults [254], which is an improvement over the previous straight-line model [253]. Another modification and improvement is the incorporation of interactions between dislocations [255–257], which improved the accuracy of the equations, but also significantly increased the complexity of the mathematical equations.

Finally, the most significant contribution of this model is its successful description of the grain size effect on deformation mechanisms. As shown in Fig. 41, the critical stresses for moving all dislocations increase with decreasing grains size. However, the rate at which the critical stress increases with decreasing diameter varies with the type of the dislocation. For example, below a critical grain size the critical stress τ_P for the leading partial will be lower than that for the lattice dislocation τ_L. The physical reason for the grain size effect is the deposition of the dislocation lines (see Fig. 40) on the grain boundaries as a dislocation glides forward under an applied stress. The deposited dislocation lines add strain energy to the system and act to drag the gliding dislocation. The dragging force does not change with grain size d, while the driving force for the dislocation slip is proportional to the length of the gliding section of the dislocation, which is equal to the grain size d. The difference in grain size dependences of the dragging and driving forces makes it more difficult for dislocations to move in smaller grains.

Table 2
The critical stress and optimum grain size for the formation of deformation twinning in Ag, Al, Au, Cu and Ni, predicted by the twinning partial from the grain boundary model (Eqs. (27) and (30)) as well as parameters used for the calculation [54,57,59].

	G (GPa)	v	γ (mJ m^{-2})	A (Å)	τ_m (GPa)	d_m (nm)
Ag	30	0.37	22	4.090	0.16	73
Al	26.5	0.345	122	4.04	0.89	6
Au	27	0.44	45	4.080	0.31	30
Cu	54.6	0.343	45	3.6146	0.37	46
Ni	94.7	0.312	125	3.5232	1.06	23

5.8.4. General-planar-fault-energy (GPFE) based models

It is generally agreed that GPFE curves have significant effect on the deformation twinning of materials [10,29,35,49,79,171,201,258–264]. However, how the GPFE curves affect the deformation twinning in nc materials have not been rigorously modeled. Most modeling works involving GPFEs have so far either focused on twinning at a crack tip in a single crystal [29,258] or using the GPFE concept to qualitatively explain MD modeling results [10]. The grain size, which has been experimentally observed to significantly affect the twinning, is conspicuously missing in these models. In other words, the GPFE models reported so far are not specific for nc materials and their validity for nc materials may be limited. For example, the GPFEs alone cannot explain the experimentally observed normal and inverse grain size effect shown in Fig. 36 and discussed in Section 5.4.

Using Rice's Peierls approach [30], Tadmor and Hai [258] derived an equation describing the twinning criterion:

$$T = \lambda_{crit}\sqrt{\frac{\gamma_{usf}}{\gamma_{utf}}} \tag{31}$$

where T is the twining tendency, λ_{crit} is dimensionless factor that characterize the extra load to nucleate the trailing partial in comparison to the leading partial, γ_{usf} and γ_{utf} are the unstable stacking fault energy and the unstable twin fault energy, respectively, as defined in Fig. 37. The value of λ_{crit} depends on the materials parameters γ_{utf}, stable stacking fault energy γ_{sf}, v, and geometric parameters. More details can be found in [258]. A two layer twin can nucleate if $T > 1$, and a trailing partial will nucleate if $T < 1$. It should be noted that grain size is not considered in the Eq. (31).

Asaro and Suresh [29] further explored Eq. (31) for a special case where the Burgers vector of the leading partial is orthogonal to the crack front, and applied shear stress is parallel to the Burgers vector of the leading partial. They developed Eq. (31) into the following equation

$$T = \sqrt{(1+\beta)\frac{\gamma_{usf}}{\gamma_{utf}}} \tag{32}$$

where $\beta = 1 - \gamma_{sf}/\gamma_{usf}$. Therefore, T is only determined by the GPFEs.

Van Swygenhoven et al. [10] used the GPFE curves to explain the differences in deformation mechanisms of nc Al, Cu and Ni with a small grain size of 12 nm. Particularly, although both Al and Ni have similar high stacking fault energy, γ_{sf}, they deform via very different mechanisms. Al deforms via lattice dislocation slip because its γ_{sf}/γ_{usf} is very small, making the trailing partial easy to nucleate and emit, while Ni deforms via partial slip because γ_{sf}/γ_{usf} is very large, making the trailing partial difficult to nucleate and emit. In addition, twinning is rarely observed in three-dimensional nc Al, Ni and Cu because of their high unstable twin fault energy, γ_{utf}. However, these results from MD simulations cannot be extrapolated to nc materials with larger grain sizes, due to the grain size effect observed experimentally [171]. In other words, when the grain sizes become larger and near the optimum grain size for twinning, deformation twins were observed [59,171]. Therefore, there is a need to do MD simulations in which grain sizes are systematically varied.

Kibey et al. [79,260] recently developed a sequential, multi-scale approach to predict the twinning stress. GPFEs were incorporated into the model, and a closed-form expression for twinning stress was obtained, which was simplified into the following approximate form:

$$\tau_{crit} = \frac{2}{3Nb_{twin}}\left(\frac{3N}{4} - 1\right)\left(\gamma_{utf} + \frac{2\gamma_{tsf} + \gamma_{sf}}{2}\right) - \frac{2}{3N}\frac{\gamma_{usf} + \gamma_{sf}}{b_{twin}} \tag{33}$$

where $N = 3$ represents a three-layer critical twin nucleus. γ_{tsf} is the energy of the twin boundary. γ_{tsf} can be approximated as half of the stacking fault energy γ_{tsf}, but this may not be obeyed by inhomogeneous alloys [261,265]. It is obvious from Eq. (33) that the grain size effect is not considered in this model.

5.8.5. Future issues on modeling

As discussed above, both grain size and GPFEs have significant effect on the formation of deformation twins and stacking faults. None of the current models has considered both factors. One possible approach is to incorporate the GPFEs into the analytical model. However, this is not trivial and also needs experimental verification of any assumptions that are used in the analytical model. The GPFEs can affect both the nucleation and glide of the dislocations.

Two fundamental issues need to be investigated. First, how do the GPFEs affect the nucleation of first partials and twinning partials? This issue needs to be studied experimentally. One question that remains is if the GPFE curves affect the nucleation of dislocations since the grain boundaries of nc materials may be in a non-equilibrium state with excess dislocations existing in them. Second, how do the GPFEs affect the slip of the first and twinning partials. In other words, how the GPFE curves affect the Peierls stresses for these partials. There have been several reports on calculating the Peierls stresses from GPFEs [264,266–268]. However, a formula for calculating the Peierls stress from the GPFEs remains to be derived.

It should be noted that any analytical descriptions of twinning models should be based on observed deformation physics instead of on convenient, arbitrary assumptions. The most important quality of an analytical model is to capture the deformation physics instead of fitting experimental data, because only such models can predict comprehensive experimental phenomena.

For MD simulations, it will be of great interest to systematically vary the grain size from 10 nm to 100 nm so that the experimentally observed effect of grain size on twinning can be studied. Ideally, MD simulations can investigate simultaneously the effects of both GPFEs and grain sizes on deformation twinning. However, this could be currently difficult because the computational power available to most researchers may limit the grain sizes that can be practically investigated.

6. Deformation twinning in non-fcc metals

The study on deformation mechanisms of nc materials has been mostly focused on fcc metals. Nanomaterials with other crystal structures such as nc bcc and hcp metals have not been studied much, although such studies have recently been reported. In this section, we will give a brief overview on recent progress on the deformation twinning in nc bcc and hcp metals. It should be noted that studies on deformation mechanisms of nc bcc and hcp metals are at their very early stages, and many issues and controversies are to be investigated and resolved.

6.1. Deformation twinning in nanocrystalline bcc metals

Compared with the nc fcc metals, the deformation mechanisms of bcc metals are much less studied. Tang and Wang observed twin formation from crack tips in Mo in MD simulations [269]. Frederiksen et al. [270] did MD simulation studies of the deformation mechanisms of nc bcc Mo with a grain size of 12 nm, and observed deformation twinning. Although crack formations at grain boundaries were extensively observed, only some twins were emitted from cracks. Marian et al. [271] modeled single crystal bcc Fe using MD simulations and found that with increasing strain rate and shear stress, screw dislocation motion changed from smooth to rough and eventually twinning became the dominant deformation mechanism. Wang et al. [31] deformed nc bcc Ta with grain sizes of 10–30 nm by nano-indentation. Subsequent HREM investigation revealed extensive deformation twins in the nano-sized grains and some grains contain multiple twins with different twin orientations, indicating that twinning is a major deformation mechanism in nc Ta. These observations in nc bcc metals are consistent with observations in nc fcc metals and alloys.

6.2. Deformation twinning in nanocrystalline hcp metals

The twinning behavior of hcp materials is very different from that of fcc metals. As discussed earlier, for fcc metals, with decreasing grain size it becomes more difficult to deform by twinning in the coarse-grain size range [11], but twinning becomes easier once the grain size is smaller than 100 nm

[9], although twinning may become difficult again when the grain size is too small (inverse grain size effect) [171]. In contrast, coarse-grained hcp metals usually need twinning to accommodate plastic deformation in addition to dislocation slip [170,272,273], because there are not five independent deformation systems, as required by the von Mises criterion for compatibility [165]. However, twinning is rarely observed in nc hcp metals and alloys, with an exception of nc Zr processed by surface mechanical attrition [274]. It appears that the deformation twinning becomes more difficult with decreasing grain size and twinning is rarely observed below a certain grain size. The reason for the observed grain size effect on twinning in hcp materials is not clear.

The twinning mechanisms in hcp metals are still under intensive study. Capolungo and Beyerlein proposed a twin-nucleation model based on the nonplanar dissociation of the leading dislocation in a pileup of basal slip dislocations [163]. Wang et al. studied the nucleation of $[10\bar{1}2](\bar{1}012)$ twin in Mg by atomic simulations, and found that the twin nucleus consists of one $-50/107[10\bar{1}1]$ partial and multiple $1/15[10\bar{1}1]$ partials [159]. Kucherov and Tadmor revealed twin nucleation formed by partial emission at a crack tip in their MD simulation [275]. Li and Ma observed deformation twinning mediated by the nucleation and glide of zonal dislocations followed by atomic shuffling in hcp Mg in their MD simulation [164]. They also found that the most favorable zonal dislocation under compression has a Burgers vector of $\frac{1}{2}\frac{1}{2}\langle10\bar{1}2\rangle$, i.e. the twinning mode is $\{10\bar{1}1\}\langle10\bar{1}2\rangle$. This zonal dislocation involves two $(10\bar{1}1)$ planes, forming a two-layer step on the twin boundary. Tomé et al. studied another twinning mode, $\{10\bar{1}2\}\langle10\bar{1}1\rangle$, in hcp metals by means of *ab initio* (density function theory) and MD simulations [159,161,276]. Kim et al. recently studied the twinning mechanism in nc hcp Mg with $[11\bar{2}0]$ texture (2D columnar structure) [277]. However, no zonal dislocation is involved in the formation of the $\{10\bar{1}2\}\langle10\bar{1}1\rangle$ twin in their simulation results. It is expected that these issues and controversies will be further clarified and resolved by future investigations.

We have recently observed deformation twins in nc hcp Mg–10 at.% Ti alloy processed by ball milling [278]. Fig. 43 shows the HREM image of a deformation twin in the as-processed nc Mg–Ti alloy. The images are viewed from a $[11\bar{2}3]$ zone axis. Importantly, a two-atomic-layer step (marked by 2) and a one-layer step (marked by 1) on the coherent twin boundaries are shown. This is a $\{10\bar{1}1\}\langle10\bar{1}2\rangle$ deformation twin, which is consistent with the twinning mode observed in MD simulation of Mg under compression [164]. The two-layer step shown here is consistent with the zonal twinning dislocation predicted by the MD simulation. The MD simulation also predicted that the one-layer steps are immobile and the four-layer steps are unstable and can spontaneously dissociate into two two-layer steps [164]. The one-layer step is experimentally observed in Fig. 43, while no four-layer steps have been observed in our samples. Interestingly, this twinning system was also observed in hcp Ti and Zr processed by severe plastic deformation under pressure, although the twinning only happened in large grains [272,279].
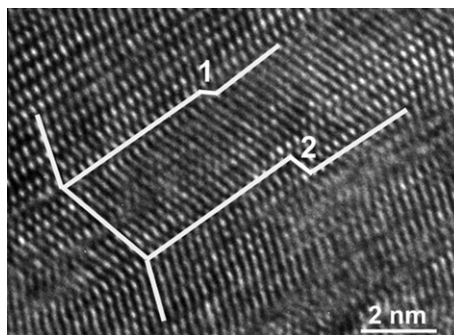

Fig. 43. HREM micrograph showing a deformation twin in the nc Mg–Ti alloy, viewed along a $[11\bar{2}3]$ zone axis. The twin system is $\{10\bar{1}1\}\langle10\bar{1}2\rangle$. A two-atomic-layer step and a one-layer step are on the twin boundary [278].

7. Interaction between dislocations and twin boundaries

Deformation twinning usually occurs simultaneously with the slip of perfect and partial dislocations, making it inevitable to have interactions between twins and gliding dislocations at twin boundaries, which have been observed both experimentally [40–44,218,280,281] and by molecular dynamics simulations [45–50,282]. These interactions are believed to make twins effective in simultaneously increasing the strength and ductility of nc materials [40,47,51,153,221,282,283]. When a dislocation glides on a slip plane and stops on a twin boundary, the dislocation line becomes parallel to the cross-line between the slip plane and the twin boundary before any dislocation reaction with the twin boundary occurs. Consequently, in fcc metals there are only four types possible dislocations to react with the twin boundary: 30° Shockley partial, 90° Shockley partial, screw perfect dislocation, and 60° perfect dislocation. To understand these dislocation-twin boundary reactions, we need to invoke the double Thompson tetrahedron [217,282,284], which is illustrated in Fig. 44. As shown, the Thompson tetrahedron above the (1 1 1) twin boundary represents slip systems in the matrix, while the bottom tetrahedron represents slip systems in the twin. The twin boundary plane is shared by the matrix above it and the twin below it. Therefore, the tetrahedron in the matrix and the tetrahedron in the twin should share the same base, which is ABC, as shown in Fig. 44. In other words, dislocations with Burgers vectors of **AB**, **BC**, **CA**, **Aδ**, **Bδ**, and **Cδ** can slip both in the matrix and in the twin.

Below we will describe all possible reactions between dislocations and twin boundaries. Any reaction could happen provided that applied stress is high enough and in the right orientation. The energy barrier for dislocation reaction could be used to qualitatively measure how easy the reaction is. Nanocrystalline materials have much higher flow stress than their coarse-grained counterparts during plastic deformation, which should help overcome the energy barriers. Therefore, some dislocation reactions with relatively high energy barriers might happen in nc materials but not in coarse-grained materials.

7.1. Cross slip of a 30° partial [285]

When a 30° Shockley partial dislocation cross-slips into the ABC plane at the twin boundary (see Fig. 44), it can react at the twin boundary to grow the twin [42], or cause detwinning [285,286].
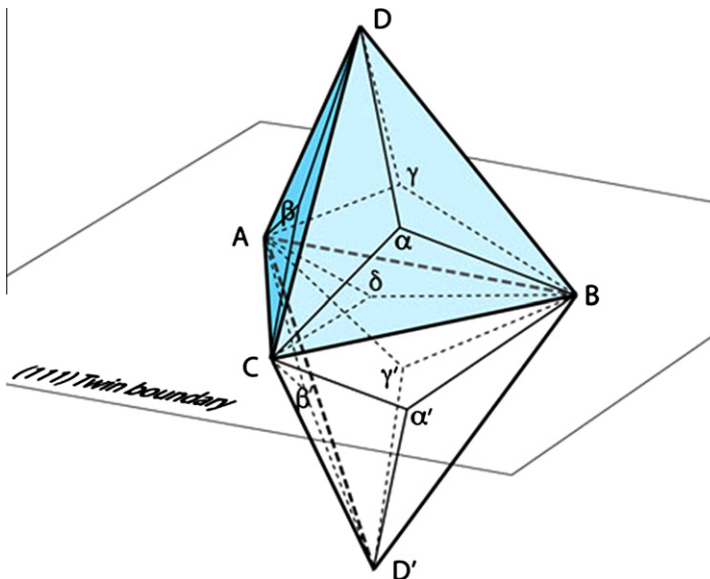

Fig. 44. Illustration of a double Thompson tetrahedron. The top tetrahedron above the (1 1 1) twin boundary represents slip systems in the matrix, while the bottom tetrahedron represents slip systems in the twin [159].

The detwinning process is very similar to the twin growth process, except that the partial glides toward the opposite direction after the cross-slip. Below we will describe the detwinning process only, since the twinning process has been described in Section 5.3.6.

As shown in Fig. 45, the 30° partial, **Bα**, glides on the BCD plane, leaving behind a stacking fault (SF), and stops at the twin boundary, **TB**. Under appropriate applied stress, the following dislocation reaction occurs (see Fig. 1 and 2):

$$\mathbf{B\alpha} \rightarrow \mathbf{B\delta} + \mathbf{\delta\alpha} \tag{34}$$

Bδ glides to the left to move the twin boundary toward the twin interior by one atomic plane. This also leaves a step on the twin boundary, and a stair-rod dislocation at the twin step, as shown in Fig. 45b.

The stair-rode dislocation **δα** could further dissociate into two partial dislocations according to the Thompson tetrahedron:

$$\mathbf{\delta\alpha} \rightarrow \mathbf{\delta B} + \mathbf{B\alpha} \tag{35}$$

where the partial **δB** will glide on the twin boundary to the opposite direction of **Bδ** under the same applied stress, because they represent partials with opposite Burgers vectors.

As shown in Fig. 45c, after the **δB** glides to the right, the twin thickness is reduced by one atomic plane, i.e. detwinning occurred during the above process. The partial **Bα** advances to the new twin boundary under the original applied stress, and can repeat the above process to annihilate the whole twin.

The energy barrier, which is the energy increase for a dislocation reaction, for the dislocation reactions described in Eq. (34) can be described as [285]:

$$\Delta E_{Eq34} = \widehat{E} + 2.0\tilde{E} \tag{36}$$

where $\widehat{E} = \frac{Ga^2}{72\pi(1-v)} \ln \frac{\sqrt{2}d}{a}$ and $\tilde{E} = \frac{Ga^2}{72\pi(1-v)}$, a is the lattice parameter, d is the grain size, G is the shear modulus and v is the Poisson's ratio, which is assumed to be 1/3, which is a reasonable approximation for most fcc metals. Note that energy barrier described in Eq. (36) and hereafter are based on the assumption of isotropic elasticity.

The energy barrier for the dislocation reaction in Eq. (35) is [285]

$$\Delta E_{Eq35} = 3.5\widehat{E} + 5.5\tilde{E} \tag{37}$$

Eq. (37) indicates that the reaction in Eq. (35) requires much higher applied stress than the reaction in Eq. (34) to overcome the energy barrier. If the applied stress is high enough to activate the reaction described in Eq. (34) but not the reaction in Eq. (35), then a step will be produced on the twin boundary. Twin boundaries with steps have been extensively observed experimentally [65,218,281] and by MD simulations [45,22,157]. Some of these steps could be formed by the mechanism described here.

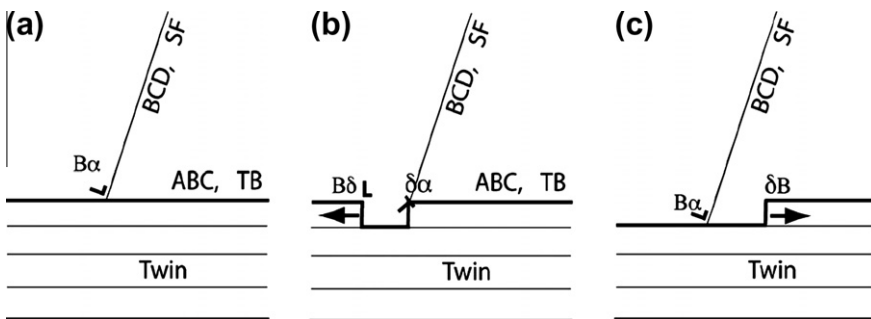**Fig. 45.** Detwinning process caused by the interaction of a 30° partial, **Bα**, with the twin boundary. SF marks the stacking fault, TB marks the twin boundary (thick black lines). BCD and ABC represent the BCD and ABC slip planes in the Thompson tetrahedron, respectively [159].

7.2. Transmission of a 30° partial across twin boundary

As shown in the double Thompson tetrahedron (Fig. 44), the tetrahedron in the matrix and the tetrahedron in the twin share the same base, which is ABC, as shown in Fig. 44. In other words, dislocations with Burgers vectors of **AB**, **BC**, **CA**, **Aδ**, **Bδ**, and **Cδ** can slip both in the matrix and in the twin. The 30° partial, **Bα**, on the BCD slip plane in the matrix, can have the following dislocation reaction to release another partial in the twin:

$$\mathbf{B\alpha} \rightarrow \mathbf{B\alpha'} + \mathbf{\alpha'\alpha} \tag{38}$$

where **Bα'** is a partial that can slip away in the twin from the twin boundary on the BCD plane, and **α'α** is a new type of stationary stair-rod dislocation across the twin boundary. The energy barrier of the dislocation reaction described in Eq. (38) can be calculated as

$$\Delta E_{Eq38} \approx 2.7\widehat{E} + 4.1\widetilde{E} \tag{39}$$

This indicates that the energy barrier for the 30° partial, **Bα**, to transmit across the twin boundary is energetically plausible under appropriate applied stress.

It can be seen from Fig. 44 that **α'α** is an edge dislocation with its Burgers vector perpendicular to both the dislocation line BC and the twin boundary (1 1 1). The dislocation configuration after the reaction is illustrated in Fig. 46, which shows two stacking faults from both sides of the twin boundary meeting at the twin boundary and connected by the stair-rod dislocation **α'α**.

7.3. Reaction of a 90° partial at twin boundary [285]

The cross-slip of 90° partials at the coherent twin boundary has been described in Section 5.3.5, and therefore won't be discussed here. The energy barrier for the cross-slip of the 90° partials is zero [285].

Below we will describe the transmission of 90° partial across the twin boundary. As shown in Fig. 44, the 90° partial **Dα** can dissociate as

$$\mathbf{D\alpha} \rightarrow \mathbf{D\delta} + \mathbf{\delta\alpha} \tag{40}$$
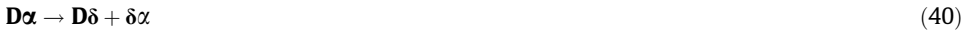
The double Thompson tetrahedron indicates that the Burgers vector **Dδ** is identical to the δD' in the twin, i.e. **Dδ** = δD', which can dissociate into a 90° partial **α'D'** and a stair-rod dislocation δα', i.e.

$$\mathbf{D\delta} = \delta\mathbf{D'} \rightarrow \delta\mathbf{\alpha'} + \mathbf{\alpha'D'} \tag{41}$$

Substituting Eq. (41) into Eq. (40) yields:

$$\mathbf{D\alpha} \rightarrow \delta\mathbf{\alpha} + \delta\mathbf{\alpha'} + \mathbf{\alpha'D'} \tag{42}$$

There are two stair-rod dislocations in Eq. (42). Both of them stay at the twin boundary and could react to form a dislocation structure with lower energy. With the help of the double Thompson tetrahedron, the stair-rod reactions can be described below
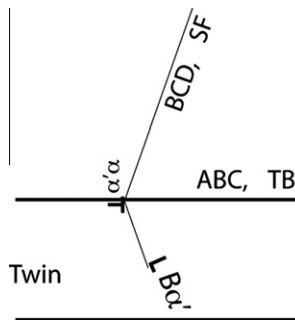

Fig. 46. The dislocation configuration after the partial **Bα** penetrates the twin boundary to release another partial **Bα'** on the BCD' plane inside the twin, leaving a stair-rod dislocation **α'α** on the twin boundary [285].

$$\delta\boldsymbol{\alpha} + \delta\boldsymbol{\alpha}' \rightarrow \frac{4}{9}\mathbf{A}\delta \tag{43}$$

Substituting Eq. (43) into the Eq. (42) yields

$$\mathbf{D}\boldsymbol{\alpha} \rightarrow \frac{4}{9}\mathbf{A}\delta + \boldsymbol{\alpha}'\mathbf{D}' \tag{44}$$

According to Eq. (44), a partial $\boldsymbol{\alpha}'\mathbf{D}'$ will be emitted from the twin boundary to slip on the BCD′ plane. The partial $\mathbf{D}\boldsymbol{\alpha}$ can also transmit across the twin boundary to emit a partial on the ACD′ plane or BAD′ plane [285]:

$$\mathbf{D}\boldsymbol{\alpha} \rightarrow \frac{2}{9}\delta\mathbf{C} + \boldsymbol{\beta}'\mathbf{D}' \tag{45}$$

and

$$\mathbf{D}\boldsymbol{\alpha} \rightarrow \frac{2}{9}\delta\mathbf{B} + \boldsymbol{\gamma}'\mathbf{D}' \tag{46}$$

The energy barrier for reaction in Eq. (44) is

$$\Delta E_{Eq44} = 0.6\widehat{E} + 1.4\tilde{E} \tag{47}$$

The energy barriers for the reactions in Eqs. (45) and (46) are

$$\Delta E_{Eqs45,46} = 0.1\widehat{E} + 0.2\tilde{E} \tag{48}$$

Therefore, the energy barriers for dislocation reactions in Eqs. (44)–(46) are very low, which make it easy for the 90° partial $\mathbf{D}\boldsymbol{\alpha}$ to transmit across the twin boundary to emit another 90° partial in the twin.

7.4. Reaction of a perfect screw dislocation at twin boundary

Assume that a perfect screw dislocation $\mathbf{BC}$ glides on the BCD plane toward the twin boundary (see Fig. 44.) It could dissociate into two 30° partials with a stacking fault in between, i.e.

$$\mathbf{BC} \rightarrow \mathbf{B}\boldsymbol{\alpha} + \boldsymbol{\alpha}\mathbf{C} \tag{49}$$

When this dissociated $\mathbf{BC}$ reaches the twin boundary, it could constrict to form a perfect dislocation again. Since $\mathbf{BC}$ is parallel to the dislocation line, it can either cross-slip into the $\mathbf{ABC}$ plane on the twin boundary, or onto the BCD′ plane in the twin, depending on the orientation of the applied stress. Therefore, a screw dislocation can easily cross-slip on the twin boundary or transmit across the twin boundary.

If the stacking fault energy is very low, a scenario could occur where the leading partial cross-slips into the ABC plane while the trailing partial remains on the BCD plane, with a stair-rod dislocation at the twin boundary linking the stacking fault with the twin boundary.

7.5. Reaction of a perfect 60° dislocation at twin boundary

Assume that a perfect 60° dislocation $\mathbf{BD}$ glides on the BCD plane toward the twin boundary (see Fig. 44). It could dissociate into a 30° partial $\mathbf{B}\boldsymbol{\alpha}$ and a 90° partial $\boldsymbol{\alpha}\mathbf{D}$ with a stacking fault between them, i.e. $\mathbf{BD} \rightarrow \mathbf{B}\boldsymbol{\alpha} + \boldsymbol{\alpha}\mathbf{D}$. Partials $\mathbf{B}\boldsymbol{\alpha}$ and $\boldsymbol{\alpha}\mathbf{D}$ with a stacking fault ribbon between them glide together toward the twin boundary under applied stress. There are several plausible scenarios that could occur at the twin boundary, these are described below.

7.5.1. Partials first constrict to form a perfect 60° dislocation

The first scenario is where the partials are constricted to form the perfect dislocation $\mathbf{BD}$ first. Such a scenario can happen easily when the stacking fault energy is relatively high and the distance of the leading and trailing partials is small. It can be seen from the double Thompson tetrahedron (Fig. 44)

that **BD** has a 60° angle with the dislocation line BC. The dislocation reaction for **BD** to cross-slip onto the ABC plane is **BD → BC + CD**. The energy barrier for such a reaction is $6\hat{E}$, which is so high that such a cross-slip is almost impossible [285].

The perfect 60° dislocation **BD** can also transmit across the twin boundary to emit a perfect dislocation in the twin. The following analysis yields possible dislocation reactions. First, **BD** can dissociate according to

$$\mathbf{BD} \rightarrow \mathbf{B\delta} + \mathbf{\delta D} \tag{50}$$

where **δD** is equivalent to **D′δ**, which can further react to emit perfect dislocations in the twin according to

$$\mathbf{\delta D} = \mathbf{D'\delta} \rightarrow \mathbf{D'B} + \mathbf{B\delta} \tag{51}$$

$$\mathbf{\delta D} = \mathbf{D'\delta} \rightarrow \mathbf{D'A} + \mathbf{A\delta} \tag{52}$$

$$\mathbf{\delta D} = \mathbf{D'\delta} \rightarrow \mathbf{D'C} + \mathbf{C\delta} \tag{53}$$

Substituting Eqs. (51)–(53) into Eq. (50), and also considering **Bδ + Aδ = δC**, and **Bδ + Cδ = δA**, we have

$$\mathbf{BD} \rightarrow 2\mathbf{B\delta} + \mathbf{D'B} \tag{54}$$

$$\mathbf{BD} \rightarrow \mathbf{\delta C} + \mathbf{D'A} \tag{55}$$

$$\mathbf{BD} \rightarrow \mathbf{\delta A} + \mathbf{D'C} \tag{56}$$

The energy barrier is $\sim 4.5\hat{E}$ for the dislocation reaction in Eq. (54), and $3\hat{E}$ in Eqs. (55) and (56).

In reactions described by Eqs. (55) and (56), one partial will glide on the twin plane, which will grow or shrink the twin by one atomic plane and leave behind a step on the twin boundary depending on the gliding direction. At the same time a perfect 60° dislocation is emitted in the twin, which will also produce a step on the twin boundary. In comparison, the dislocation reaction in Eq. (54) will release two partials on the ABC plane to grow or shrink the twin by two atomic planes, which is why it has higher energy barrier.

7.5.2. 30° leading partial reacts first at twin boundary

The 60° dislocation **BD** glides on the BCD plane toward the twin boundary. It can dissociate as **BD → Bα + αD**, with the 30° partial **Bα** as the leading partial. The leading partial **Bα** could either cross-slip onto the twin boundary plane or transmit across the twin boundary. The reaction of the leading partial is identical to what are described in Sections 7.1 and 7.2. The trailing partials can either stay on the original slip plane in the matrix, cross-slip onto the twin boundary, or transmit across the twin boundary. We will discuss these scenarios below.

The first scenario is the cross-slip of leading 30° partial **Bα** onto the twin boundary plane, while the trailing 90° partial **αD** remains on the BCD plane, forming a dislocation structure with a stair-rod dislocation, as shown in Fig. 47a. Such a dislocation structure has been observed both experimentally and by MD simulations [46,47,77]. It has been assumed very effective in blocking other dislocations and consequently causes strain hardening [77].

As shown in Fig. 47a, under high applied stress, the trailing partial **αD** may be driven to the twin boundary to react with the stair-rod dislocation **δα**:

$$\mathbf{\delta\alpha} + \mathbf{\alpha D} \rightarrow \mathbf{\delta D} \tag{57}$$

From the double Thompson tetrahedron, **δD** is equivalent to **D′δ**. The latter can dissociate as **D′δ → D′α′ + α′δ**. Therefore, Eq. (57) can be rewritten as

$$\mathbf{\delta\alpha} + \mathbf{\alpha D} \rightarrow \mathbf{D'\alpha'} + \mathbf{\alpha'\delta} \tag{58}$$

The energy barrier for this reaction is 0. This scenario is schematically illustrated in Fig. 47b.
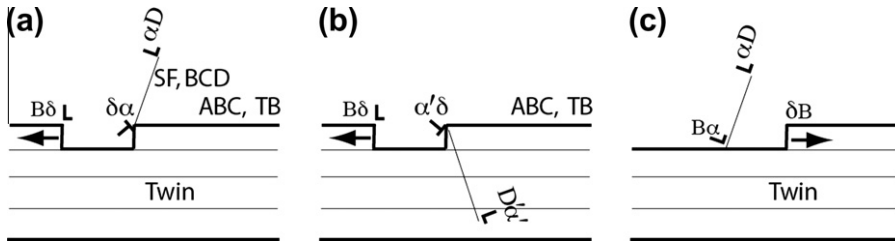
Fig. 47. Reaction of dissociated 60° dislocation **BD** with a 30° leading partial at the twin boundary. (a) The leading partial cross-slips onto the ABC twin boundary, leaving behind a stair-rod dislocation and the 90° trailing partial still on the original BCD slip plane. (b) After the trailing partial **αD** reacts with the stair-rod dislocation δα and transmit across the twin boundary. (c) The stair-rod dislocation dissociates according to δα → δ**B** + **B**α to reduce the twin by one atomic layer [285].

The second scenario is for the leading 30° partial **B**α to transmit across the twin boundary. As discussed in Section 7.2, the 30° partial **B**α may transmit across the twin boundary, leaving behind a large stair rod dislocation αα′. If the trailing partial **α**D remains on the BCD plane, it will have a unique dislocation configuration where a stacking fault links the αα′ with partial **B**α′, and another stacking fault links the αα′ with the trailing partial **α**D, as sown in Fig. 48a. The trailing partial **α**D can also cross-slip onto the twin boundary plane, becoming a partial δ**A** to slip to the left to increase the twin by one atomic plane, as shown in Fig. 48b.

The third scenario is for the stair-rode dislocation δα in Fig. 47a to further dissociate into two partial dislocations, δα → δ**B** + **B**α, where the partial δ**B** glides on the twin boundary to the opposite direction of **B**δ to reduce the twin thickness by one atomic plane, as illustrated in Fig. 47c. Such a process can be repeated to reduce the twin, as described in Section 7.1. The energy barrier for such a reaction is about $3.5\hat{E}$, making it relatively difficult.

The trailing 90° partial **α**D can also react with the stair-rod αα and transmit across the twin boundary [285]. However, the dislocation reactions have very high energy barriers, and are not likely to occur [285]. Therefore, the transmission of the trailing 90° partial will not be discussed in detail here.

7.5.3. 90° leading partial reacts first at twin boundary

If the 90° partial **α**D is the leading partial, **α**D could either cross-slip onto the twin boundary plane or transmit across the twin boundary. The first scenario is for the 90° leading partial to cross-slip onto the twin boundary plane ABC, as described in Section 7.3. The trailing partial **B**α can also cross-slip onto the twin boundary to form **B**δ on the ABC plane, following the procedure described in Section 7.1, leaving behind a stair-rod dislocation δα. **B**δ and δ**A** can glide together on the twin boundary with a stacking fault between them. On the other hand, the trailing 30° partial **B**α can also transmit across the twin boundary to emit a parital **B**α′ in the twin, as described in Section 7.2. This leaves behind a stair-rod α′α at the twin boundary.
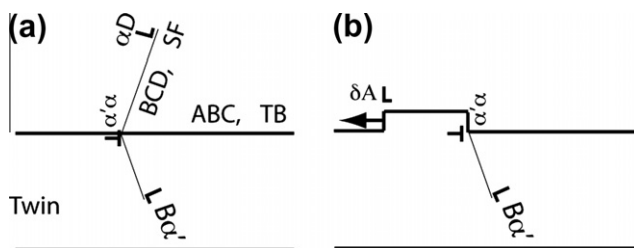

Fig. 48. (a) Dislocation configuration after the leading 30° partial **B**α transmits across twin boundary and the trailing 90° partial **α**D remains on the BCD plane. (b) After the trailing partial **α**D cross-slips into the ABC plane to grow the twin by one atomic plane [285].

The second scenario is for the leading partial **αD** to transmit across the twin boundary, as described in Section 7.3. The 90° partial **αD** can transmit across the twin boundary after one of the following reactions:

$$\mathbf{\alpha D} \rightarrow \mathbf{\alpha \delta} + \mathbf{\alpha'\delta} + \mathbf{D'\alpha'} \tag{59}$$

$$\mathbf{\alpha D} \rightarrow \mathbf{\alpha \delta} + \mathbf{\beta'\delta} + \mathbf{D'\beta'} \tag{60}$$

and

$$\mathbf{\alpha D} \rightarrow \mathbf{\alpha \delta} + \mathbf{\gamma'\delta} + \mathbf{D'\gamma'} \tag{61}$$

where the partial dislocations **D'α'**, **D'β'**, or **D'γ'** will glide away in the twin, leaving behind two stair rod dislocations at the twin boundary. When the trailing 30° partial **Bα** reaches the twin boundary, it can react with stair-rod dislocation, i.e.

$$\mathbf{B\alpha} + \mathbf{\alpha \delta} \rightarrow \mathbf{B\delta} \tag{62}$$

This reaction is energetically favorable with an energy reduction of $-\widehat{E}$. The **Bδ** can glide on the ABC plane, which either increase or reduce the twin thickness by one atomic plane, depending on its slip direction.

The trailing partial **Bα** can also react with stair-rod dislocations (as shown in Eqs. (59)–(61)) at the twin boundary to release a Shockley partial dislocation in the twin:

$$\mathbf{B\alpha} + \mathbf{\alpha \delta} + \mathbf{\alpha'\delta} \rightarrow \mathbf{B\alpha'} + 2\mathbf{\alpha'\delta} \tag{63}$$

$$\mathbf{B\alpha} + \mathbf{\alpha \delta} + \mathbf{\beta'\delta} \rightarrow \mathbf{B\alpha'} + \mathbf{\alpha'\delta} + \mathbf{\beta'\delta} \tag{64}$$

and

$$\mathbf{B\alpha} + \mathbf{\alpha \delta} + \mathbf{\gamma'\delta} \rightarrow \mathbf{B\alpha'} + \mathbf{\alpha'\delta} + \mathbf{\gamma'\delta} \tag{65}$$

A first inspection suggests that the energy barrier should be zero for the reactions in Eqs. (63)–(65) because the number of partial dislocations and stair-rod dislocations does not change. However, the reacting stair-rod dislocation pairs on the left can combine to form a dislocation with lower energy, while the stair-rod dislocation pairs on the right form a dislocation with higher energy when they combine together [285]. This energy differences can be regarded as the energy barrier, which are about $3.4\widehat{E}$ for Eq. (63) and $2.8\widehat{E}$ for Eqs. (64) and (65). Therefore, the energy barrier for the trailing partial to transmit across the twin boundary is relatively high.

8. Effect of twinning on properties

The interaction between the twin boundary and dislocations will inevitably affect the mechanical and physical properties. The existence of twin boundaries significantly increases the dislocation storage capability in materials, and twin structure may also affect physical properties. These are discussed in the following sections. Since deformation twins and growth twins should have similar effect on the properties, no differentiation is made between them in the following discussion.

8.1. Strain rate sensitivity

Strain rate sensitivity (SRS) m is defined as $m = \frac{\partial \ln \sigma}{\sigma \partial \ln \dot{\varepsilon}}\big|_{\varepsilon,T}$, where σ is the flow stress and $\dot{\varepsilon}$ is the strain rate [287]. By defining the activation volume, which is the rate of decrease of the activation enthalpy with respect to flow stress at a fixed temperature, $v^* = \sqrt{3}kT\left(\frac{\partial \ln \dot{\varepsilon}}{\partial \ln \sigma}\right)$, where k is the Boltzmann constant and T is the absolute temperature, SRS can be re-written as $m = \frac{\sqrt{3}kT}{\sigma v^*}$ [287,288]. Experimental results have shown that nc materials are highly sensitive to strain rates and that the SRS of nominally defect-free nc Cu and Ni are several times higher than that of their coarse-grained counterparts [289–291]. The activation volume of nc materials is about two order of magnitude smaller than that of conventional coarse-grained materials [288].

Tensile strain rate jump tests of UFG copper with and without nanoscale twins over a wide range of strain rates indicated that twinned structures significantly increase the strain rate sensitivity [195]. Fig. 49 shows that increasing strain rate reduces moderately the SRS of twinned samples, while the SRS of the untwinned sample is independent of the strain rate. The SRS of nano-twinned Cu sample with a small twin boundary spacing of 15 nm is significantly higher than that of the nano-twinned Cu sample with a larger twin boundary spacing of 100 nm, while the SRS of the untwinned sample is the lowest among the three samples.

Lu et al. [292] carried out a series of systematic experiments of depth-sensing instrumented indentation with varying loading rates by three orders of magnitude, demonstrating that increasing the density of growth twins in UFG pure Cu leads to a significant increase in the strain rate-sensitivity. Fig. 50 shows nanoindentation hardness plotted as a function of loading rate for UFG Cu with different twin densities. By assuming indentation hardness and loading rate are equivalent to stress and strain rate, respectively, the SRS m for the three materials are calculated using the relationship of $\sigma \propto \dot{\varepsilon}^m$. The results indicate that the SRS m for Cu with a lower twin density (average twin boundary spacing $\sim$90 nm) and with a higher twin density (twin boundary spacing $\sim$20 nm) is 0.025 ± 0.009 and 0.036 ± 0.009, while the SRS for UFG Cu without twin, evaluated from tension tests instead of indentation because of the large scatter in the indentation response, is only 0.005 ± 0.001. TEM microstructural investigation suggested that deformation-induced displacement of coherent twin boundaries (CTBs), formation of steps and jogs along CTBs, and blockage of dislocations at CTBs significantly
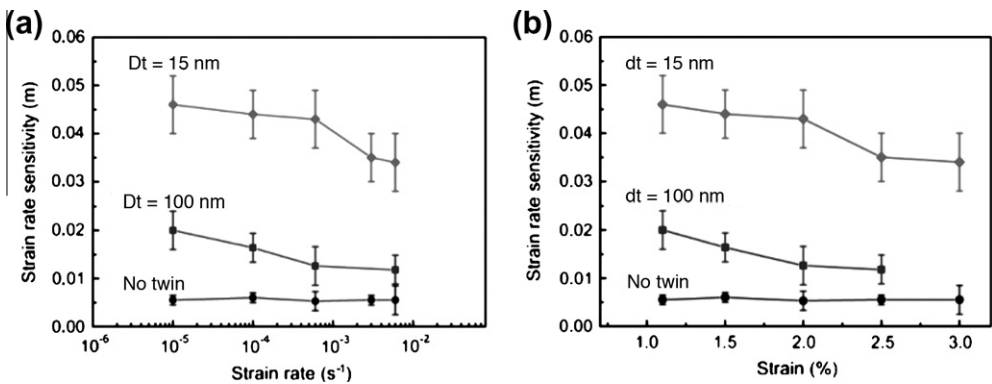

Fig. 49. The strain rate sensitivity as a function of (a) strain rate and (b) grain size for UFG coppers with no twin, twin boundary spacing is 100 ± 15 nm, and twin boundary spacing is 15 ± 7 nm [195].
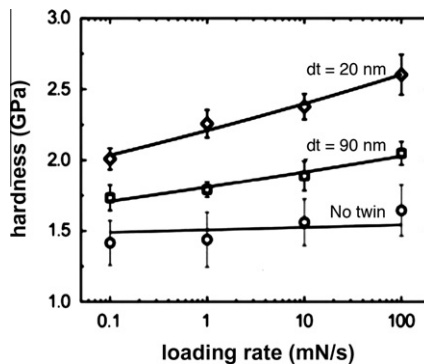

Fig. 50. The hardness as a function of loading for UFG coppers with no twin, twin boundary spacing is 90 nm, and twin boundary spacing is 20 nm [292].

influence the evolution of thermal activation volume for plastic flow, which is some three orders of magnitude smaller than that known for microcrystalline Cu.

Lu et al. [293] summarized the experimental results on the effect of twin lamellar thickness d (or λ) on the strain rate sensitivity m of nano-twinned copper, as shown in Fig. 51. They reported that m can be one order of magnitude higher than conventional coarse-grained materials when λ is reduced down to about 15 nm. For comparison purpose, the m values of nanocrystalline copper, with grain size d replacing twin lamellar thickness λ, are also plotted in the figure. It is very clear that the dependence of m on λ and d are very similar.

Asaro and Suresh [29] proposed that the rate-controlling mechanism for nc materials is grain boundary mediated dislocation activity, which is different from the bulk dislocation–dislocation interaction (forest hardening) in coarse-grained materials [294]. They developed mechanism-based models that rationalize the distinct deformation characteristics of fcc metals with grain size and twin dimensions in the nanometer regime. They developed estimates of flow stress as a function of strain rate and activation volume by exploring the roles of crystal stacking energies, such as the intrinsic stacking fault and the unstable stacking fault energy, in the process of initiating deformation via the emission of either partial dislocations or perfect dislocations from the grain or twin boundaries of nc FCC metals. Results obtained from their models are consistent with available experimental data on activation volumes and rate sensitivity in both a quantitative and qualitative manner.

8.2. Strain hardening rate

For coarse-grained materials, twinning has been known to contribute significantly to plastic deformation in materials with low SFE [295,296]. Higher rates of strain hardening have been reported in low SFE alloys due to deformation twinning that acts as strong barriers to dislocation motion, which consequently resulted in higher tensile ductility [297–302]. Through the analysis of the barriers to slip caused by twinning in an fcc crystal, Mahajan and Chin [74] predicted that the strain-hardening rate should be increased by the formation of twins. The prediction was supported by experimental results on polycrystalline coarse-grained FCC 70/30 brass and MP35 N with low stacking fault energies [81,303]. Ma et al. reported that the strain hardening rate of nano-twinned copper is much higher than that of UFG Cu [304].

Chen and Lu [305] measured the strain hardening rates of four UFG Cu samples – nt-Cu-20 with twin spacing of ~20 ± 4 nm (nt = nanotwin), nt-Cu-36 with twin spacing of ~36 ± 7 nm, nt-Cu-90 with twin spacing of 90 ± 26 nm, and UFG-Cu without twin, using uniaxial tensile tests. Fig. 52 shows strain hardening rates plotted against the true strain for the four samples. As shown, the strain-hardening rate is achieved in nt-Cu-20 at stresses that is higher than that of the other three samples. The highest strain-hardening rate is also seen in nt-Cu-20 over a range of strains. Comparison of the values of the strain hardening rates obtained from the three nt-Cu specimens leads to the conclusion that introducing nanoscale twins into UFG grains enhances strain hardening rate significantly.
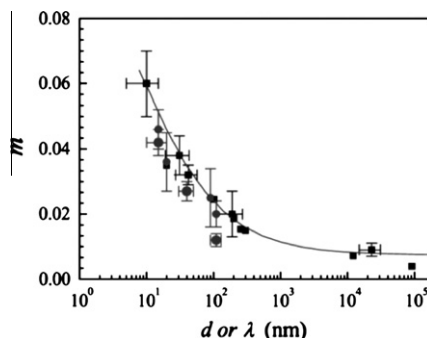

Fig. 51. The effect of the twin lamellar thickness d (or λ) on the strain rate sensitivity m [283].
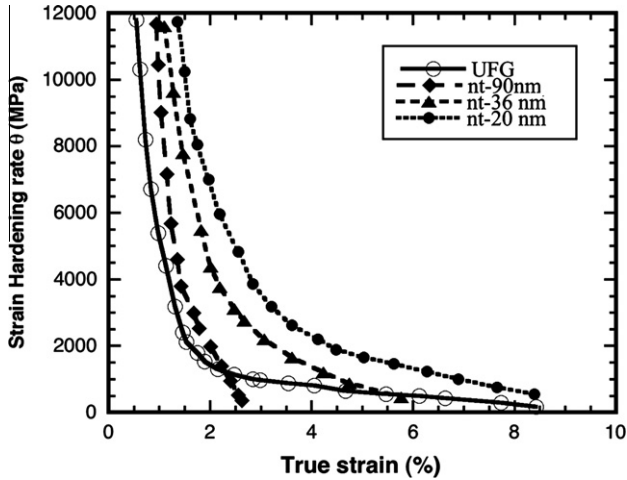
Fig. 52. The strain hardening rates of four copper samples measured by tensile tests: nano twinned sample with a twin spacing of 20 nm (nt-20 nm), nano twinned sample with a twin spacing of 36 nm (nt-36 nm), nano twinned sample with a twin spacing of 90 nm (nt-90 nm), and UFG sample without twin [305].

8.3. Strength and ductility

It has been well accepted that twin boundaries are equivalent to conventional grain boundaries with respect to the H–P effect [306–312], i.e., the same H–P slope for both twin boundaries and grain boundaries [290], because twin boundaries are strong barriers for dislocation motion [310–313]. Significant enhancement of tensile strength in copper [40,314] and hardness in fcc γ phase 330 stainless steel thin films [315] as well as fcc Cu/330 stainless steel multilayer films [316,317] was achieved by nano twins. Growth twins in Copper [291] and Nickel [195] and deformation twins in steel [292] with twin boundary spacing of tens to hundreds of nanometers show H–P behavior.

Nano-twinned FCC 330 stainless steel [294] with an average columnar grain size of ∼30 nm and an average twin spacing of ∼4 nm is observed to have a hardness of ∼6.5 GPa, while the hardness of bulk conventional 330 SS is only ∼200 MPa. However, the hardness value cannot be explained using the H–P relationship extrapolated from data of other similar steels [294]. This phenomenon is explained as that, instead of dislocation pile-ups at twin boundaries, materials with this extremely fine twin spacing are strengthened via single dislocations transmission across twin boundaries, in which the twin boundaries act as strong barriers for the transmission of dislocations. The mechanism has also been used to explain the observed phenomena that in FCC Cu/330 stainless steel multilayer films with high densities of twins in the nano Cu and 330 SS layers, the increase of hardness with decreasing layer thickness follows the Hall–Petch law for layer thickness greater than about 50 nm, but at lower layer thickness the hardness saturates to a value of about 5 GPa [296].

Lu et al. [41] reported that reducing the thickness of twins down to 15 nm in nano-twinned (nt) Cu samples resulted in continuous increase in strength. However, further reducing the thickness resulted in softening accompanied by enhanced strain hardening and tensile ductility, i.e., the maximum strength of nt-Cu samples exists at a twin thickness of 15 nm (see Fig. 53). They suggested that the strongest twin thickness originates from a transition in the yielding mechanism from the slip transfer across twin boundaries to the activity of preexisting easy dislocation sources. Curves for a twin-free UFG-Cu with a mean grain size of 500 nm and for a coarse-grained-Cu with a mean grain size of 10 mm are included for the comparison purpose.

The maximum strength observed by Lu et al. [41] is consistent with an MD simulation [50], and was further investigated using large-scale MD simulations and a kinetic theory of dislocation nucleation by Li et al. [318]. They proposed a dislocation–nucleation-controlled mechanism in
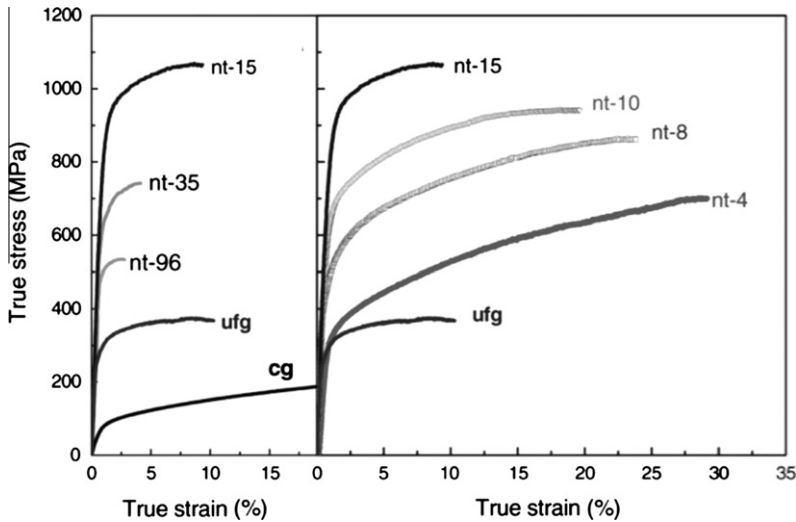
Fig. 53. Tensile true stress–strain curves of nano twinned copper tested at a strain rate of $6 \times 10^{-2}\,\text{s}^{-1}$ [41].

nano-twinned metals, in which there are plenty of dislocation nucleation sites but dislocation motion is not confined. They showed that dislocation nucleation governs the strength of such materials, resulting in the softening of the materials below a critical twin thickness. They found that there exists a transition in deformation mechanism, occurring at a critical twin-boundary spacing for which strength is maximized. At this point, the classical Hall–Petch type of strengthening due to dislocation pile-up and cutting through twin planes switches to a dislocation–nucleation-controlled softening mechanism with twin-boundary migration resulting from nucleation and motion of partial dislocations parallel to the twin planes.

Deformation twins produced by plastic deformation can also significantly improve the strength and ductility of nanostructured materials [51,153,221,319,320]. It has been reported that lowering SFE can simultaneously increase the strength and ductility of nanostructured materials [51]. Zhao et al. produced nanostructured Cu, Cu–10 wt.% Zn, and Cu–30 wt.% Zn alloys using HPT to study their mechanical properties. Their stacking fault energies decrease with increasing Zn content and are 41 mJ/m^2, 22 mJ/m^2, and 7 mJ/m^2, respectively [221,321]. TEM and X-ray analysis revealed that as the stacking fault energy decreased from 41 mJ/m^2 to 7 mJ/m^2, the grain size decreased from 180 nm to 10 nm, the dislocation density increased from $0.23 \times 10^{15}\,\text{m}^{-2}$ to $3.10 \times 10^{15}\,\text{m}^{-2}$, and twin density, defined as the probability of finding a twin boundary between any two adjacent {1 1 1} planes, increased from 0.1% to 8.0% [221].

Fig. 54 shows the engineering stress–strain curves of the three samples. As shown, the strength increases monotonically with decreasing stacking fault energy. However, the ductility first increases (the Cu–10 wt.% Zn sample) and then decreases, indicating an optimum stacking fault energy for the best ductility. X-ray analysis revealed that the Cu–10 wt.% Zn sample has the best capability to accumulate dislocations, twins and stacking faults, and therefore has the highest hardening capability during the tensile testing. On the other hand, the Cu–30 wt.% Zn sample has the highest densities of twins and dislocations, which are already saturated before the tensile testing, making it impossible to further accumulate these crystalline defects during the tensile testing. This leads to very low strain hardening rate and consequently low ductility. It will be interesting to see if a controlled annealing of the sample could reduce the initial defect density and recover the strain hardening.

Note that the strength increase shown in Fig. 54 is partially caused by the solution hardening of the Zn solute. To isolate the effect of stacking fault energy, Sun et al. recently investigated the Co–Ni alloy, which has a systematic decrease in stacking fault energy with increasing Co content, but very little solution hardening [319]. The results confirmed that lower stacking fault energy improves both
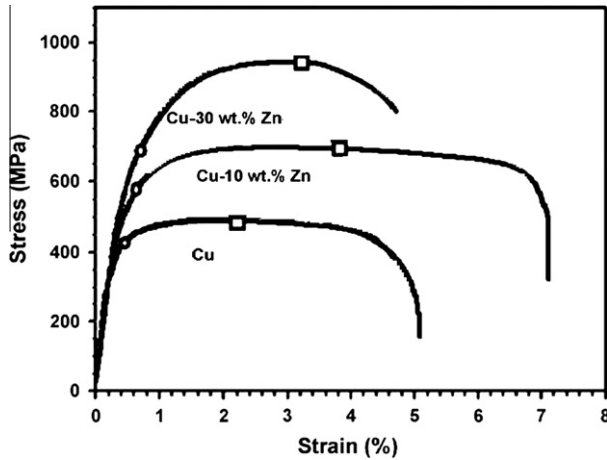
Fig. 54. The engineering stress–strain curves Cu, Cu–10 wt.% Zn, and Cu–30 wt.% Zn samples processed by HPT [221]. The gage dimension is 0.15 mm × 2 mm × 10 mm.

strength and ductility of NS materials. These data are very preliminary and further study is needed to probe this issue, especially when the stacking fault energy is very low.

8.4. Fatigue

This has not been extensively studied. A study on the effect of cyclic deformation on multilayer Cu/ Cu samples with nanoscale twinning showed that (1) nano-twinned Cu is much more stable under cyclic deformation than equiaxed nanocrystalline Cu and (2) the fatigue of nano-twinned Cu is improved significantly over that of coarse-grained Cu [322]. However, although twin boundaries are strong in resisting fatigue cracking, it is also observed that some fatigue cracks could propagate along the twin boundary [323]. Another recent study found that detwinning happened during the cyclic deformation of nanocrystalline NiFe [324].

8.5. Conductivity

It is desirable for conducting metals to have both high strength and high electrical conductivity for many applications. However, many strengthening mechanisms including grain size refinement, cold working and alloying produce crystalline imperfections that serve as the scattering centers for conduction electrons in metals and therefore lower the conductivity. On the other hand, coherent twin boundaries, which are very effective in increasing strength, have an electron scattering coefficient that is an order of magnitude lower than that of conventional high-angle grain boundaries. Indeed, Anderoglu et al. reported that single-crystal-like nano-twinned copper films with average twin lamella thickness of 7–16 nm produced by magnetron sputtering exhibited much higher ratio of conductivity to strength as compared to nc columnar, textured, nano-twinned copper [325].

Lu et al. synthesized pure copper samples with a high density of nanoscale growth twins [40]. They showed a tensile strength about 10 times higher than that of conventional coarse-grained copper, while retaining an electrical conductivity comparable to that of pure copper. In comparison, the electrical conductivity values of the nc Cu foil without twins were at least one order of magnitude lower. The electrical resistivity can be described using the empirical Matthiessen's Rule, $\rho_{total} = \rho_t + \rho_i + \rho_d$, where ρ_{total} is the total resistivity of a metal, ρ_t, ρ_i, and ρ_d are the contributions from vibrations, impurities, and lattice defects such as dislocations and grain boundaries, respectively. The difference in the lattice dislocation density among the samples could be ignored, the major factor that contributes to the difference in electrical resistivity should be grain boundaries and twin boundaries. It has been

known that electrical resistivity of grain boundaries [326] and twin boundaries [327] in Cu at 295 K is about $3.6 \times 10^{-16}\,\Omega\,m^2$ and about $1.7 \times 10^{-17}\,\Omega\,m^2$, respectively. Therefore, the contribution to electrical conductivity from twin boundaries is much smaller than that from grain boundaries. This explains why the nano-twinned samples have conductivity that is close to that of the coarse-grained Cu.

9. Outstanding issues

There are still many outstanding issues for the materials community to solve. Most studies on deformation twinning in nc metals have focused on the fcc systems, while very few studies have concerned the nc bcc and hcp metals and alloys. Furthermore, the mechanisms for the formation of deformation twins are not very well studied even for coarse-grained bcc and hcp metals and alloys. Although the twinning mechanisms for coarse-grained and nc hcp metals are already under investigation [159–161,163,166,170,241,273,277,328–333], it is not clear if the twinning phenomena and mechanisms observed in nc fcc metals also occur in nc bcc and fcc systems. For example, it is unknown if the grain size effect on deformation twinning observed in nc fcc metals also exists in nc bcc and hcp metals. In fact, as discussed in Section 6.2, deformation twinning is rarely observed in nc hcp systems. It will take significant efforts by researchers using both MD simulation and experimental observations to establish the basic understanding of deformation twinning in nc bcc and hcp metals and alloys.

Even for nc fcc metals and alloys, there are still issues that need further study. As discussed in Section 5.8.5, to establish a comprehensive model to describe the twinning behavior of nc fcc metals, we need to understand how the GPFEs affect the nucleation of first partials and twinning partials. Currently, it is not clear if the GPFE curves affect the nucleation of dislocations since non-equilibrium grain boundaries existing in nc metals can also act as a dislocation source. More experimental studies are needed to clarify this issue. In addition, the GPFEs may also affect the slip of the first and twinning partials. Theoretical modeling is needed to develop a formula for calculating the Peierls stress for the slip of these partials from the GPFEs.

Another outstanding issue is the grain size effect on the detwinning in nc metals and alloys. Almost all studies so far have focused on the formation of deformation twins. There have been recent studies on the detwinning process in nc materials also occurs in the nc fcc metals [131,156,227,246,285,286,334,335]. However, issues that are of interest for future studies include: (a) more experimental observations on the de-twinning process to compare with the proposed mechanisms [285,335], (b) the grain size effect of de-twinning, and (c) the existence of an equilibrium twin density and thickness.

10. Implications of deformation twinning within materials science

The discovery of new mechanisms for the formation of deformation twins in nc fcc metals has significantly extended our understanding of the deformation physics of metals and alloys as well as the role of grain boundaries in the deformation of fcc metals. It gives us a more complete picture on how the deformation mechanisms change with grain size [3]. As the grains of an fcc metal become smaller, dislocation sources that are active in coarse-grains, such as the Frank-Reed dislocation source, become inactive or more and more marginalized. Concurrently, grain boundary-mediated deformation mechanisms become active and eventually dominant [336]. In grain size range of a few tens to above 100 nm, grain boundaries become the source and sink of dislocations. Particularly, the emission of partial dislocations from grain boundaries becomes significant in nc fcc metals, even in systems with medium to high stacking fault energies. This leads to the formation stacking faults and deformation twins, which also shows grain size dependence. When the grain sizes decrease further, grain rotation and grain boundary sliding becomes dominant, which may also be assisted by diffusion and dislocation activities.

The new deformation mechanisms and deformation twinning discussed in this paper also provide fundamental physics for materials scientists to model the mechanical behavior of nc materials. For example, the strength of nc materials have been observed to deviate from the Hall–Petch relationship,

and even exhibit an inverse Hall–Petch relationship in some cases. Numerous analytical models and computational simulations have been carried out to describe and investigate this phenomenon [336–355]. The analytical Hall–Petch models are based on various assumptions and all of them can qualitatively describe the inverse grain size effect on strength. This makes it difficult to judge which models are physically better and more valuable. Any valuable analytical model or computer simulation on the mechanical properties must be based on real deformation physics. It is hoped that the deformation physics and deformation twinning of nc materials discussed in this review will be useful for future modeling of mechanical properties.

The deformation twinning also provides an effective approach for simultaneously improve the strength and ductility of nc materials, as discussed in Section 8.3. Due to the lack of dislocation accumulation in the interior of grains, nc materials usually have low tensile ductility. The twins could act as the barrier to dislocation slip and to enable dislocation accumulation, which increases both the strength and ductility. However, the effect of twins and deformation twinning on many other mechanical and physical properties needs to be further studied.

11. Summary and concluding remarks

In summary, nanocrystalline fcc metals deform by twinning more readily than their coarse-grained counterparts. Deformation twins in nanocrystalline fcc metals are largely formed by the emissions of Shockley partial dislocations from grain boundaries of nano-sized grains. In other words, the grain boundary acts as the source of partial dislocations in most cases. Another important source for partial dislocations is the dislocation reactions at the twin boundaries, which is the primary mechanism for the formation of multiple twins. Non-equilibrium grain boundaries play an important role in the deformation twinning because they may provide ready partials for the nucleation of stacking faults and twins. The partials emitted from grain boundaries may not have the same Burgers vector, which leads to twins with reduced or even zero shape change in the twinned grain. This is in sharp contrast to twins formed by mechanisms in coarse-grained metals, which have the same Burgers vector.

Both grain size and generalized stacking fault energy influences the formation of deformation twins in nanocrystalline fcc metals. There is an optimum grain size in nanocrystalline fcc metals at which the twinning is easiest, and this optimum grain size can be estimated from an analytical equation. Factors that affect the optimum grain size for twinning include the stacking fault energy and the shear modulus. When grains are smaller than the optimized grain size for twinning, an inverse grain size effect exists, where the twinning becomes more difficult with decreasing grain size. However, no inverse grain size effect on stacking fault formation exists. This difference is explained by the generalized planar fault energy effect, where the unstable twin fault energy is higher than unstable stacking fault energy. Therefore, both grain size effect and the generalized planar fault energy effect need to be considered in an analytical model to describe more accurately the twinning mechanisms in nanocrystalline fcc metals. Such a model is yet to be developed.

Deformation twinning and dislocation slip usually occur simultaneously during the deformation of nanocrystalline metals. The interactions of the dislocations with twins are very complex and the proposed interactions need to be further verified experimentally. Twin boundaries are effective barriers to dislocation slip, and consequently twins can increase the strength of nanocrystalline and nanostructured materials. Twins are also found to increase the strain hardening rate and the strain rate sensitivity, which leads to increase in ductility. Therefore, twinning is a mechanism that can simultaneously increase the strength and ductility. In the design of new nanocrystalline alloys for high strength, ductility and toughness, stacking fault energy can be adjusted by alloying to promote deformation winning.

References

[1] Christian JW, Mahajan S. Prog Mater Sci 1995;39:1.
[2] Wu XL, Liao XZ, Srinivasan SG, Zhou F, Lavernia EJ, Valiev RZ. Phys Rev Lett 2008;100:095701.
[3] Zhu YT, Langdon TG. Mater Sci Eng A 2005;409:234.
[4] Humphreys FJ, Hatherly S. Recrystallization and related annealing phenomena. New York: Pergamon; 1995.
[5] Gubicza J, Chinh NQ, Labar JL, Hegedus Z, Langdon TG. J Mater Sci 2009;44:1656.
[6] Chen MW, Ma E, Hemker KJ, Sheng HW, Wang YM, Cheng XM. Science 2003;300:1275.
[7] Liao XZ, Zhao YH, Zhu YT, Valiev RZ, Gunderov DV. J Appl Phys 2004;96:636.
[8] Liao XZ, Zhao YH, Srinivasan SG, Zhu YT, Valiev RZ, Gunderov DV. Appl Phys Lett 2004;84:592.
[9] Yamakov V, Wolf D, Phillpot SR, Mukherjee AK, Gleiter H. Nature Mater 2002;1:45.
[10] Van Swygenhoven H, Derlet PM, Froseth AG. Nature Mater 2004;3:399.
[11] Meyers MA, Vohringer O, Lubarda VA. Acta Mater 2001;49:4025.
[12] Koch CC. Bulk behavior of nanostructured materials. In: Siegel RW, HuE., Roco MC, editors. Final report by WTEC panel; 1999. p. 93.
[13] Koch CC. Scripta Mater 2003;49:657.
[14] Nieman GW, Weertman JR, Siegel RW. J Mater Res 1991;6:1012.
[15] Gleiter H. Prog Mater Sci 1989;33:223.
[16] Valiev RZ, Estrin Y, Horita Z, Langdon TG, Zehetbauer MJ, Zhu YT. JOM 2006;58(4):33.
[17] Valiev RZ. Nature Mater 2004;3:511.
[18] Zhu YT, Langdon TG. JOM 2004;56(10):58.
[19] Agnew SR, Elliott BR, Youngdahl CJ, Hemker KJ, Weertman JR. Mater Sci Eng A 2000;285:391.
[20] Zhao YH, Guo YZ, Wei Q, Topping TD, Dangelewicz AM, Zhu YT. Mater Sci Eng A 2009;525:68.
[21] Zhao YH, Guo YZ, Wei Q, Dangelewiez AM, Zhu YT, Langdon TG. Scripta Mater 2008;59:627.
[22] Wolf D, Yamakov V, Phillpot SR, Mukherjee A, Gleiter H. Acta Mater 2005;53:1.
[23] Liao XZ, Zhou F, Lavernia EJ, Srinivasan SG, Baskes MI, He DW. Appl Phys Lett 2003;83:632.
[24] Schiotz J, Di Tolla FD, Jacobsen KW. Nature 1998;391:561.
[25] Shan ZW, Stach EA, Wiezorek JMK, Knapp JA, Follstaedt DM, Mao SX. Science 2004;305:654.
[26] Van Swygenhoven H, Derlet PM, Hasnaoui A. Phys Rev B 2002;66:024101.
[27] Kumar KS, Suresh S, Chisholm MF, Horton JA, Wang P. Acta Mater 2003;51:387.
[28] Liao XZ, Kilmametov AR, Valiev RZ, Gao HS, Li XD, Mukherjee AK. Appl Phys Lett 2006;88:021909.
[29] Asaro RJ, Suresh S. Acta Mater 2005;53:3369.
[30] Rice JR. J Mech Phys Solids 1992;40:239.
[31] Wang YM, Hodge AM, Biener J, Hamza AV, Barnes DE, Liu K. Appl Phys Lett 2005;86:101915.
[32] Huang CX, Wang K, Wu SD, Zhang ZF, Li GY, Li S. Acta Mater 2006;54:655.
[33] Wu XL, Ma E. Appl Phys Lett 2006;88:061905.
[34] Wu X, Zhu YT, Chen MW, Ma E. Scripta Mater 2006;54:1685.
[35] Wu XL, Zhu YT, Ma E. Appl Phys Lett 2006;88:121905.
[36] Van Swygenhoven H, Derlet PA. Phys Rev B 2001;64:224105.
[37] Yamakov V, Wolf D, Phillpot SR, Mukherjee AK, Gleiter H. Nature Mater 2004;3:43.
[38] Ke M, Hackney SA, Milligan WW, Aifantis EC. Nanostruct Mater 1995;5:689.
[39] Wang YB, Ho JC, Liao XZ, Li HQ, Ringer SP, Zhu YT. Appl Phys Lett 2009;94:011908.
[40] Lu L, Shen YF, Chen XH, Qian LH, Lu K. Science 2004;304:422.
[41] Lu K, Lu L, Suresh S. Science 2009;324:349.
[42] Zhu YT, Narayan J, Hirth JP, Mahajan S, Wu XL, Liao XZ. Acta Mater 2009;57:3763.
[43] Sennour M, Lartigue-Korinek S, Champion Y, Hytch MJ. Philos Mag 2007;87:1465.
[44] Sennour M, Lartigue-Korinek S, Champion Y, Hytch MJ. J Mater Sci 2008;43:3806.
[45] Yamakov V, Wolf D, Phillpot SR, Gleiter H. Acta Mater 2003;51:4135.
[46] Sansoz F, Huang HC, Warner DH. JOM 2008;60(9):79.
[47] Afanasyev KA, Sansoz F. Nano Lett 2007;7:2056.
[48] Henager CH, Hoagland RG. Scripta Mater 2004;50:701.
[49] Jin J, Shevlin SA, Guo ZX. Acta Mater 2008;56:4358.
[50] Shabib I, Miller RE. Acta Mater 2009;57:4364.
[51] Zhao YH, Zhu YT, Liao XZ, Horita Z, Langdon TG. Appl Phys Lett 2006;89:121906.
[52] Chen KC, Wu WW, Liao CN, Chen LJ, Tu KN. Science 2008;321:1066.
[53] Smith WF, Hashemi J. Foundations of materials science and engineering. Boston: McGraw-Hill; 2006.
[54] Hirth JP, Lothe J. Theory of dislocations. Malabar (FL): Krieger Publishing Company; 1992.
[55] Arzaghi M, Beausir B, Toth LS. Acta Mater 2009;57:2440.
[56] Zhu YT, Liao XZ, Wu XL. JOM 2008;60(9):60.
[57] Zhu YT, Liao XZ, Srinivasan SG, Zhao YH, Baskes MI, Zhou F. Appl Phys Lett 2004;85:5049.
[58] Li J, Wang CZ, Chang JP, Cai W, Bulatov VV, Ho KM. Phys Rev B 2004;70:104113.
[59] Zhu YT, Liao XZ, Srinivasan SG, Lavernia EJ. J Appl Phys 2005;98:034319.
[60] Valiev RZ, Alexandrov IV, Zhu YT, Lowe TC. J Mater Res 2002;17:5.
[61] Zhu YT, Huang JY, Gubicza J, Ungar T, Wang YM, Ma E. J Mater Res 2003;18:1908.
[62] Raab GJ, Valiev RZ, Lowe TC, Zhu YT. Mater Sci Eng A 2004;382:30.
[63] Lowe TC, Zhu YT. Adv Eng Mater 2003;5:373.

[64] Valiev RZ, Islamgaliev RK, Alexandrov IV. Prog Mater Sci 2000;45:103.
[65] Liao XZ, Huang JY, Zhu YT, Zhou F, Lavernia EJ. Philos Mag 2003;83:3065.
[66] Liao XZ, Zhou F, Lavernia EJ, He DW, Zhu YT. Appl Phys Lett 2003;83:5062.
[67] Narayana J, Zhu YT. Appl Phys Lett 2008;92:151908.
[68] Wu XL, Ma E, Zhu YT. J Mater Sci 2007;42:1427.
[69] Wu XL, Narayan J, Zhu YT. Appl Phys Lett 2008;93:031910.
[70] Zhu YT, Liao XZ, Valiev RZ. Appl Phys Lett 2005;86:103112.
[71] Ookawa A. J Phys Soc Jpn 1957;12:825.
[72] Venables JA. Philos Mag 1961;6:379.
[73] Niewczas M, Saada G. Philos Mag A 2002;82:167.
[74] Mahajan S, Chin GY. Acta Metall 1973;21:1353.
[75] Mahajan S, Green ML, Brasen D. Metall Trans A 1977;8:283.
[76] Thompson N. Proc Phys Soc Lond Sect B 1953;66:481.
[77] Wu XL, Zhu YT, Wei YG, Wei Q. Phys Rev Lett 2009;103:205504.
[78] Youssef KM, Scattergood RO, Murty KL, Horton JA, Koch CC. Appl Phys Lett 2005;87:091904.
[79] Kibey S, Liu JB, Johnson DD, Sehitoglu H. Acta Mater 2007;55:6843.
[80] Meyers MA, Mishra A, Benson DJ. Prog Mater Sci 2006;51:427.
[81] El-Danaf E, Kalidindi SR, Doherty RD. Metall Mater Trans A 1999;30:1223.
[82] Romhanji E, Milenkovic V, Drobnjak D. Z Metall 1992;83:110.
[83] Lahaie D, Embury JD, Chadwick MM, Gray GT. Scripta Metall Mater 1992;27:139.
[84] Meyers MA, Andrade UR, Chokshi AH. Metall Mater Trans A 1995;26:2881.
[85] Blewitt TH, Coltman RR, Redman JK. J Appl Phys 1957;28:651.
[86] Meyers MA, Gregori F, Kad BK, Schneider MS, Kalantar DH, Remington BA. Acta Mater 2003;51:1211.
[87] Murr LE. Residual microstructure–mechanical property relationships in shock-loaded metals and alloys. New York (NY): Plenum Press; 1981.
[88] Cao F, Beyerlein IJ, Addessio FL, Sencer BH, Trujillo CP, Cerreta EK. Acta Mater 2010;58:549.
[89] Bell RL, Cahn RW. Proc Phys Soc Lond Ser A 1957;239:494.
[90] Bolling GF, Richman RH. Acta Metall 1965;13:709.
[91] Venables JA. Deformation twinning. New York: Gordon & Breach; 1964.
[92] Reed-Hill RE. Inhomogeneity of plastic deformation. Metals Park (OH): ASM; 1973.
[93] Harding J. Mem Sci Rev Metall 1968;65:245.
[94] Harding J. Proc Phys Soc Lond Ser A 1967;299:464.
[95] Humphreys FJ, Hatherly M. Recrystallization and related annealing phenomena. Kidlington: Elsevier Science Ltd; 1995.
[96] Wang YM, Ma E, Valiev RZ, Zhu YT. Adv Mater 2004;16:328.
[97] Stolyarov VV, Valiev RZ, Zhu YT. Appl Phys Lett 2006;88:041905.
[98] Stolyarov VV, Zhu YT, Alexandrov IV, Lowe TC, Valiev RZ. Mater Sci Eng A 2003;343:43.
[99] Stolyarov VV, Zhu YT, Lowe TC, Valiev RZ. Mater Sci Eng A 2001;303:82.
[100] Wang YB, Ho JC, Cao Y, Liao XZ, Li HQ, Zhao YH. Appl Phys Lett 2009;94:091911.
[101] Wang ZW, Wang YB, Liao XZ, Zhao YH, Lavernia EJ, Zhu YT. Scripta Mater 2009;60:52.
[102] Wang YM, Ma E. Acta Mater 2004;52:1699.
[103] Li YS, Tao NR, Lu K. Acta Mater 2008;56:230.
[104] Xiao GH, Tao NR, Lu K. Mater Sci Eng A 2009;513–514:13.
[105] Hasnaoui A, Van Swygenhoven H, Derlet PM. Phys Rev B 2002;66:184112.
[106] Sergueeva AV, Mara NA, Krasilnikov NA, Valiev RZ, Mukherjee AK. Philos Mag 2006;86:5797.
[107] Ivanisenko Y, Kurmanaeva L, Weissmueller J, Yang K, Markmann J, Rosner H. Acta Mater 2009;57:3391.
[108] Chinh NQ, Szommer P, Horita Z, Langdon TG. Adv Mater 2006;18:34.
[109] Ovid'ko IA, Sheinerman AG. Acta Mater 2009;57:2217.
[110] Bobylev SV, Ovid'ko IA. Appl Phys Lett 2008;92:081914.
[111] Gutkin MY, Ovid'ko IA, Skiba NV. Acta Mater 2003;51:4059.
[112] Gutkin MY, Ovid'ko IA, Skiba NV. Phys Solid State 2005;47:1662.
[113] Zelin MG, Mukherjee AK. Philos Mag A 1993;68:1183.
[114] Zelin MG, James RW, Mukherjee AK. J Mater Sci 1993;12:176.
[115] Bobylev SV, Morozov NF, Ovid'ko IA. Phys Rev Lett 2010:105.
[116] Zelin MG, Dunlap MR, Rosen R, Mukherjee AK. J Appl Phys 1993;74:4972.
[117] Shan ZW, Wiezorek JMK, Knapp JA, Follstaedt DM, Stach EA, Mao SX. Appl Phys Lett 2008;92:091917.
[118] Jin M, Minor AM, Stach EA, Morris JW. Acta Mater 2004;52:5381.
[119] Wang YB, Li BQ, Sui ML, Mao SX. Appl Phys Lett 2008;92:011903.
[120] Farkas D, Mohanty S, Monk J. Mater Sci Eng A 2008;493:33.
[121] Sansoz F, Dupont V. Appl Phys Lett 2006;89:111901.
[122] Gutkin MY, Ovid'ko IA. Appl Phys Lett 2005;87:251916.
[123] Ovid'ko IA. Science 2002;295:1.
[124] Fan GJ, Fu LF, Wang YD, Ren Y, Choo H, Liaw PK. Appl Phys Lett 2006;89:101918.
[125] Yang B, Vehoff H, Hohenwarter A, Hafok M, Pippan R. Scripta Mater 2008;58:790.
[126] Markmann J, Bunzel P, Rosner H, Liu KW, Padmanabhan KA, Birringer R. Scripta Mater 2003;49:637.
[127] Weissmuller J, Markmann J. Adv Eng Mater 2005;7:202.
[128] Haslam AJ, Moldovan D, Yamakov V, Wolf D, Phillpot SR, Gleiter H. Acta Mater 2003;51:2097.
[129] Zhang K, Weertman JR, Eastman JA. Appl Phys Lett 2005;87.
[130] Zhang K, Weertman JR, Eastman JA. Appl Phys Lett 2004;85:5197.
[131] Li L, Ungar T, Wang YD, Morris JR, Tichy G, Lendvai J. Acta Mater 2009;57:4988.
[132] Li L, Ungar T, Wang YD, Fan GJ, Yang YL, Jia N. Scripta Mater 2009;60:317.

[133] Legros M, Dehm G, Keller-Flaig RM, Arzt E, Hemker KJ, Suresh S. Mater Sci Eng A 2001;309:463.
[134] Gianola DS, Warner DH, Molinari JF, Hemker KJ. Scripta Mater 2006;55:649.
[135] Gianola DS, Van Petegem S, Legros M, Brandstetter S, Van Swygenhoven H, Hemker KJ. Acta Mater 2006;54:2253.
[136] Fan GJ, Li L, Yang B, Choo H, Liaw PK, Saleh TA. Mater Sci Eng A 2009;506:187.
[137] Brandstetter S, Zhang K, Escuadro A, Weertman JR, Van Swygenhoven H. Scripta Mater 2008;58:61.
[138] Moldovan D, Yamakov V, Wolf D, Phillpot SR. Phys Rev Lett 2002;89:206101.
[139] Sharon JA, Su P-C, Prinz FB, Hemker KJ. Scripta Mater 2011;64:25.
[140] Zhu YT, Liao XZ. Nature Mater 2004;3:351.
[141] Budrovic Z, Van Swygenhoven H, Derlet PM, Van Petegem S, Schmitt B. Science 2004;304:273.
[142] Zhu YT, Kolobov YR, Grabovetskaya GP, Stolyarov VV, Girsova NV, Valiev RZ. J Mater Res 2003;18:1011.
[143] Wang LH, Han XD, Liu P, Yue YH, Zhang Z, Ma E. Phys Rev Lett 2010;105.
[144] Yamakov V, Wolf D, Salazar M, Phillpot SR, Gleiter H. Acta Mater 2001;49:2713.
[145] Xu C, Xia KN, Langdon TG. Acta Mater 2007;55:2351.
[146] Harai Y, Ito Y, Horita Z. Scripta Mater 2008;58:469.
[147] Xu C, Horita Z, Langdon TG. Acta Mater 2007;55:203.
[148] Zhao YH, Zhu YT, Liao XZ, Horita Z, Langdon TG. Mater Sci Eng A 2007;463:22.
[149] Zhao YH, Topping T, Bingert JF, Thornton JJ, Dangelewicz AM, Li Y. Adv Mater 2008;20:3028.
[150] Zhao YH, Liao XZ, Jin Z, Valiev RZ, Zhu YT. Acta Mater 2004;52:4589.
[151] Zhao YH, Liao XZ, Cheng S, Ma E, Zhu YT. Adv Mater 2006;18:2280.
[152] Zhao YH, Bingert JF, Zhu YT, Liao XZ, Valiev RZ, Horita Z. Appl Phys Lett 2008;92:081903.
[153] Zhao YH, Bingert JE, Liao XZ, Cui BZ, Han K, Sergueeva AV. Adv Mater 2006;18:2949.
[154] Mompiou F, Legros M, Caillard D, Mughrabi H. J Phys Conf Ser 2010;240:012137.
[155] Shan ZW, Wiezorek JMK, Stach EA, Follstaedt DM, Knapp JA, Mao SX. Phys Rev Lett 2007;98:095502.
[156] Wang YB, Sui ML, Ma E. Philos Mag Lett 2007;87:935.
[157] Yamakov V, Wolf D, Phillpot SR, Gleiter H. Acta Mater 2002;50:5005.
[158] Van Swygenhoven H, Derlet PM, Froseth AG. Acta Mater 2006;54:1975.
[159] Wang J, Hoagland RG, Hirth JP, Capolungo L, Beyerlein IJ, Tome CN. Scripta Mater 2009;61:903.
[160] Capolungo L, Marshall PE, McCabe RJ, Beyerlein IJ, Tome CN. Acta Mater 2009;57:6047.
[161] Capolungo L, Beyerlein IJ, Tome CN. Scripta Mater 2009;60:32.
[162] Capolungo L, Beyerlein IJ, Kaschner GC, Tome CN. Mater Sci Eng A – Struct Mater Proper Microstruct Process 2009;513–514:42.
[163] Capolungo L, Beyerlein IJ. Phys Rev B 2008;78:024117.
[164] Li B, Ma E. Acta Mater 2009;57:1734.
[165] Hosford WF. The mechanics of crystals and textured polycrystals. New York (NY): Oxford University Press; 1993.
[166] Chino Y, Kimura K, Mabuchi M. Mater Sci Eng A 2008;486:481.
[167] Wang YN, Huang JC. Acta Mater 2007;55:897.
[168] Wang YM, Huang JY, Jiao T, Zhu YT, Hamza AV. J Mater Sci 2007;42:1751.
[169] Sun HQ, Shi YN, Zhang MA, Lu K. Acta Mater 2007;55:975.
[170] Yapici GG, Karaman I, Luo ZP. Acta Mater 2006;54:3755.
[171] Wu XL, Zhu YT. Phys Rev Lett 2008;101:025503.
[172] Phillpot SR, Wolf D, Gleiter H. Scripta Metall Mater 1995;33:1245.
[173] Phillpot SR, Wolf D, Gleiter H. J Appl Phys 1995;78:847.
[174] VanSwygenhoven H, Caro A. Appl Phys Lett 1997;71:1652.
[175] Yamakov V, Wolf D, Phillpot SR, Gleiter H. Acta Mater 2002;50:61.
[176] Hasnaoui A, Van Swygenhoven H, Derlet PM. Acta Mater 2002;50:3927.
[177] Gleiter H. Adv Mater 1992;4:474.
[178] Gleiter H, Marquardt P. Z Metall 1984;75:263.
[179] Gleiter H. Nanostruct Mater 1995;6:3.
[180] Nieman GW, Weertman JR, Siegel RW. Scripta Metall 1989;23:2013.
[181] Fougere GE, Riester L, Ferber M, Weertman JR, Siegel RW. Mater Sci Eng A 1995;204:1.
[182] Fougere GE, Weertman JR, Siegel RW. Nanostruct Mater 1995;5:127.
[183] Sanders PG, Witney AB, Weertman JR, Valiev RZ, Siegel RW. Mater Sci Eng A 1995;204:7.
[184] Sanders PG, Eastman JA, Weertman JR. Acta Mater 1997;45:4019.
[185] Schiotz J, Jacobsen KW. Science 2003;301:1357.
[186] Rosner H, Markmann J, Weissmuller J. Philos Mag Lett 2004;84:321.
[187] Wu XL, Zhu YT. Appl Phys Lett 2006;89:031922.
[188] Wu XL, Qi Y, Zhu YT. Appl Phys Lett 2007;90:221911.
[189] Wang YM, Bringa EM, McNaney JM, Victoria M, Caro A, Hodge AM. Appl Phys Lett 2006;88:061917.
[190] Karch J, Birringer R, Gleiter H. Nature 1987;330:556.
[191] Chokshi AH, Rosen A, Karch J, Gleiter H. Scripta Metall 1989;23:1679.
[192] Gertsman VY, Hoffmann M, Gleiter H, Birringer R. Acta Metall Mater 1994;42:3539.
[193] Warner DH, Curtin WA, Qu S. Nature Mater 2007;6:876.
[194] Yamakov VI, Glaessgen EH. Nature Mater 2007;6:795.
[195] Shen YF, Lu L, Dao M, Suresh S. Scripta Mater 2006;55:319.
[196] Derlet PM, Van Swygenhoven H, Hasnaoui A. Philos Mag 2003;83:3569.
[197] Van Swygenhoven H. Science 2002;296:66.
[198] Froseth AG, Derlet PM, Van Swygenhoven H. Acta Mater 2004;52:5863.
[199] Hasnaoui A, Derlet PM, Van Swygenhoven H. Acta Mater 2004;52:2251.
[200] Farkas D, Van Petegem S, Derlet PM, Van Swygenhoven H. Acta Mater 2005;53:3115.
[201] Siegel DJ. Appl Phys Lett 2005;87:121901.

[202] Caturla MJ, Nieh TG, Stolken JS. Appl Phys Lett 2004;84:598.
[203] Wang J, Huang HC. Appl Phys Lett 2004;85:5983.
[204] Bringa EM, Caro A, Wang YM, Victoria M, McNaney JM, Remington BA. Science 2005;309:1838.
[205] Li XY, Wei YJ, Yang W, Gao HJ. Proc Natl Acad Sci USA 2009;106:16108.
[206] Cao AJ, Wei YG. J Appl Phys 2007;102:083511.
[207] Cao AJ, Wei YG. Phys Rev B 2007;76:024113.
[208] Tschopp MA, McDowell DL. Scripta Mater 2008;58:299.
[209] Zhu T, Li J, Samanta A, Kim HG, Suresh S. Proc Natl Acad Sci USA 2007;104:3031.
[210] Dupont V, Sansoz F. Acta Mater 2008;56:6013.
[211] Huang JY, Liao XZ, Zhu YT, Zhou F, Lavernia EJ. Philos Mag 2003;83:1407.
[212] Liao XZ, Srinivasan SG, Zhao YH, Baskes MI, Zhu YT, Zhou F. Appl Phys Lett 2004;84:3564.
[213] He JH, Chung KH, Liao XZ, Zhu YT, Lavernia EJ. Metall Mater Trans A 2003;34:707.
[214] Zhu YT, Wu XL, Liao XZ, Narayan J, Mathaudhu SN, Kecskes LJ. Appl Phys Lett 2009;95:031909.
[215] Li BQ, Sui ML, Li B, Ma E, Mao SX. Phys Rev Lett 2009;102:205504.
[216] Cao AJ, Wei YG. Appl Phys Lett 2006;89:041919.
[217] Wang YB, Wu B, Sui ML. Appl Phys Lett 2008;93:041906.
[218] Wang YB, Sui ML. Appl Phys Lett 2009;94:021909.
[219] Balogh L, Ungar T, Zhao Y, Zhu YT, Horita Z, Xu C. Acta Mater 2008;56:809.
[220] Gubicza J, Dragomir LC, Ribarik G, Zhu YT, Valiev R, Ungar T. Mater Sci Test Inform 2003;414–4:229.
[221] Zhao YH, Liao XZ, Horita Z, Langdon TG, Zhu YT. Mater Sci Eng A 2008;493:123.
[222] Zhao YH, Liao XZ, Zhu YT, Horita Z, Langdon TG. Mater Sci Eng A 2005;410:188.
[223] Tao NR, Wu XL, Sui ML, Lu J, Lu K. J Mater Res 2004;19:1623.
[224] Lu K, Lu J. J Mater Sci Technol 1999;15:193.
[225] Huang JY, Zhu YT, Jiang H, Lowe TC. Acta Mater 2001;49:1497.
[226] Froseth AG, Derlet PM, Van Swygenhoven H. Adv Eng Mater 2005;7:16.
[227] Wang J, Li N, Anderoglu O, Zhang X, Misra A, Huang JY. Acta Mater 2010;58:2262.
[228] Ashby MF, Harper E. Harvard report September. Cambridge (MA): Harvard University; 1967.
[229] Gryaznov VG, Heydenreich J, Kaprelov AM, Nepijko SA, Romanov AE, Urban J. Cryst Res Technol 1999;34:
     1091.
[230] Huang P, Dai GQ, Wang F, Xu KW, Li YH. Appl Phys Lett 2009;95:203101.
[231] Bringa EM, Farkas D, Caro A, Wang YM, McNaney J, Smith R. Scripta Mater 2008;59:1267.
[232] Kim C, Gu WH, Briceno M, Robertson IM, Choi H, Kim K. Adv Mater 2008;20:1859.
[233] Wu B, Heidelberg A, Boland JJ, Sader JE, Sun XM, Li YD. Nano Lett 2006;6:468.
[234] Huang JY, Wu YK, Ye HQ. Acta Mater 1996;44:1211.
[235] An XL, Lin QY, Wu SD, Zhang ZF, Figueiredo RB, Gao N. Scripta Mater 2011;64:249.
[236] Hall CR, Fawzi SAH. Philos Mag A 1986;54:805.
[237] Fujita H, Mori T. Scripta Metall 1975;9:631.
[238] Akarapu S, Zbib H, Hirth JP. Scripta Mater 2008;59:265.
[239] Dregia SA, Hirth JP. J Appl Phys 1991;69:2169.
[240] Fu HH, Benson DJ, Meyers MA. Acta Mater 2001;49:2567.
[241] Yu Q, Shan ZW, Li J, Huang XX, Xiao L, Sun J. Nature 2010;463:335.
[242] Cheng S, Stoica AD, Wang XL, Ren Y, Almer J, Horton JA. Phys Rev Lett 2009:103.
[243] Zhang JY, Liu G, Wang RH, Li J, Sun J, Ma E. Phys Rev B 2010;81:172104.
[244] Zhang Y, Tao NR, Lu K. Scripta Mater 2009;60:211.
[245] Zhao YH, Horita Z, Langdon TG, Zhu YT. Mater Sci Eng A 2008;474:342.
[246] Hu SY, Henager CH, Chen LQ. Acta Mater 2010;58:6554.
[247] Zhang XY, Wu XL, Zhu AW. Appl Phys Lett 2009;94:121907.
[248] Zimmerman JA, Gao HJ, Abraham FF. Modell Simul Mater Sci Eng 2000;8:103.
[249] Zhu YT, Jiang HG, Huang JY, Lowe TC. Metall Mater Trans A 2001;32:1559.
[250] Horita Z, Smith DJ, Nemoto M, Valiev RZ, Langdon TG. J Mater Res 1998;13:446.
[251] Valiev RZ, Gertsman VY, Kaibyshev OA. Phys Status Solidi a 1986;97:11.
[252] Zhao WS, Tao NR, Guo JY, Lu QH, Lu K. Scripta Mater 2005;53:745.
[253] Asaro RJ, Krysl P, Kad B. Philos Mag Lett 2003;83:733.
[254] Gu P, Kad BK, Dao M. Scripta Mater 2010;62:361.
[255] Bobylev SV, Ovid'ko IA. Rev Adv Mater Sci 2004;7:75.
[256] Bobylev SV, Gutkin MY, Ovid'ko IA. Phys Rev B 2006;73.
[257] Gutkin MY, Ovid'ko IA, Skiba NV. Phys Rev B 2006;74.
[258] Tadmor EB, Hai S. J Mech Phys Solids 2003;51:765.
[259] Kibey SA, Wang LL, Liu JB, Johnson HT, Sehitoglu H, Johnson DD. Phys Rev B 2009;79:214202.
[260] Kibey S, Liu JB, Johnson DD, Sehitoglu H. Appl Phys Lett 2007;91:181916.
[261] Kibey S, Liu JB, Johnson DD, Sehitoglu H. Appl Phys Lett 2006;89:191911.
[262] Kibey S, Liu JB, Curtis MJ, Johnson DD, Sehitoglu H. Acta Mater 2006;54:2991.
[263] Brandl C, Derlet PM, Van Swygenhoven H. Phys Rev B 2007;76:054124.
[264] Ogata S, Li J, Yip S. Phys Rev B 2005;71:224102.
[265] Finkenstadt D, Johnson DD. Phys Rev B 2006;73:024101.
[266] Nabarro FRN. Proc Phys Soc Lond 1947;59:256.
[267] Bulatov VV, Kaxiras E. Phys Rev Lett 1997;78:4221.
[268] Joos B, Duesbery MS. Phys Rev Lett 1997;78:266.
[269] Tang QH, Wang TC. Acta Mater 1998;46:5313.
[270] Frederiksen SL, Jacobsen KW, Schiotz J. Acta Mater 2004;52:5019.

[271] Marian J, Cai W, Bulatov VV. Nature Mater 2004;3:158.
[272] Kim I, Kim J, Shin DH, Laio XZ, Zhu YT. Scripta Mater 2003;48:813.
[273] Li YJ, Chen YJ, Walmsley JC, Mathinsen RH, Dumoulin S, Roven HJ. Scripta Mater 2010;62:443.
[274] Zhang L, Han Y. Mater Sci Eng A 2009;523:130.
[275] Kucherov L, Tadmor EB. Acta Mater 2007;55:2065.
[276] Wang J, Hirth JP, Tome CN. Acta Mater 2009;57:5521.
[277] Kim DH, Manuel MV, Ebrahimi F, Tulenko JS, Phillpot SR. Acta Mater 2010;58:6217.
[278] Wu XL, Youssef KM, Koch CC, Mathaudhu SN, Kecskes LJ, Zhu YT. Scripta Mater 2011;64:213.
[279] Wang YB, Louie M, Cao Y, Liao XZ, Li HJ, Ringer SP. Scripta Mater 2010;62:214.
[280] Marquis EA, Medlin DL, Leonard F. Acta Mater 2007;55:5917.
[281] Chen AY, Ruan HH, Wang J, Chan HL, Wang Q, Li Q, et al. Acta Mater 2011:XXX.
[282] Wu ZX, Zhang YW, Srolovitz DJ. Acta Mater 2009;57:4508.
[283] You ZS, Lu L, Lu K. Scripta Mater 2010;62:415.
[284] Hartley CS, Blachon DLA. J Appl Phys 1978;49:4788.
[285] Zhu YT, Wu XL, Liao XZ, Narayan J, Kecskes LJ, Mathaudhu SN. Acta Mater 2011;59:812.
[286] Wen HM, Zhao YH, Li Y, Ertorer O, Nesterov KM, Islamgaliev RK. Philos Mag 2010;90:4541.
[287] Conrad H. In: Zackey VF, editor. High-strength materials. New York (NY): Wiley; 1964.
[288] Wei Q, Cheng S, Ramesh KT, Ma E. Mater Sci Eng A 2004;381:71.
[289] Lu L, Li SX, Lu K. Scripta Mater 2001;45:1163.
[290] Wang YM, Ma E. Appl Phys Lett 2003;83:3165.
[291] Schwaiger R, Moser B, Dao M, Chollacoop N, Suresh S. Acta Mater 2003;51:5159.
[292] Lu L, Schwaiger R, Shan ZW, Dao M, Lu K, Suresh S. Acta Mater 2005;53:2169.
[293] Lu L, Dao M, Zhu T, Li J. Scripta Mater 2009;60:1062.
[294] Chen J, Lu L, Lu K. Scripta Mater 2006;54:1913.
[295] Sevillano JG, Vanhoutte P, Aernoudt E. Prog Mater Sci 1980;25:71.
[296] Hirsch J, Lucke K, Hatherly M. Acta Metall 1988;36:2905.
[297] Remy L. Metall Trans A 1981;12:387.
[298] Mullner P, Solenthaler C, Speidel MO. Acta Metall Mater 1994;42:1727.
[299] Thompson AW, Baskes MI, Flanagan WF. Acta Metall 1973;21:1017.
[300] Singh RP, Doherty RD. Metall Trans A 1992;23:307.
[301] Remy L. Acta Metall 1978;26:443.
[302] Bressane Jp, Moskowit A. Asm Trans Quart 1966;59:223.
[303] Asgari S, ElDanaf E, Kalidindi SR, Doherty RD. Metall Mater Trans A 1997;28:1781.
[304] Ma E, Wang YM, Lu QH, Sui ML, Lu L, Lu K. Appl Phys Lett 2004;85:4932.
[305] Chen XH, Lu L. Scripta Mater 2007;57:133.
[306] Babyak WJ, Rhines FN. Trans Am Inst Min Metall Eng 1960;218:21.
[307] Merz MD, Dahlgren SD. J Appl Phys 1975;46:3235.
[308] Murr LE, Moin E, Greulich F, Staudhammer KP. Scripta Metall 1978;12:1031.
[309] Shen YF, Lu L, Lu QH, Jin ZH, Lu K. Scripta Mater 2005;52:989.
[310] Youngdahl CJ, Weertman JR, Hugo RC, Kung HH. Scripta Mater 2001;44:1475.
[311] Kaschner GC, Tome CN, Beyerlein IJ, Vogel SC, Brown DW, McCabe RJ. Acta Mater 2006;54:2887.
[312] Subhash G, Ravichandran G, Pletka BJ. Metall Mater Trans A 1997;28:1479.
[313] Sangid MD, Ezaz T, Sehitoglu H, Robertson IM. Acta Mater 2011;59:283.
[314] Wang GY, Li GY, Zhao L, Lian JS, Jiang ZH, Jiang Q. Mater Sci Eng A 2010;527:4270.
[315] Zhang X, Misra A, Wang H, Nastasi M, Embury JD, Mitchell TE. Appl Phys Lett 2004;84:1096.
[316] Zhang X, Misra A, Wang H, Shen TD, Nastasi M, Mitchell TE. Acta Mater 2004;52:995.
[317] Misra RDK, Zhang Z, Jia Z, Somani MC, Karjalainen LP. Scripta Mater 2010;63:1057.
[318] Li XY, Wei YJ, Lu L, Lu K, Gao HJ. Nature 2010;464:877.
[319] Sun PL, Zhao YH, Cooley JC, Kassner ME, Horita Z, Langdon TG. Mater Sci Eng A 2009;525:83.
[320] Dao M, Lu L, Shen YF, Suresh S. Acta Mater 2006;54:5421.
[321] Carter CB, Ray ILF. Philos Mag 1977;35:189.
[322] Shute CJ, Myers BD, Xie S, Barbee TW, Hodge AM, Weertman JR. Scripta Mater 2009;60:1073.
[323] Qu S, Zhang P, Wu SD, Zang QS, Zhang ZF. Scripta Mater 2008;59:1131.
[324] Cheng S, Zhao YH, Wang YM, Li Y, Wang XL, Liaw PK. Phys Rev Lett 2010:104.
[325] Anderoglu O, Misra A, Wang H, Ronning F, Hundley MF, Zhang X. Appl Phys Lett 2008;93:083108.
[326] Mannan KM, Karim KR. J Phys F 1975;5:1687.
[327] Yoshinag H. Phys Status Solidi 1966;18:625.
[328] Capolungo L, Beyerlein IJ, Kaschner GC, Tome CN. Mater Sci Eng A 2009;513–514:42.
[329] Yoo MH, Lee JK. Philos Mag A 1991;63:987.
[330] Thornburg DR, Piehler HR. Metall Trans A 1975;6:1511.
[331] Vaidya S, Mahajan S. Acta Metall 1980;28:1123.
[332] Barnett MR. Mater Sci Eng A 2007;464:1.
[333] Barnett MR. Mater Sci Eng A 2007;464:8.
[334] Li N, Wang J, Huang JY, Misra A, Zhang X. Scripta Mater 2011;64:149.
[335] Wei Y. Mater Sci Eng A 2011;528:1558.
[336] Malygin GA. Phys Solid State 2008;50:1056.
[337] Cho MK, Cho JW, Wu JH, Cho JU, Choi YJ, Kim YK. Curr Appl Phys 2010;10:57.
[338] Aifantis KE, Konstantinidis AA. Mater Sci Eng B 2009;163:139.
[339] Pande CS, Cooper KP. Prog Mater Sci 2009;54:689.
[340] Pan Y, Zhou ZF, Fu SY, Nie YG, Sun CQ. Nano 2008;3:175.

[341] Dahlberg CFO, Gudmundson P. Philos Mag 2008:88.
[342] Trelewicz JR, Schuh CA. Appl Phys Lett 2008:93.
[343] Desai TG, Millett P, Wolf D. Mater Sci Eng A 2008;493:41.
[344] Mohammadabadi AS, Dehghani K. J Mater Eng Perform 2008;17:662.
[345] Shen TD, Schwarz RB, Feng S, Swadener JG, Huang JY, Tang M. Acta Mater 2007;55:5007.
[346] Carlton CE, Ferreira PJ. Acta Mater 2007;55:3749.
[347] Jerusalem A, Stainier L, Radovitzky R. Philos Mag 2007;87:2541.
[348] Xiang Q, Guo XM. Int J Solids Struct 2006;43:7793.
[349] Giga A, Kimoto Y, Takigawa Y, Higashi K. Scripta Mater 2006;55:143.
[350] Nieh TG, Wang JG. Intermetallics 2005;13:377.
[351] Kadau K, Germann TC, Lomdahl PS, Holian BL, Kadau D, Entel P. Metall Mater Trans A 2004;35A: 2719.
[352] Conrad H, Narayan J. Appl Phys Lett 2002;81:2241.
[353] Takeuchi S. Scripta Mater 2001;44:1483.
[354] Chattopadhyay PP, Pabi SK, Manna I. Z Metall 2000;91:1049.
[355] Song HW, Guo SR, Hu ZQ. Nanostruct Mater 1999;11:203.